Roles of Cftr-dependent Fluid Secretion During Organ Morphogenesis and Function

by

Adam Navis

Department of Cell Biology
Duke University

Date:_____

Approved:

_____
Michel Bagnat, Supervisor

_____
Vann Bennett, Chair

_____
Blanche Capel

_____
Kenneth Poss

_____
John Rawls

Dissertation submitted in partial fulfillment of
the requirements for the degree of Doctor
of Philosophy in the Department of
Cell Biology in the Graduate School
of Duke University

2014

ABSTRACT

Roles of Cftr-dependent Fluid Secretion During Organ Morphogenesis and Function

by

Adam Navis

Department of Cell Biology
Duke University

Date:_____

Approved:

_____
Michel Bagnat, Supervisor

_____
Vann Bennett, Chair

_____
Blanche Capel

_____
Kenneth Poss

_____
John Rawls

An abstract of a dissertation submitted in partial fulfillment of the requirements for the degree of Doctor of Philosophy in the Department of Cell Biology in the Graduate School of Duke University

2014

Abstract

Fluid secretion is essential to organ development and function, yet relatively little is known about the roles of fluid secretion *in vivo*. Early in development, fluid secretion plays important roles during the process of lumen formation and is necessary for organ homeostasis throughout life. A human disease, cystic fibrosis (CF) is caused by loss of cystic fibrosis transmembrane conductance regulator (CFTR) function, a chloride channel and key regulator of vertebrate fluid secretion. CFTR regulates fluid secretion by governing ion transport and osmotic gradients across epithelia.

To identify the developmental requirements for *cftr* function, we generated *cftr* mutant zebrafish using transcription activator like effector nucleases (TALENs). In *cftr* mutant zebrafish, we observed defects in the specification of left-right (LR) asymmetry. In the zebrafish, LR asymmetry is specified in part by directional fluid flow within a ciliated structure, Kupffer's vesicle (KV). Using live imaging of several transgenic markers in KV, we determined that lumen expansion is impaired in *cftr* mutants, which prevents directional fluid flow necessary for KV function. To examine *cftr* expression, we generated bacterial artificial chromosome (BAC) transgenic zebrafish expressing fluorescent Cftr fusion proteins under the control of the *cftr* promoter. These transgenes express Cftr within the KV epithelium and the protein localizes to the apical membrane. These transgenes rescue the KV function and the specification of LR asymmetry. These

studies reveal a new role for *cftr* during KV morphogenesis and function in the zebrafish.

In the zebrafish pancreas, we found that loss of *cftr* function leads to defects reminiscent of CF including destruction of exocrine tissue and changes in islet morphology. Additionally, we observed exocrine pancreatic destruction by 3 weeks post fertilization (wpf). Analysis of *cftr* BAC expression in the adult and larval zebrafish pancreata revealed that *cftr* is expressed specifically within the ducts, localized to the apical membrane throughout life. Adult *cftr* mutant pancreata developed substantial degeneration of exocrine tissue and experienced reduced growth rates. In contrast, we found that *cftr* is not necessary for the specification or initial development of the larval pancreas. Exocrine and endocrine tissues developed similarly in WT and *cftr* mutant larvae. These results indicate that *cftr*-dependent fluid secretion is important for maintenance of the zebrafish pancreas. Altogether, these studies of *cftr* function in KV and the pancreas demonstrate that fluid secretion is an essential component of lumen morphogenesis and organ function.

Contents

List of Tables

List of Figures

Acknowledgements

I am deeply indebted to the many people who have guided me on my sometimes circuitous journey to science. Their discussions and guidance have been instrumental in shaping and refining my interests in the ways animals take shape.

First, I am grateful to my brilliant advisor, Michel Bagnat, for his indispensable guidance and support. His lab has provided immense freedom for pursuing important questions from new directions. I am so thankful for his supreme confidence in me, even while mine waned, and for the many professional opportunities I have been provided. I am also grateful for the deep insights and guidance provided by the members of my thesis committee, Vann Bennett, Blanche Capel, Ken Poss, and John Rawls. Their advice was essential for focusing my efforts as I worked to complete my project.

I am also grateful to the other members of the Bagnat lab, Ashley Alvers, Lindsay Marjoram, Kathryn Ellis, Sean Ryan, and Jennifer Bagwell, for their friendship, discussions, and advice over the years. The numerous coffee runs and lighter-hearted moments like helicopter spotting and a shark-infested space birthday helped make the lab a fantastic environment.

I am also grateful for the guidance provided by my undergraduate advisor Alan Rawls who gave me a project that inspired my love of live imaging and also for instrumental advice that helped steer my early career. I am also especially grateful to a

former Rawls lab member, Doug Anderson, who despite not wanting undergraduate assistance, helped me in innumerable ways. He taught me fundamental molecular techniques and provided a model for scientific enthusiasm I hoped to emulate.

I am thankful to my parents for instilling in me the value of inquisition and for their unconditional support of my fluctuating dreams. I am deeply grateful to my wife, Allison Navis, for her friendship and immeasurable support through the trials of graduate school. Her companionship has been vital on this adventure and the adventures to come.

1. Introduction

1.1 Mechanisms of fluid secretion

The formation and function of many organs depends on fluid secretion driven by osmotic gradients generated by several types of ion channels. Classically, the Na^+/K^+-ATPase, localized to the basolateral membrane of the mammalian intestine, generates an extracellular sodium gradient by hydrolyzing ATP to pump potassium ions in and sodium ions out of the cell (Fig. 1A). The extracellular sodium gradient drives the import of chloride through a sodium, potassium, and chloride co-transporter, NKCC1. The increased intracellular concentration of chloride ions can be released through apical anion channels leading to an electrochemical gradient in the lumen. The electrochemical gradient draws positively charged sodium ions into the lumen establishing an osmotic gradient, which is thought to drive luminal fluid secretion (Barrett and Keely, 2000).

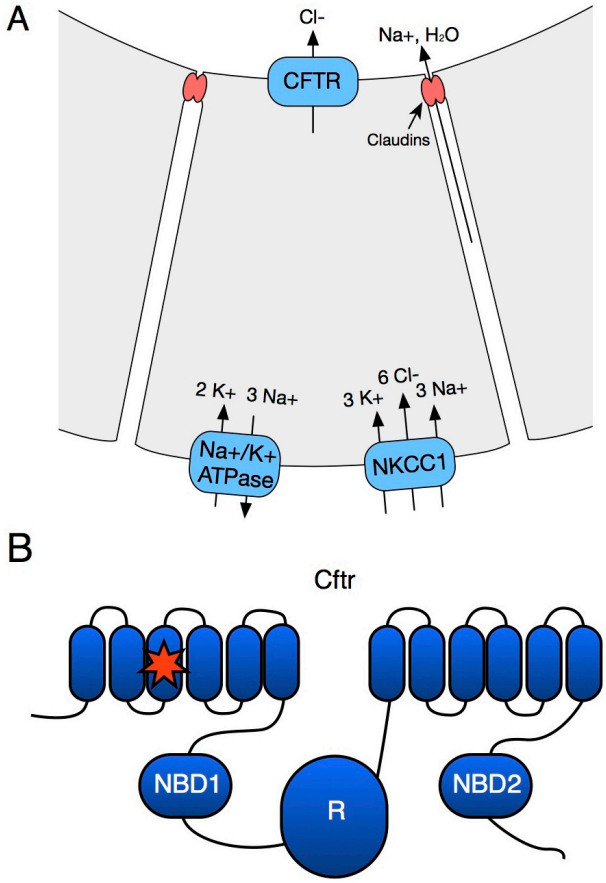

Figure 1: Fluid secretion is regulated by ion channels.

(A) Schematic representation of the ion gradients that regulate intestinal fluid secretion. (B) Schematic structure of Cftr including twelve transmembrane domains, two nucleotide binding domains (NBD), and a regulatory domain (R-domain).

Fluid secretion is required for several types of lumen morphogenesis. In the zebrafish gut, the Na^+/K^+-ATPase helps drive fluid secretion necessary for single lumen formation (Bagnat et al., 2007), although fluid secretion alone is insufficient to complete lumen coalescence (Alvers et al., 2014). Fluid pressure can also help drive organ morphogenesis by inflating a lumen. In the zebrafish brain, Na^+/K^+-ATPase activity is required for expansion of the brain ventricles (Lowery and Sive, 2005). In zebrafish Na^+/K^+-ATPase mutants, the brain contains a continuous, uninflated single lumen. Hydrostatic fluid pressure is also required for lumen expansion in the *Ciona intestinalis* notochord. An Slc26 family chloride/bicarbonate exchanger regulates ion transport and pH levels necessary for notochord expansion in the ascidian notochord (Deng et al., 2013). *Ciona* lacking Slc26 function also demonstrate normal apical membrane specification and luminal connections in the notochord indicating that in some systems, lumen formation and expansion are discrete processes. These studies indicate that fluid secretion is essential for several processes during lumen formation.

A properly regulated epithelial barrier is necessary to form and maintain electrochemical gradients essential for fluid secretion. Claudin-family adhesion molecules are key regulators of epithelial barrier function (Furuse et al., 2002). In addition to restricting ion flow, claudins also selectively permit paracellular ion transport. Claudin 4 and 8 coordinate the paracellular flow of chloride ions in the mammalian kidney, helping to regulate fluid absorption in the organ (Fujita et al., 2012;

Hou et al., 2010). Absorption of sodium ions across the kidney epithelium, also important for renal fluid absorption, is regulated by Claudin 2 (Muto et al., 2010). Claudin15 is a key regulator of fluid secretion in the zebrafish gut and was shown to be essential for lumen coalescence (Bagnat et al., 2007). Similarly, fluid secretion that drives expansion of the zebrafish brain ventricles depends on Claudin5a function, which helps establish a paracellular barrier (Zhang et al., 2010). These studies demonstrate that a properly regulated epithelial barrier is essential for fluid transport during lumen morphogenesis and function.

Aquaporins facilitate fluid secretion by allowing water molecules, driven by osmotic gradients, to diffuse through the plasma membrane. Expansion of the *C. elegans* excretory canal is regulated in part by Aquaporin-8 (AQP-8) (Khan et al., 2013; Kolotuev et al., 2013). Loss of AQP-8 activity by blocking expression or treatment with mercury inhibits lumen expansion in the excretory canal (Khan et al., 2013). Taken together, these studies indicate that fluid secretion is an essential component of lumen morphogenesis in a wide variety of systems.

1.2 CFTR

A chloride channel, the cystic fibrosis transmembrane conductance regulator (CFTR), is composed of several domains crucial for its function. A member of the ATP-binding cassette (ABC) transporter family, CFTR passively transports anions in contrast to the active transport performed by most family members (Dean and Annilo, 2005;

Riordan et al., 1989). The protein contains twelve transmembrane domains organized into two membrane spanning domains, two nucleotide binding domains (NBD), and a regulatory domain (R-domain) (Fig. 1B) (Riordan et al., 1989). The CFTR NBDs regulate channel gating by binding to ATP, which governs opening of the pore (Carson et al., 1995). The CFTR NBDs are capable of ATP hydrolysis, but require new ATP for channel activity. CFTR activity is further regulated by phosphorylation of the R-domain, a domain unique among the ABC family (Cheng et al., 1991). The R-domain can be phosphorylated by PKA, in response to increased cyclic AMP (cAMP) levels, which activates the channel.

Zebrafish Cftr is similar to human CFTR. The protein maintains 55% identity overall and the domains important for Cftr function are even more highly conserved (Bagnat et al., 2010). Additionally, zebrafish Cftr is responsive to many of the same activators and inhibitors of human CFTR indicating conserved functionality between the proteins.

Defects in CFTR-dependent fluid secretion are associated with the progression of several human diseases. Increased fluid secretion has been associated with polycystic kidney disease (PKD) and secretory diarrheas. In PKD, fluid accumulates in the kidneys causing formation of large, painful cysts (Wilson, 2004). Fluid secretion into these cysts is thought to be driven in part by channel activity of CFTR (Hanaoka et al., 1996; Yang et al., 2008). In the intestine, misregulated fluid secretion leads to secretory diarrheas, a

leading cause of death in the developing world. Cholera is a bacterial pathogen that causes secretory diarrheas by stimulating increased production of cAMP, which in turn activates CFTR (Field et al., 1972). The increased CFTR activity drives excessive fluid secretion into the intestine and quickly leads to dehydration (Barrett and Keely, 2000). The primary therapy for affected patients is oral rehydration therapy, which overcomes the osmotic gradients by providing a large dose of glucose to drive import of water molecules back into the cells (Wright and Loo, 2000).

Excessive fluid secretion can be modeled in the zebrafish. In zebrafish mutant for *cse1l*, fluid secretion becomes misregulated, leading to increased luminal fluid and dramatic expansion of the gut (Bagnat et al., 2010). Cse1l was found to function as a negative regulator of Cftr, which normally limits Cftr activity in the gut. Misregulated chloride channel activity leads to increased fluid secretion and expansion of the gut lumen. Properly regulated CFTR activity and fluid secretion is crucial for organ homeostasis.

1.3 Cystic fibrosis

Loss of CFTR function leads to defects in fluid secretion and cystic fibrosis (CF). CF is a multi-organ disease characterized most prominently by a loss of fluid secretion causing mucosal buildup, blocking organ ducts, and preventing normal organ function.

CF was initially described in the 1938 as a disease affecting the pancreas (Andersen, 1938). Due to the obvious pancreatic defects in CF patients, the disease was

first titled cystic fibrosis of the pancreas. Infants born with CF typically failed to thrive due to blockage of the pancreatic ducts causing pancreatic insufficiency (PI), which prevents delivery of digestive enzymes necessary for metabolizing food (DiMagno et al., 1973). As a hint to the root cause of the disease, CF patients were discovered to have high concentrations of salt in their sweat, an early indication of the involvement of ion transport in the progression of the disease (Di Sant'Agnese et al., 1953). In fact, testing the chloride levels in sweat remains a standard diagnostic indicator for CF (Rosenstein and Cutting, 1998). As treatment for pancreatic disease and patient life-span has improved, several other symptoms have emerged including lung disease and cystic fibrosis related diabetes (CFRD) (Lyczak et al., 2002; Mackie et al., 2003).

CFTR was identified as the causative gene for CF in a landmark paper (Riordan et al., 1989). CF was a particularly good candidate because it followed simple Mendelian frequencies indicative of a single causative gene. The identification of CFTR allowed for a more detailed investigation of the mutations responsible for the disease. The most common allele in CF is a deleted phenylalanine at amino acid 508 (CFTR-ΔF508), present in more than 90% of patients (Riordan, 2008; Riordan et al., 1989). The CFTR-ΔF508 allele disrupts protein stability, targeting the channel for premature degradation and reducing apical membrane localization. CFTR-ΔF508 is partially active at room temperature, suggesting that the primary defect is a loss of folding leading to decreased retention at the plasma membrane (Thibodeau et al., 2005). Loss of CFTR activity leads to a loss of

fluid secretion and defects in hydration of luminal mucus, which causes blockages in several organs.

In the pancreas, CFTR is expressed along the pancreatic ducts, where it is thought to regulate ion gradients that hydrate luminal mucus and drive secretion of pancreatic juices (Marino et al., 1991). In the pancreas, loss of chloride transport leads to mucosal buildup and blockage of the pancreatic ducts (Quinton, 1990). This prevents delivery of digestive enzymes to the stomach and is thought to drive degeneration of the exocrine pancreas. More than 85% of CF patients develop PI due to loss of exocrine pancreatic function (Consortium, 1993; Wilschanski and Novak, 2013). CF patients with PI are treated with oral digestive enzymes. Even with enzyme supplements, CF patients have reduced growth rates. (Sproul and Huang, 1964). In many CF patients and in some animal models of CF, much of the exocrine pancreas is destroyed and replaced by fibrotic tissue (Imrie et al., 1979; Rogers et al., 2008; Sturgess, 1984; Sun et al., 2010).

Functionally, the pancreas is composed of two main tissues, the exocrine pancreas, responsible for producing digestive enzymes and the endocrine pancreas, which produces several hormones (Gittes, 2009; Shih et al., 2013). In addition to the destruction of the exocrine pancreas, many CF patients develop deficiencies in endocrine pancreatic function. The endocrine pancreas contains several cell types including α, β, δ, PP, and ε cells (Shih et al., 2013). The α and β cells are the most prevalent cell-type in the islet and regulate blood glucose levels (Baetens et al., 1979). The α cells secrete glucagon,

which increases blood glucose levels by stimulating the liver to convert stored glucagon into glucose. Conversely, the β cells reduce blood glucose by promoting the uptake of glucose by cells throughout the body (Baetens et al., 1979; Unger, 1985). Many CF patients that develop PI go on to develop CFRD, which shares similarities with type 1 and type 2 diabetes (Mackie et al., 2003). CFRD patients develop defects in blood glucose regulation and progressive exocrine degeneration leads to changes in islet morphology (Löhr et al., 1989; Mackie et al., 2003).

In the lung, loss of CFTR-dependent chloride channel activity also leads to defects in fluid secretion. Typically, mucus coats the airway and is hydrated by water secreted from the lung epithelium. Properly hydrated mucous is gradually cleared from the lung by coordinated beating of cilia present on the epithelial surface, which push the mucus up and out of the airway. In CF patients, the mucus becomes dried-out and compacted preventing normal ciliary clearance (Knowles et al., 1997). This causes continued mucosal buildup and allows opportunistic pathogens including *Pseudomonas aeruginosa* and *Burkholderia cepacia* to colonize the lung (Callaghan and McClean, 2012). Chronic *Pseudomonas* infection is associated with persistent inflammation in the lung and *Burkholderia cepacia* is associated with rapid declines in lung function of CF patients (Callaghan and McClean, 2012).

CF patients also have defects in several other organs, which have been less well characterized. In many patients, bile ducts become blocked by mucus leading to liver

disease (Tanner and Taylor, 1995). In the immune system, bacterial killing is compromised in CF patients since immune cells drive high chloride concentrations to kill engulfed bacterial cells (Di et al., 2006). CF patients also have abnormal responses to immune signaling causing inappropriate immune responses (Bruscia et al., 2011). Additionally, the bone density of CF patients is often below normal leading to a higher incidence of fractures (Elkin et al., 2001). This may be due to a variety of effects including poor nutrition due to pancreatic insufficiency, defective mineral absorption, or osteoblast dysfunction leading to defects in bone mineralization (Elkin et al., 2001). Altogether, these symptoms highlight the importance of CFTR function throughout the body and emphasize the challenges associated with treating CF.

In recent years, several new CF models have been developed, including a pig and ferret model to complement the existing CFTR mutant mouse (Rogers et al., 2008; Sun et al., 2010; van Doorninck et al., 1995). Investigating the pathophysiology of CF in mice has proven challenging because the mouse does not develop severe pancreatic disease and has compensatory ion channels in the lung that rescue loss of CFTR function (Colledge et al., 1995; Zeiher et al., 1995). The CFTR mutant pig and ferret models develop several hallmarks of human CF including defects in lung function, pancreatic disease, and intestinal defects (Rogers et al., 2008; Sun et al., 2010). In recent years, the pig and ferret have been instrumental in providing new insights into the progression of CF.

Pancreatic degeneration can be observed in CF infants (Waters et al., 1990), though it remains unclear whether these defects arise during organogenesis or secondarily due to pancreatic blockage and subsequent inflammation in the pancreas. Similarly, severe pancreatic degeneration has been observed in newborn piglets (Abu-El-Haija et al., 2012). In ferrets, pancreatic inflammation is initially less severe and degeneration occurs over the course of the first month of life (Olivier et al., 2012). Whether pancreatic disease arises during organogenesis or secondarily to pancreatic blockage and inflammation has remained an open question due to challenges associated with observing development in existing models. The ferret and pig are not easily accessible developmental model systems and mouse knockouts do not develop the severe pancreatic disease characteristic of CF. To address these limitations, we generated a zebrafish model to investigate developmental functions for *cftr*.

1.4 Types of lumen formation

Cells may coordinate to form a lumen through several distinct processes (Lubarsky and Krasnow, 2003). During epithelial wrapping, a sheet of polarized cells undergoes apical constriction to drive cell shape changes that bend a tissue and enclose a lumen. Lumen morphogenesis in the gut and neural tube of mammals, chicks, and frogs is driven by epithelial wrapping (Sawyer et al., 2010).

A rod of cells may form a lumen through cavitation or cord hollowing. Cavitation in the mammalian salivary gland and mammary tissue is characterized by

apoptosis and clearance of the cells in the interior of a rod, generating an epithelium that surrounds a central lumen (Mailleux et al., 2007; Melnick and Jaskoll, 2000; Tucker, 2007). Alternatively, lumen formation may occur through cord hollowing by cellular rearrangements within a rod of cells to generate a central lumen (Fig. 2). During cord hollowing, the organ initially forms several small lumens, which must coalesce to complete lumen formation. The mammalian kidney, pancreas, zebrafish gut, and Kupffer's vesicle form a central lumen through cord hollowing (Amack et al., 2007; Bagnat et al., 2007; Horne-Badovinac et al., 2003; Kesavan et al., 2009; Yang et al., 2013).

New tubes may also form through budding to branch a lumen. In the lung, apical constriction along the luminal epithelium drives the early phases of branching morphogenesis (Kim et al., 2013). Budding is observed during morphogenesis of the mammalian lung, vasculature, *Drosophila* tracheal system, and salivary gland (Hogan and Kolodziej, 2002; Kim et al., 2013; Uv et al., 2003).

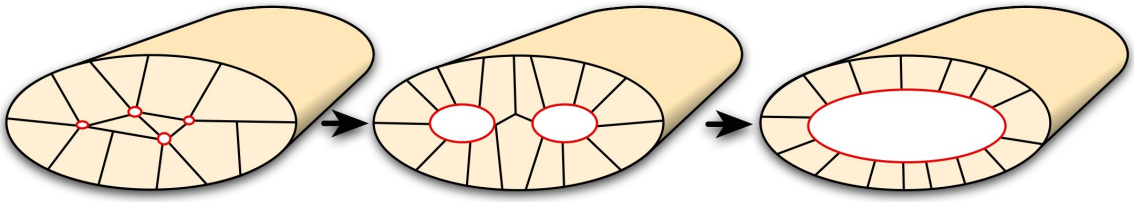

Figure 2: Lumen formation by cord hollowing

Cartoon depicting the morphogenetic events leading to single lumen formation by cord hollowing. Several small lumens coalesce to form a single central lumen.

Within a single cell, a lumen may form through cell hollowing. During cell hollowing, apical membrane is typically localized to an intracellular compartment, which extends and connects to neighboring cells. Lumen formation by cell hollowing occurs in small blood vessels, the terminal and fusion branches of the *Drosophila* trachea, the ascidian notochord, and in the *C. elegans* excretory system (Buechner, 2002; Dong et al., 2009a; Kamei et al., 2006; Levi et al., 2006). Lumen formation by these diverse mechanisms is a crucial component of organogenesis and is necessary for organ function.

1.5 Kupffer's vesicle morphogenesis

Kupffer's vesicle (KV) is the zebrafish organ of asymmetry and is functionally analogous to the organs of asymmetry in other vertebrates including the mouse node and frog gastrocoel roof plate (Essner et al., 2005; Nonaka et al., 2002; Schweickert et al., 2007). KV is a transient organ that develops from a group of dorsal forerunner cells (DFCs), which migrate toward the vegetal pole during epiboly (Essner et al., 2005). After migration completes, KV forms a fluid-filled lumen through cord hollowing beginning at the 1 somite stage (ss) (Fig. 2) (Amack et al., 2007). Although cilia-driven fluid flow is important for the specification of left-right (LR) asymmetry in nearly all vertebrates, KV is the only organ of asymmetry known to form a complete lumen. After the specification of LR asymmetry, KV is disassembled and resorbed by the embryo before 24 hpf.

Inside the lumen, counterclockwise fluid flow is essential to KV function (Essner et al., 2005; Essner et al., 2002). KV contains two types of cilia: motile cilia, which rapidly beat to drive directional fluid flow, and immotile sensory cilia which are thought to detect the flow and transmit asymmetric signaling outside KV. The cilia develop a posterior tilt, which is thought to help translate anterior-posterior asymmetry into left-right asymmetry (Wang et al., 2011a). Sensory cilia contain a mechanosensitive ion channel, Pkd2, which has been proposed to generate a calcium flux in response to mechanical signals (Kramer-Zucker et al., 2005; Schottenfeld et al., 2007). This calcium flux initiates numerous downstream signaling events that regulate LR asymmetry.

1.6 Specification of left-right asymmetry

Symmetry breaking in the early embryo is essential for the formation of the vertebrate body plan. Loss of proper specification of LR asymmetry leads to a variety of defects, including a complete mirroring of the body plan (*situs inversus totalis*). Incomplete specification of LR asymmetry can lead to indeterminate organ positioning or heterotaxia, which can have drastic effects on the circulatory system and other physiological processes (Levin, 2005).

In many vertebrates, the specification of LR asymmetry is determined by two distinct processes. Early in embryogenesis, ion gradients regulated by the H^+/K^+-ATPase are necessary for LR asymmetry in the fish and frog (Kawakami et al., 2005; Levin et al., 2002). The earliest asymmetric gene expression in the frog is the H^+/K^+-ATPaseα subunit

(Aw et al., 2008). In the fish, H^+/K^+-ATPase activity is asymmetric, with no observed asymmetry in gene expression (Kawakami et al., 2005). Importantly, H^+/K^+-ATPase activity does not appear to regulate LR asymmetry during mammalian embryogenesis (Vandenberg and Levin, 2013).

A second key step in vertebrate LR specification is the development of organs of asymmetry. In several homologous organs, the mouse node, frog gastrocoel roof plate, and zebrafish KV, cilia drive fluid flow necessary for the specification of LR asymmetry (Essner et al., 2005; Nonaka et al., 2002; Schweickert et al., 2007). Interestingly, the chick and pig do not have nodal cilia, suggesting that they use alternative mechanisms for the determination of LR asymmetry. Alternatively, cell movements have been proposed to drive LR asymmetry in Hensen's node in the chick (Gros et al., 2009).

Directional fluid flow drives left-sided signaling and downstream gene expression in zebrafish and many other vertebrate species (Fig. 3). The mechanisms translating directional flow to asymmetric gene expression in the ciliated organs of asymmetry are not completely understood. Two models have been proposed: fluid flow may move ligands to receptors on the left side of the node (Hirokawa et al., 2006) or sensory cilia may mechanically detect nodal flow (McGrath et al., 2003). In either case, this leads to an asymmetric calcium flux in the left side of the mouse node through calcium channels, Pkd1 and Pkd2, in sensory cilia (Field et al., 2011). In the zebrafish, *pkd2* also regulates KV calcium signaling (Bisgrove et al., 2005; Schottenfeld et al., 2007).

One of the earliest examples of asymmetric gene expression downstream of the node and KV is Cerl2 in the mouse and *charon* in the zebrafish (Hashimoto et al., 2004; Marques et al., 2004). The gene is responsive to calcium signaling and acts as a Nodal antagonist. Charon is expressed more highly on the right side of the perinodal tissue, opposite the pattern of calcium signaling (Hashimoto et al., 2004; Superina et al., 2014).

Asymmetric signaling leads to left-sided expression of Nodal, a secreted signaling molecule and key left-side determinant (Brennan et al., 2002; Long et al., 2003; Saijoh et al., 2003). Nodal drives its own expression in positive feedback loop and also drives expression of Lefty, a TGF-β ligand that rapidly diffuses and inhibits Nodal expression (Nakamura et al., 2006). This arrangement establishes a self-enhancement and lateral-inhibition system to promote local activation of Nodal on the left, while restricting Nodal expression on the right (Marjoram and Wright, 2011). Signals are restricted to the left side of the animal by the midline barrier (Lenhart et al., 2011). Interestingly, loss of *pkd2* (*curly up*) in the zebrafish leads to bilateral *southpaw*, the zebrafish ortholog of Nodal, expression, while loss of Pkd2 in the mouse leads to an absence of Nodal expression indicating some differences exist between the mechanisms that direct asymmetric gene expression in these systems (Pennekamp et al., 2002; Schottenfeld et al., 2007).

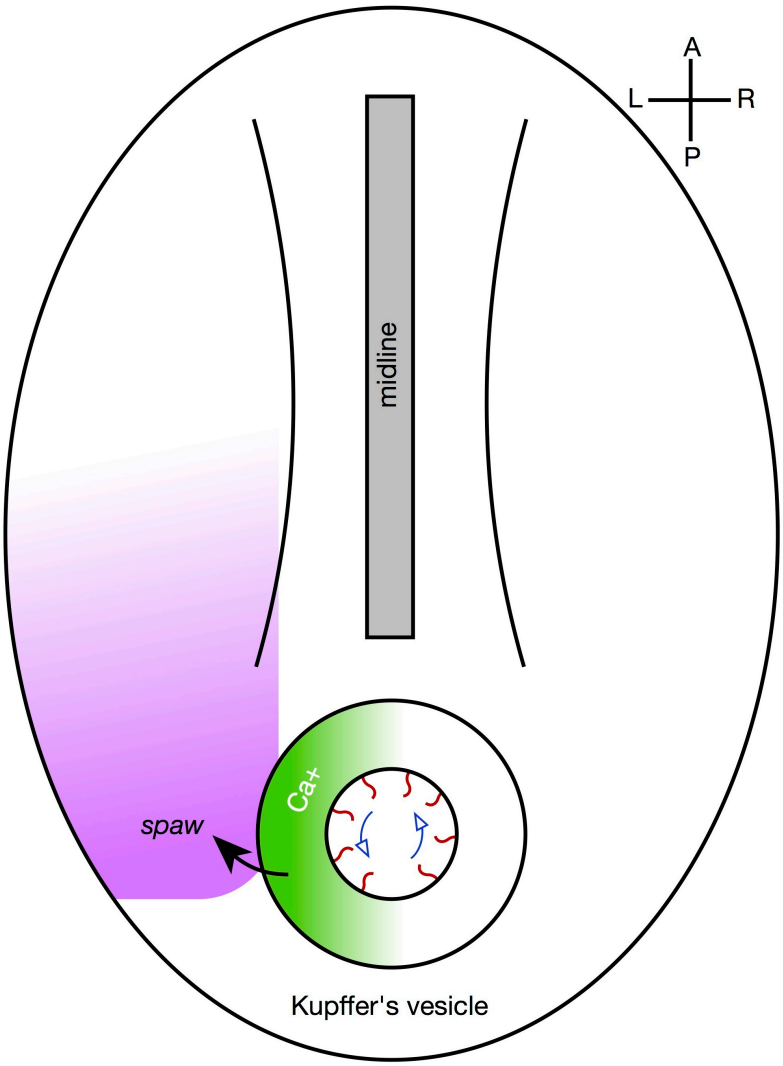

Figure 3: Specification of LR asymmetry by KV in zebrafish

Schematic representation of the basic mechanisms underlying specification of LR asymmetry in zebrafish. Cilia (red) within KV drive directional fluid flow (blue), which stimulates calcium signaling (green) on the left side of KV. This process drives expression of *spaw* (purple), which propagates up the left side of the embryo. The midline barrier (gray) restricts diffusion of signaling molecules from one side to the other. Anterior is oriented upward in this schematic dorsal view of the embryo.

Left-sided signaling is important for asymmetric expression of several downstream genes that regulate positioning of the heart, pancreas, liver, and intestine (Levin, 2005). During development of the heart tube, Nodal signals drive asymmetric cell motility, which is necessary for jogging the heart tube to the left side of the body from its initial midline position (Veerkamp et al., 2013). The specification of the LR axis is an integral step in vertebrate development, regulated by ion channels and fluid flow. To better understand the mechanisms regulating LR determination, it will be important to determine the interplay between the early mechanisms that specify LR signaling.

1.7 Pancreatic development

The zebrafish pancreas is similar to the mammalian pancreas in morphology and function (Tiso et al., 2009). Initially, the zebrafish pancreas develops from two distinct domains, dorsal and ventral buds formed at 24 and 40 hours post fertilization (hpf) respectively (Field et al., 2003) (Fig. 4). As the pancreas forms, these buds join at 52 hpf with the ventral bud contributing the exocrine tissue, and the dorsal bud contributing endocrine tissue, forming the principal islet (Field et al., 2003). Once the buds join, the tail of the pancreas extends and ductal cells generate a lumen through cord hollowing (Kesavan et al., 2009). The principal islet is located at the head of the pancreas and the pancreatic duct can be observed extending along the length of the pancreas. As the pancreas continues to develop, the organ increases in size and the duct undergoes

branching to extend throughout the exocrine tissue. Importantly, the transparency of the larval zebrafish allows for detailed analysis of pancreatic development in live animals.

As the fish grows, new secondary islets are specified and develop near the pancreatic ducts. Lineage tracing in the mouse and zebrafish has established that new β cells can be specified from progenitors located in the pancreatic ducts (Parsons et al., 2009; Solar et al., 2009; Wang et al., 2011b). In zebrafish, the ductal progenitors are responsive to Notch signaling. Inhibiting Notch signaling in these cells can stimulate formation of new secondary islet β cells (Parsons et al., 2009). These β cells incorporate into new, secondary islets that embed in the surrounding exocrine tissue throughout the pancreas. In contrast to the zebrafish pancreas, the mammalian pancreas does not contain a principal islet specified during the initial stages of pancreatic development (Chen et al., 2007). Instead mammalian islets are specified through a process more similar to secondary islet formation in zebrafish (Parsons et al., 2009).

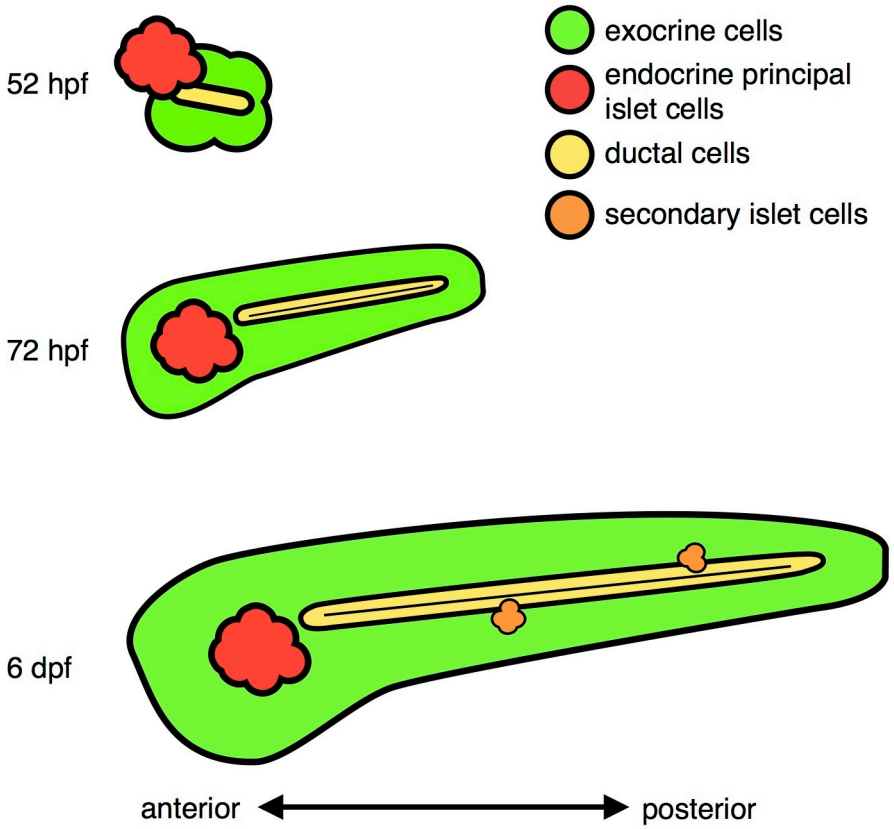

Figure 4: Zebrafish pancreatic development.

Schematic representation of pancreatic development in the zebrafish. A dorsal bud contributes early endocrine tissue to the principal islet and a ventral bud contributes exocrine and ductal cells, which fuse by 54 hpf. The pancreatic duct extends posteriorly by 72 hpf and secondary islets begin to develop from ductal progenitors around 6 dpf.

1.8 Summary

Here we use the zebrafish to investigate the function of *cftr*-dependent fluid secretion during zebrafish development and disease. Importantly, we found that early in embryogenesis, *cftr* functions during the specification of LR asymmetry. Cftr activity is necessary to inflate the KV lumen and to facilitate cilia-driven fluid flow that drives asymmetric signaling. We found that loss of KV lumen expansion leads to defects in LR asymmetry. Later in development, *cftr* is important for the function of the zebrafish pancreas. In mammals, loss of Cftr activity leads to blockage of the pancreatic ducts and degeneration of the exocrine pancreas, a symptom characteristic of CF. In the adult zebrafish, we found degeneration of the exocrine pancreas, which is replaced by fibrotic tissue similar to mammalian disease. Zebrafish mutant for *cftr* have defects in growth and pancreatic degeneration evident by 3 wpf. We found that *cftr* is required for the function in the pancreatic ducts. Altogether, these studies reveal a key role for *cftr* during fluid secretion necessary for organ morphogenesis and function.

The findings presented in chapter 3 were published in *Development* in April 2013 [Navis, A., Marjoram, L. and Bagnat, M. (2013). Cftr controls lumen expansion and function of Kupffer's vesicle in zebrafish. *Development* 140, 1703–1712.].

2. Methods

2.1 TALEN mutagenesis

Three TALENs (Miller et al., 2011) were designed to target the sixth exon of *cftr* using TALEN targeter (Doyle et al., 2012) and constructed using Golden Gate assembly (Cermak et al., 2011). The TALEN used to generate the *cftr* mutant alleles reported here was composed of the following repeat variable domains (RVDs): NN NN NN NG NI NG NN NN HD HD HD NI NG NG NG NG NI NG NI NG and NN NG NI HD NI HD NI NN NN NI NG NN HD NI NG NG. Two *cav1* mutant alleles were generated by two TALEN pairs, *cav1*-T1 is expected to disrupt the *cav1α* isoform, while *cav1*-T2 is expected to disrupt the α and β isoforms. *Cav1*-T1 was composed of the following RVDs: NG NG HD NG NG NG NN NN NI NI HD HD NN HD NI and NG NG HD HD NG NN NI NG NI NI NI HD NN NN HD. *Cav1*-T2 was composed of NN NN NI NG NI NI HD NN NI HD NI NN HD NI NG and HD NG HD HD NG NG NN NN NG NN NG NN NN NI HD NI NG RVDs. The *cav1* mutant alleles were generated using a modified TALEN backbone for improved nuclease activity (Dahlem et al., 2012). Zebrafish were injected into the yolk at the one-cell stage with 100 pg total TALEN RNA and 50 pg of dsRed RNA to mark expressing embryos. Mutant alleles were identified by *Eco*RV digestion of a PCR product generated with the following primers: cftr-exon6-F, TTGGGCCTAAATTTCAAATGAT; and cftr-exon6-R, TTTGGATGCACAGTAGGCTAA.

2.2 BAC recombineering

A BAC containing *cftr* (DKEY-270I2) was modified using Red/ET BAC modification plasmids (Genebridges, Heidelberg, Germany). A positive selection cassette for generating C-terminal fusions was developed by constructing a plasmid containing a 20-aa spacer (DLPAEQKLISEEDLDPPVAT), GFP or mRFP-Ruby, an SV40 poly-adenylation sequence, and an FRT-kanamycin-FRT cassette (Lee et al., 2001) into pBluescript. Recombination was performed by amplifying the cassette with the following primers, which contained 50 bp of homology flanking the stop codon of *cftr*: cftr-spGFP-hom-F, CGCAGACCCTGCAAGAGGAGGCAGAGGACAACATCCAGGACACTCGCCTCGATCTCCCCGCCGAACAGAAA and cftr-spGFP-hom-R, TTTAATGTACCATTGGGTGACGGCCTGGGTCACTGAGTCTTTTGGAACGCATTGGAGCTCCACCGCGGTG. The amplicon was then transformed into Red/ET-induced *Escherichia coli*. The kanamycin was removed from the BAC by expressing Flpase from the p707-Flpe plasmid (Genebridges). The *cftr-RFP* BAC was further modified by recombining the iTol2-Amp cassette into the loxP site of the pIndigoBAC-536 backbone (Suster et al., 2009). The modified BAC was purified using the Nucleobond BAC-100 Kit (Clontech, Mountain View, CA, USA).

The *cav1-GFP* and *cftr:Gal4* BACs were generated using the SW105 strain (Warming et al., 2005). The BACs were first transformed into the SW105 cells. The GFP-

SV40-FKF cassette above was amplified using the following primers: cav1-spGFP-hom-F,

ccatggggaaatgctttagtaacgtccgggtcactgctactaaggtggtgGATCTCCCCGCCGAACAGAAA

and cav1-spGFP-hom-R,

cattcccccatcccacccgatccctctggctcttctctttcactctgtccATTGGAGCTCCACCGCGGTG. To generate the *cftr-Gal4* BAC, a plasmid was generated containing a Gal4-SV40-FRT-kanamycin-FRT cassette and was amplified using the following primers: cftr-Gal4-hom-F, gatacccgtaacccgatgtgagcgctttcacccccggggtacttttttaggATGAAGCTACTGTCTTCTAT

and cftr-Gal4-hom-R,

caaaagaagtatctggagaggcagttggcatcctccacaggtgatctctgCAGTGTGATGGATATCTGCAG. The recombination machinery for inserting the cassette and removing the kanamycin resistance gene are encoded within the SW105 genome. The protocol was performed as previously described (Warming et al., 2005). Briefly, the recombinase is expressed in response to heat induction and the flppase is induced by arabinose and the cells must be otherwise maintained below 31°C. After the GFP cassette was added, iTol2-amp was inserted into the backbone for transgenesis.

2.3 Zebrafish transgenesis

The *cftr-GFP* BAC was linearized using *Sfi*I (NEB) and injected into one-cell-stage embryos. The *cftr-RFP* and *cav1-GFP* BACs were co-injected with 50 pg of transposase RNA into one-cell-stage embryos (Kawakami, 2004; Kwan et al., 2007). Several

transgenic lines were established: *TgBAC(cftr-GFP)pd1041*, *TgBAC(cftr-RFP)pd1042*, *TgBAC(cftr:Gal4)*pd1101 and *TgBAC(cav1-GFP)pd1097*. The *cftr:Gal4* BAC was co-injected with a circular plasmid expressing RFP and without Tol2 sites to mark expressing cells without integrating. Founders were identified by crossing to *Tg(UAS:GFP)zf82* to generate the *TgBAC(cftr:Gal4)pd1101* line.

The *Tg(hsp70l:GFP-podxl)pd1080* line was generated by Gateway recombination with the Tol2Kit (Kwan et al., 2007). GFP-podocalyxin (Meder et al., 2005) was subcloned into pME and assembled with p5E-hsp70l, p3E-polyA and pDestTol2pA2. The resulting plasmid was co-injected into one-cell-stage embryos with 50 pg Transposase RNA. To induce expression, embryos at 50% epiboly were heat-shocked for 30 minutes in a 39°C water bath. GFP-podocalyxin was imaged in conjunction with GFP Counterstain BODIPY TR Methyl Ester dye (Invitrogen).

Table 1: List of transgenic lines used in this study.

Name	Allele number
TgBAC(cftr-GFP)	pd1041
TgBAC(cftr-RFP)	pd1042
TgBAC(cftr:Gal4)	pd1101
TgBAC(cav1-GFP)	pd1097
Tg(UAS:GFP)	zf82
Tg(sox17:GFP)	s870
Tg(hsp:GFP-podxl)	pd1080
Tg(ela:GFP, lfabp:dsRed)	gz12
Tg(ins:dsRed)	m108
Tg(ins:NTR-mCherry)	jh4

2.4 In situ hybridization

The probe to detect the *cftr* transcript by *in situ* hybridization was PCR amplified from cDNA and ligated into pGEMT-Easy (Promega, Madison, WI, USA) with the following primers: cftr-ish-F, CCAAACCAGACAAAGGCAAA; and cftr-ish-R, GGTGCCATCTCACGATAACTCAA. *In situ* hybridization to detect *cftr* in the early embryo was performed as previously described (Marjoram and Wright, 2011; Snelson et al., 2008). *In situ* hybridization to detect *cftr* at 3 and 5 dpf was performed similarly with the addition of a 20 min proteinase K step to better permeablize the larvae. Detection of *spaw*, *cmlc2* (*myl7* – Zebrafish Information Network), *lefty1* and *no tail* transcripts were performed as previously described (Long et al., 2003; Yelon et al., 1999). The plasmids were linearized and digoxygenin-labeled RNA was generated using the DIG RNA Labeling Kit (Roche). Stained embryos were imaged on a Discovery.V20 stereoscope (Zeiss, Oberkochen, Germany) with an Achromat S 1.0× lens.

2.5 Immunofluorescence

Whole-mount immunofluorescence using aPKC (Santa Cruz Biotechnology; 1:100), pan-cadherin (Santa Cruz Biotechnology; 1:1200) and ZO-1 (Invitrogen; 1:500) primary antibodies with goat anti-mouse Alexa568 or goat anti-rabbit Alexa647 secondary antibodies (Molecular Probes; 1:100) was performed as previously described (Li et al., 2011). Acetylated tubulin staining was performed as previously described (Zaghloul and Katsanis, 2011) with the following modifications. Embryos were fixed

overnight at 4°C in Dent's fixative, treated with 10 μg/ml Proteinase K (Sigma) for 1 minute and post-fixed with 4% paraformaldehyde. Mouse anti-acetylated tubulin (Sigma; 1:1000) was detected with goat anti-mouse Alexa568 (Molecular Probes; 1:100). Tailbuds were dissected with a microknife (Fine Science Tools, Foster City, CA, USA), mounted in SlowFade Gold (Invitrogen) and imaged using a Leica SP5 confocal microscope.

Immunofluorescence using insulin (Dako, 1:100), glucagon (Sigma, 1:100), carboxypeptidase (Rockland, 1:500), and ZN-5 (ZIRC, 1:100) antibodies in the pancreas was performed as previously described (Dong et al., 2007; Moss et al., 2009). Larvae were fixed overnight in 3% formaldehyde in PEM (100 mM PIPES, 2 mM EGTA, and 1 mM MgSO4). For whole-mount immunofluorescence, fixed larvae were washed with PBS and the ventral skin and remaining yolk was removed using forceps before blocking with 4% BSA in PBS with 0.3% Triton X-100. Whole-mount samples were dehydrated and imaged in glycerol. Transverse sections were generated by embedding the fish in 4% low melt agarose in PBS at 55°C, cooling for at least 1 hour at 4°C, and sectioning on a vibratome (VT 1000S; Leica). Sections were blocked with a solution containing 4% BSA in PBS containing 0.3% Triton X-100 and washed using PBS containing 0.3% Triton X-100. Agarose sections were mounted in Vectashield Mounting Medium with DAPI (Vector Labs). Samples were imaged using a Leica SP5 confocal microscope.

2.6 Live imaging

Embryos for live confocal imaging were mounted in 4% agarose on slides and immediately imaged on an SP5 confocal microscope (Leica, Wetzlar, Germany) with an HC PL APO 20×/0.70 objective. Imaging of KV flow was performed by injecting fluorescent beads as previously described (Borovina et al., 2010). Differential interference contrast (DIC) microscopy and whole-mount epifluorescence were performed on embryos mounted in 3% methylcellulose and imaged on an Imager M1 (Zeiss) with a EC Plan-Neufluar 10×/0.3 objective.

2.7 RNA injection

The *TgBAC(cftr-GFP)* open reading frame was cloned into pCS2+ with flanking *Eco*RI sites. RFP was fused to the N-terminus of Clic5b (accession number: BC085448) and cloned into pCS2+ with flanking *Eco*RI and *Xho*I sites. Capped RNA was transcribed from *Not*I linearized plasmid using the mMESSAGE mMACHINE SP6 Kit (Ambion, Grand Island, NY, USA). Arl13b-mCherry (75 pg/embryo) (Borovina et al., 2010) or *cftr-GFP* (150 pg/embryo) RNA was injected into the yolk of one-cell-stage embryos.

2.8 Pharmacological treatments

Pharmacological reagents were purchased from Sigma (St Louis, MO, USA). Forskolin was prepared as a 10 mM stock in DMSO and fish were treated in egg water at 10 μM. IBMX (3-isobutyl-1-methylxanthine) was prepared as a 100 mM stock in DMSO and embryos were treated at 40 μM in egg water. Ouabain was prepared as a 1 mM

stock in DMSO and embryos were treated at 1 μM in egg water. Embryos were treated from 50% epiboly until they were imaged at the 10-to 12-ss.

2.9 Cell culture

Human HEK293 and Cos-7 cells were cultured in DMEM with 10% fetal bovine serum and 1% penicillin-streptomycin (Invitrogen). Cells were transfected on glass coverslips with either pCDNA-Cftr-GFP or pCDNA-Cftr^{pd1048}-GFP using Lipofectamine 2000 (Invitrogen) and fixed the following day in 4% paraformaldehyde. Fixed cells were stained with DAPI and imaged on an Imager M1 (Zeiss).

2.10 Glucose measurements

Observations of fasting blood glucose were collected by sacrificing zebrafish adults and measured using a Freestyle blood glucose meter as previously described (Moss et al., 2009).

2.11 Nitroreductase treatment

Islet β cells were targeted for ablation by treating *Tg(ins:NTR-mCherry)jh4* expressing zebrafish with 10 mM metronidazole as previously described (Pisharath et al., 2007). Larvae were treated at 56 hpf for 24 hours. The metronidazole was removed and the fish were allowed to recover for 48 hours. After recovery, the fish were fixed and processed for immunofluorescence as described above. The number of insulin positive β cells expressing either *Tg(ins:NTR-mCherry)jh4* or labeled with anti-insulin was quantified using ImageJ to analyze stacks of confocal images through complete islets.

2.12 Lipid feeding

Fluorescently labeled fatty acids were prepared as previously described (Carten et al., 2011; Semova et al., 2012). Briefly, BODIPY-C_5 fatty acids were resuspended in egg water containing 5% egg yolk. Larvae at 6 dpf were incubated for 6 hours in the 5% yolk emulsion and fixed in 4% PFA. Fixed larvae were imaged on a Leica SP5 confocal microscope.

2.13 Statistical analysis

Measurements of KV lumen area, exocrine pancreas volume, body length, number of β cells, and cilia length were performed using ImageJ (NIH, Bethesda, MD, USA) and analyzed for statistical significance using Student's *t*-test in Prism (Graphpad, La Jolla, CA, USA). Comparisons between KV phenotype and organ laterality were performed using a $\chi 2$ test in Prism (Graphpad). Error bars are reported as standard error of the mean (s.e.m.)

3. Cftr regulates Kupffer's vesicle lumen expansion

3.1 Introduction

Regulated fluid secretion is crucial for the development and function of many organs in vertebrates, including the kidney, vasculature, brain and ear (Cartwright et al., 2009). During organogenesis, fluid secretion can act as a force driving tubulogenesis. In zebrafish, fluid secretion promotes single lumen formation in the gut (Bagnat et al., 2007) and ventricle inflation in the brain (Lowery and Sive, 2005). Similarly, in mammals, fluid secretion has been shown to be crucial for lung development (Wilson et al., 2007). Loss of fluid regulation can lead to defects in organogenesis. For example, excessive fluid accumulation leads to dramatic expansion of the zebrafish gut lumen (Bagnat et al., 2010) and defects in cilia-dependent fluid clearance can lead to kidney cysts and hydrocephalus (Kramer-Zucker et al., 2005; Moyer et al., 1994; Nauli et al., 2003; Sun et al., 2004).

A major regulator of fluid secretion in vertebrates is CFTR. CFTR regulates fluid secretion by controlling the transport of chloride (Anderson et al., 1991), which draws sodium to generate osmotic gradients that drive the movement of water through a tissue. Defects in CFTR function cause CF, a disease in which loss of Cl^- and/or $HCO3^-$ transport impairs fluid secretion and also causes mucus build-up in many organs, including the lungs, intestine and pancreas (Durie and Forstner, 1989; Gaskin et al., 1988; Matsui et al., 1998). The channel is composed of several domains, including twelve

transmembrane domains, two nucleotide-binding domains and a unique regulatory domain (R-domain) (Riordan et al., 1989). The R-domain is regulated through phosphorylation by cyclic AMP-dependent protein kinase (PKA) (Berger et al., 1993). Zebrafish Cftr is highly similar to its human ortholog, particularly in domains important for CFTR function (Bagnat et al., 2010). Although CFTR activity has been well characterized *in vitro*, relatively little is known about its function *in vivo*, especially during development.

In vertebrates, fluid flow generated by ciliary beating is important for the determination of left-right (LR) asymmetry. In zebrafish, laterality is controlled by a transient, fluid-filled structure called Kupffer's vesicle (KV) (Essner et al., 2005). KV is functionally homologous to the organs of asymmetry in other vertebrates, including the mouse node and the gastrocoel roof plate in *Xenopus* (Nonaka et al., 2002; Schweickert et al., 2007). KV develops from a group of dorsal forerunner cells (DFCs) that migrate to the vegetal pole during gastrulation and coalesce to form a fluid-filled spherical structure surrounding a single lumen (Amack et al., 2007; Oteíza et al., 2008). Within the KV lumen, motile cilia drive directional fluid flow leading to asymmetric calcium signaling at the periphery, similar to the mouse node (McGrath et al., 2003; Sarmah et al., 2005). Asymmetric signaling leads to an upregulation of left-sided genes beginning with *southpaw* (*spaw*), the zebrafish ortholog of Nodal, a highly conserved signaling molecule required for the specification of LR asymmetry (Brennan et al., 2002; Long et al., 2003;

Saijoh et al., 2003). Although it is has been well established that cilia-driven fluid flow is crucial for KV function, the mechanisms that regulate secretion of fluid into KV remain uncharacterized.

Here, we describe a new role for Cftr in the development and function of KV in zebrafish. Using TAL effector nucleases (TALENs), we generated *cftr* mutants and found that loss of Cftr activity impairs KV lumen expansion and function, causing defects in LR patterning. Using BAC recombineering we generated a Cftr-GFP transgenic line and observed that *cftr* is expressed primarily in KV, where the protein localizes apically as the lumen forms. Together, our results demonstrate that Cftr-dependent fluid secretion is crucial for lumen formation and function of KV in zebrafish.

3.2 Generation of cftr mutant zebrafish

To investigate the role of Cftr during zebrafish development we generated *cftr* mutants using TALENs (Cermak et al., 2011; Huang et al., 2011; Miller et al., 2011). Three TALEN pairs for *cftr* were constructed, transiently expressed in zebrafish embryos, and then screened for activity. Embryos injected with the TALEN pair showing the highest transient activity were raised to establish mutant lines. The TALEN was targeted to the *Eco*RV site in the sixth of 27 *cftr* exons, corresponding to the third transmembrane domain. This exon precedes several domains crucial for Cftr function, including the chloride pore, regulatory domain, and both nucleotide-binding domains (Fig. 5A,B). After screening ten TALEN-injected fish for disruption of the *Eco*RV restriction site (Fig.

5C), we identified three *cftr* alleles, including a two-amino acid deletion, *cftr*^{pd1048}, and two frameshift mutations, *cftr*^{pd1049} and *cftr*^{pd1050} (Fig. 5D). The *cftr*^{pd1049} allele is predicted to code for 56 incorrect amino acids past the lesion before encountering a stop codon (Fig. 5E), whereas *cftr*^{pd1050} generates a stop codon at the site of the lesion. To characterize the *cftr*^{pd1048} mutation, we cloned and expressed GFP-tagged wild-type (WT) Cftr (Cftr-GFP) and Cftr^{pd1048}-GFP in Cos-7 cells. Unlike WT Cftr-GFP, Cftr^{pd1048}-GFP was largely absent at the cell surface and localized mostly to intracellular membranes resembling the endoplasmic reticulum, suggesting that the shortened transmembrane domain encoded by the mutant allele affects biosynthetic transport (Fig. 6A,B). Accordingly, in transfected cells Cftr^{pd1048} lacked the mature, fully glycosylated form of the protein, as judged by western blot analysis (Fig. 6C).

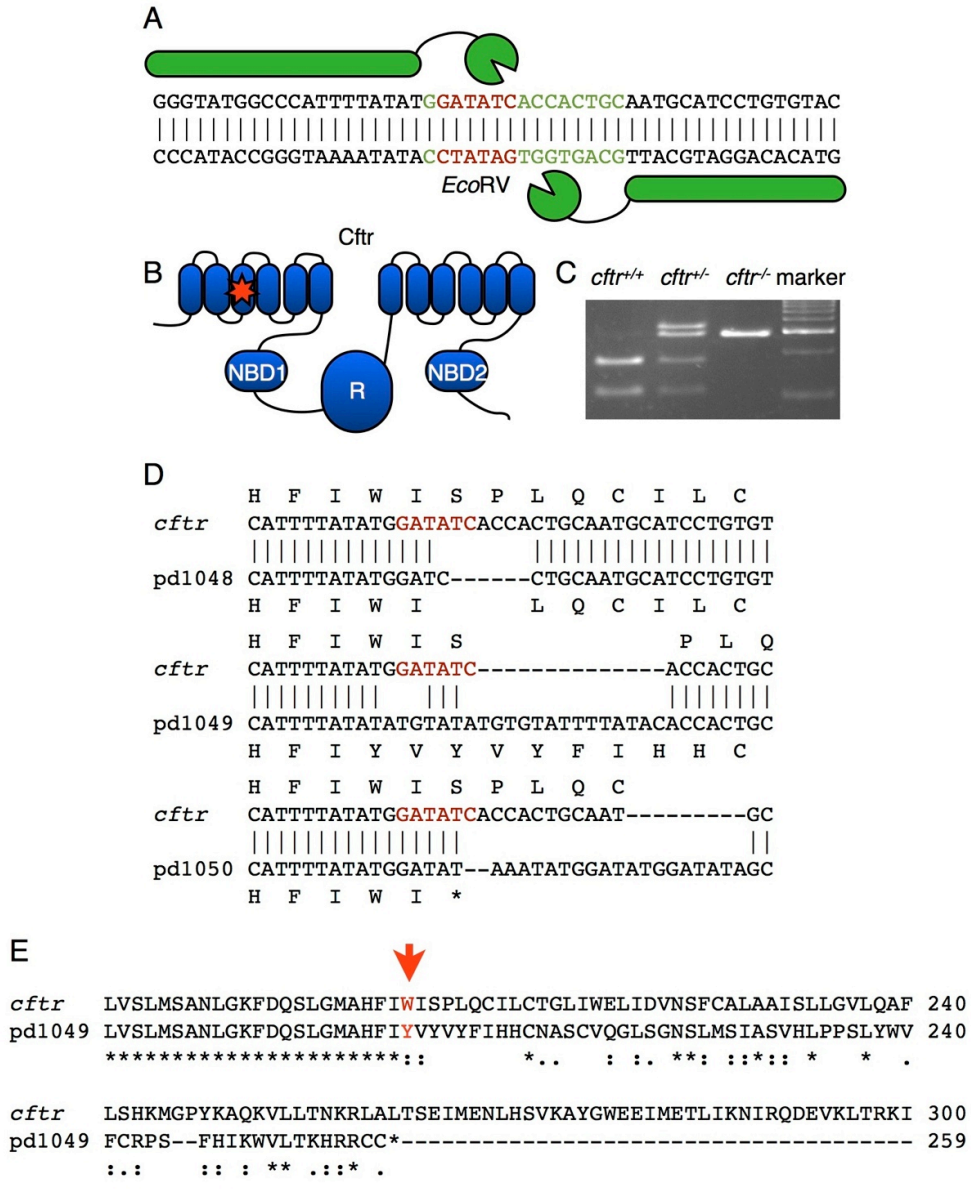

Figure 5: Generation of a *cftr* mutant zebrafish.

Figure 5: Generation of a *cftr* mutant zebrafish. (A) A TALEN was designed to target the *Eco*RV site in the sixth transmembrane domain. The spacer is marked by green text and the restriction site is denoted by red text. (B) Schematic of the domain structure of Cftr with a star indicating the TALEN target site within the third transmembrane domain of the protein. NBD, nucleotide binding domain; R, regulatory domain. (C) TALEN activity generated insertions and deletions that disrupt the *Eco*RV site. (D) Sequence alignments of the TALEN-generated alleles. *Cftr*^{pd1048} has a six-nucleotide deletion, *cftr*^{pd1049} and *cftr*^{pd1050} have nucleotide insertions and deletions causing frameshifts leading to premature stop codons. (E) An alignment of the amino acid sequences encoded by *cftr*^{pd1049} and WT *cftr*.

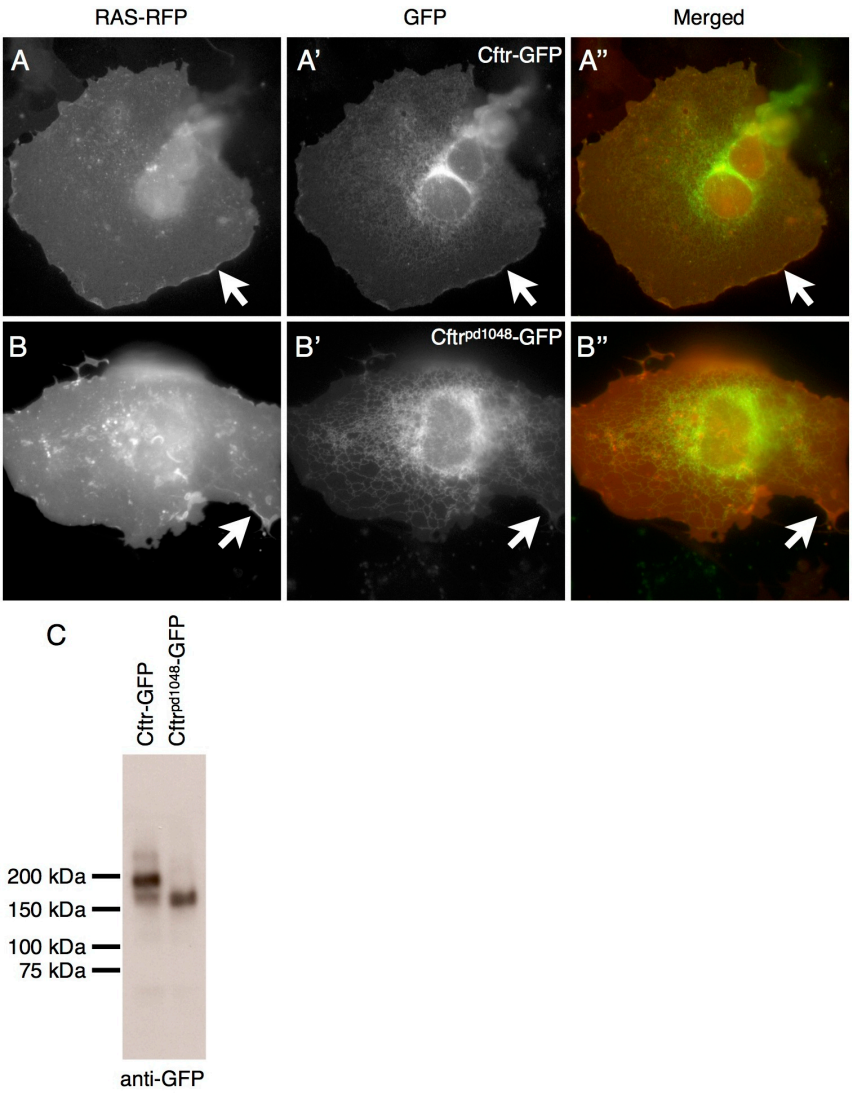

Figure 6: *cftr*^{pd1048} encodes a hypomorphic *cftr* allele.

(A) Cos7 cell expressing WT Cftr-GFP demonstrating plasma membrane localization of Cftr co-localized with the membrane marker RAS-RFP. Arrows indicate plasma membrane localization of RAS-RFP and Cftr-GFP. (B) Cos7 cell expressing Cftr^{pd1048} localized to intracellular accumulations distinct from RAS-RFP. Arrows indicate plasma membrane localization of RAS-RFP while Cftr^{pd1048}-GFP is absent from the membrane. (C) Western blot showing decreased molecular weight of Cftr^{pd1048} compared to WT Cftr.

3.3 cftr is required for the specification of left-right asymmetry

To analyze Cftr function during development, the *cftr* mutations were crossed into the *Tg(fabp10:dsRed, ela:GFP)gz12* background, which expresses dsRed in the liver and GFP in the exocrine pancreas (Farooq et al., 2008). While examining homozygous mutant embryos, we found partial randomization of liver and pancreas *situs*. In zebrafish, the liver normally develops on the left side of the abdomen; however, in 27% of $cftr^{pd1049}$ mutants the liver developed on the right (*n*=30 mutants), compared with 0% of their WT siblings (*n*=103 WT) (Fig. 7A,B).

To test whether the anatomical positioning of other organs is also affected in *cftr* mutants, we examined heart looping, one of the earliest morphological indicators of organ laterality. The heart, marked by *cmlc2* expression, normally loops to the left. In ~31% of *cftr* mutant embryos the heart looped to the right (*n*=138 mutants), in contrast to only 1% of WT siblings (*n*=408 WT) (Fig. 7C,D). Homozygous mutants survived to adulthood and the females were moderately fertile, allowing the generation of maternal zygotic $cftr^{pd1049}$ mutants. Maternal zygotic $cftr^{pd1049}$ fish were morphologically identical to zygotic $cftr^{pd1049}$ and had similar rates of reversed heart looping (31%, *n*=26). Defects in liver and heart orientation were primarily concordant and only a few cases of heterotaxia were observed.

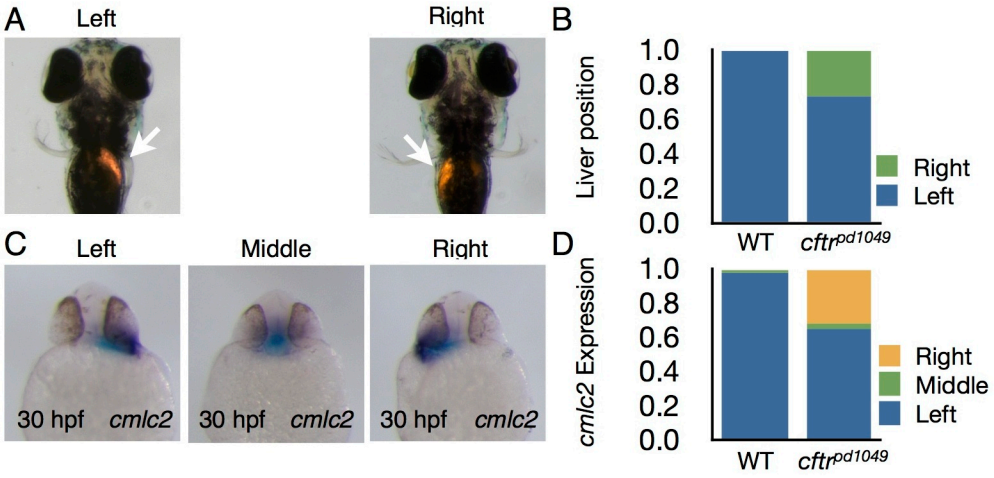

Figure 7: *cftr* mutants have defects in organ laterality.

(A) Ventral view of 4 days post-fertilization (dpf) WT and *cftr*^{pd1049} mutant larvae expressing dsRed in the liver (arrows). (B) Quantification of liver orientation in WT and *cftr*^{pd1049} mutants. Liver orientation is reversed in 27% of homozygous mutants. WT, *n*=103; *cftr*^{pd1049}, *n*=30. (C) Ventral view of representative *cftr*^{pd1049} mutants showing *cmlc2* expression pattern. (D) Quantification of heart looping in WT and *cftr*^{pd1049} mutants. WT, *n*=408; *cftr*^{pd1049}, *n*=138.

To investigate early events in LR patterning, we examined the expression of *spaw*, a gene asymmetrically expressed in the left lateral plate mesoderm of the embryo at 20 ss and an important LR patterning determinant (Long et al., 2003). Whereas 99.3% of WT siblings expressed *spaw* exclusively on the left (*n*=146), *cftr*^{pd1049} mutants displayed a range of *spaw* expression phenotypes including exclusively left (30.6%), left dominant (25.0%), bilateral (23.6%), right dominant (9.7%) and exclusively right (11.1%) (*n*=73) (Fig. 8A,B). These data indicate that *cftr* is required for the establishment of LR asymmetry in zebrafish before the onset of *spaw* expression.

Aberrant *spaw* expression and organ laterality can be caused by defects in processes that establish and restrict asymmetric signaling. Dorsal midline structures, such as the notochord and floorplate, function as a barrier to restrict *spaw* to the left side of the embryo and loss of barrier function has been shown to result in bilateral *spaw* expression (Long et al., 2003). Additionally, midline expression of *lefty1*, a *spaw* antagonist, is required for left-sided restriction of *spaw* expression (Bisgrove et al., 1999). To determine whether *cftr*^{pd1049} mutants have midline barrier defects, we examined the expression of midline markers as well as the gross morphology of WT and mutant embryos. At 22 ss, expression of the notochord marker *no tail* (*ntl*) in *cftr*^{pd1049} mutants was indistinguishable from that of WT siblings (Fig. 9A,B). We also examined the expression of *lefty1* and found that in *cftr*^{pd1049} mutant embryos *lefty1* expression was similar to that of WT siblings (Fig. 9C,D). In addition, the notochord and floorplate of

cftr^{pd1049} mutants appeared to be completely intact at 24 hours post-fertilization (hpf) as judged by DIC microscopy (Fig. 9E,F). Brightfield whole-mount imaging of *cftr*^{pd1049} mutants at 24 and 48 hpf showed no obvious morphological defects (Fig. 9G-J). Thus, defects in *spaw* expression and LR patterning in *cftr*^{pd1049} mutants are probably not due to defects in midline integrity.

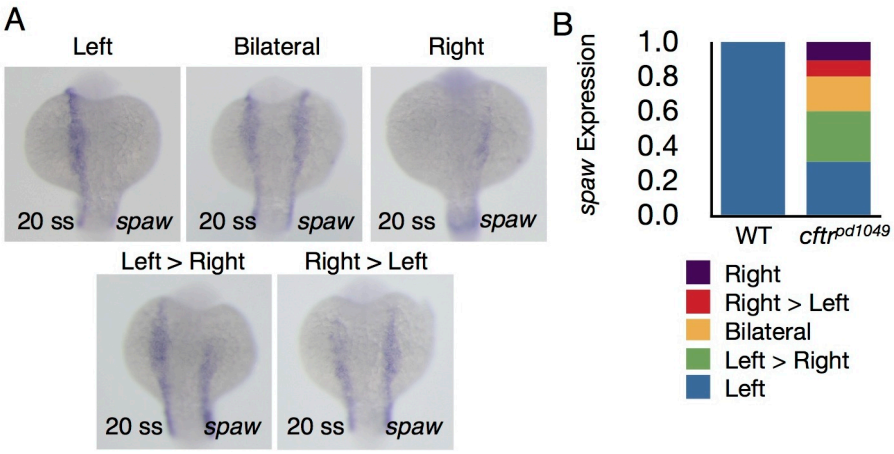

Figure 8: Early LR signaling events are disrupted in *cftr* mutants.

(A) Dorsal view of *cftr*^{pd1049} mutant embryos displaying left, right, left>right, right>left and left=right *spaw* expression patterns. (B) Quantification of *spaw* expression in WT and *cftr*^{pd1049} mutants. WT, *n*=146; *cftr*^{pd1049}, *n*=73.

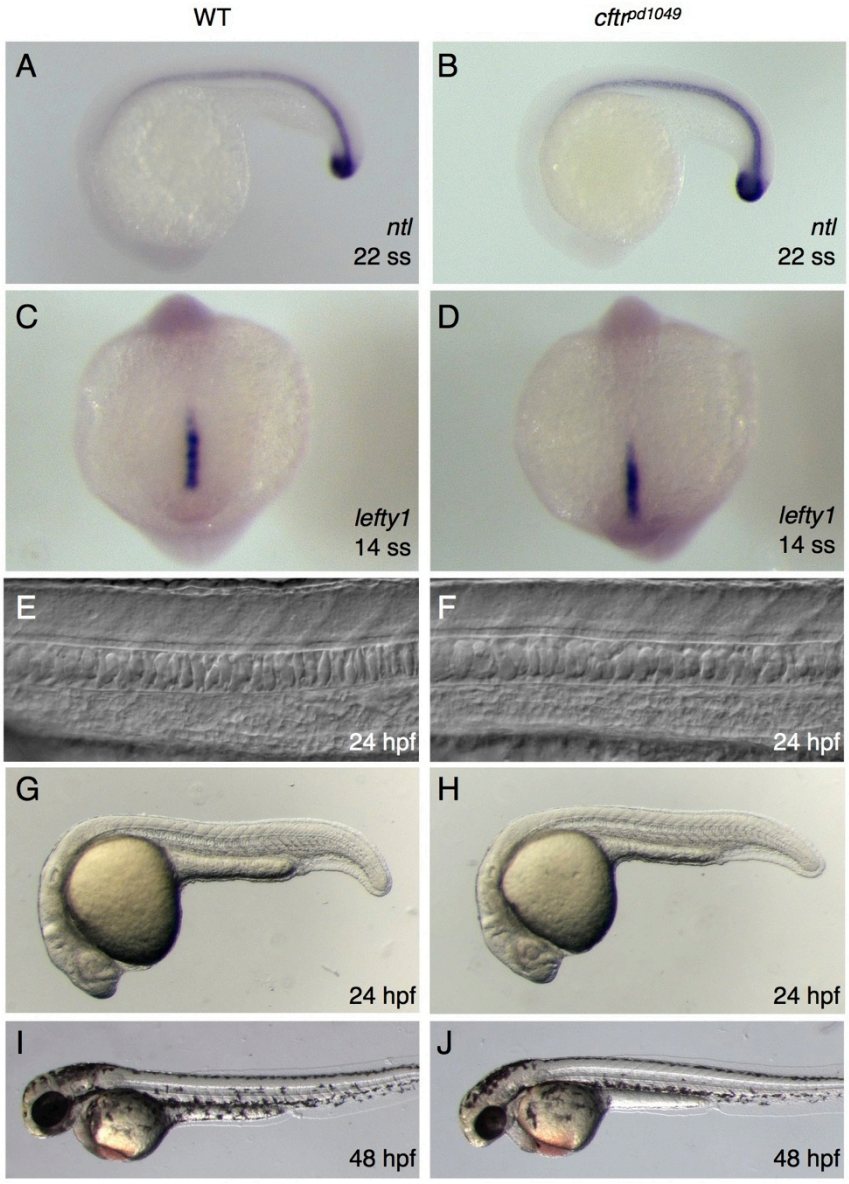

Figure 9: The midline is intact in *cftr* mutants.

(A) WT and (B) *cftr*^{pd1049} mutant embryos showing unbroken *ntl* expression in the notochord. (C) WT and (D) *cftr*^{pd1049} mutant embryos expressing lefty in the posterior notochord. (E) WT and (F) *cftr*^{pd1049} mutant embryos imaged with DIC microscopy to show an intact neural tube floorplate. (G) Brightfield imaging of WT and (H) *cftr*^{pd1049} mutant embryos demonstrating normal body extension at 24 hpf and (I,J) 48 hpf.

3.4 KV lumen expansion requires cftr

To better understand how Cftr functions in LR asymmetry, we next investigated the development of KV, a transient, fluid-filled organ important for the specification of LR asymmetry in zebrafish (Essner et al., 2005). Examination of *cftr* mutants by DIC microscopy revealed that the KV lumen was absent in the frameshift alleles *cftr*^{pd1049} and *cftr*^{pd1050} (Fig. 10A-D). This phenotype is fully penetrant; all homozygous *cftr* mutants displayed defects in KV lumen morphogenesis (n=72). In *cftr*^{pd1048}, the lumen was present, but severely reduced in size (Fig. 10E,F), suggesting that this may be a hypomorphic allele.

To investigate the morphology of KV in greater detail, we crossed *cftr* mutants into the *Tg(sox17:GFP)s870* background, a well-established marker of DFCs and KV (Oteíza et al., 2008; Sakaguchi et al., 2006). To visualize cilia, we injected RNA encoding Arl13b-mCherry into one-cell-stage embryos (Borovina et al., 2010). Using live confocal imaging, we found that in *cftr*^{pd1049} mutants the DFCs migrated and clustered to form a structure similar in size to the WT KV. However, in the mutants, lumen inflation did not occur and resulted in a central plate of ciliated, *sox17:GFP*-positive cells with no discernible luminal space (Fig. 10G,H).

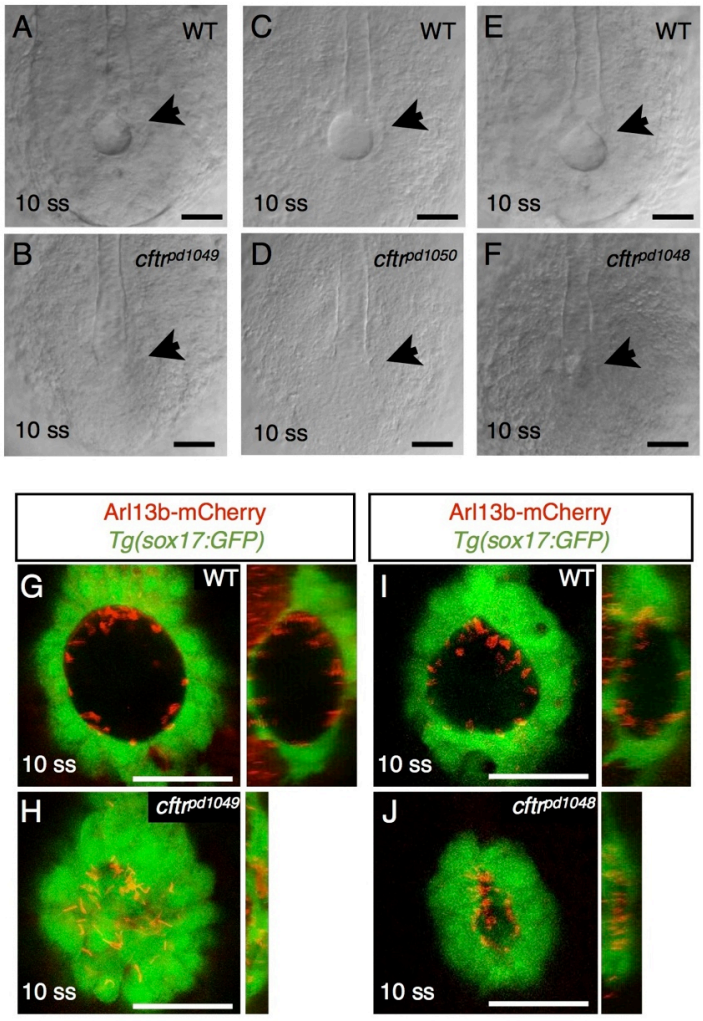

Figure 10: *cftr* is required for KV lumen expansion.

(A-F) KV lumen (arrow), imaged at 10 ss by DIC microscopy in WT (A,C,E) and mutant siblings (B,D,F respectively). (B,D) The KV lumen is undetectable by DIC in *cftr*^{pd1049} and *cftr*^{pd1050} mutants at 10 ss. (F) DIC imaging of the *cftr*^{pd1048} tailbud identified a small KV lumen. (G-J) Live confocal images showing ventral cross-section and orthogonal views of WT and mutant KV expressing *Tg(sox17:GFP)* and Arl13b-mCherry RNA at 10 ss in (G,H) WT and *cftr*^{pd1049} mutant siblings and (I,J) WT and *cftr*^{pd1048} siblings. Scale bars: 50 μm.

Next, we examined KV development in the hypomorphic *cftr*^{pd1048} allele. Using live confocal imaging we observed that, at 10 ss, mutants homozygous for this allele had a KV with a very small central lumen (~30% of the area compared with WT siblings) containing Arl13b-mCherry-positive cilia that appeared motile (Fig. 10I,J). Due to line averaging during confocal microscopy, motile cilia appear as a fan-shaped blur (Borovina et al., 2010). At 12 ss, in some rare cases, the small lumen inflated to a size large enough to reveal seemingly normal, but highly crowded motile cilia (Fig. 11A-D), suggesting that Cftr function is not required for cilia morphogenesis or motility in KV. We then investigated whether these mutants formed a lumen large enough to allow for proper specification of LR asymmetry. We examined heart looping and liver orientation in *cftr*^{pd1048} mutants and found that they had a similar rate of LR asymmetry defects compared to the null (*cftr*^{pd1049}) allele. To determine whether fluid flow is normal in the hypomorphic allele, we injected fluorescent beads into the KV lumen. In the *cftr*^{pd1048} KV, fluid flow appeared turbulent, indicating the organ does not function normally when fluid secretion and lumen size are significantly reduced (Fig. 11E,F).

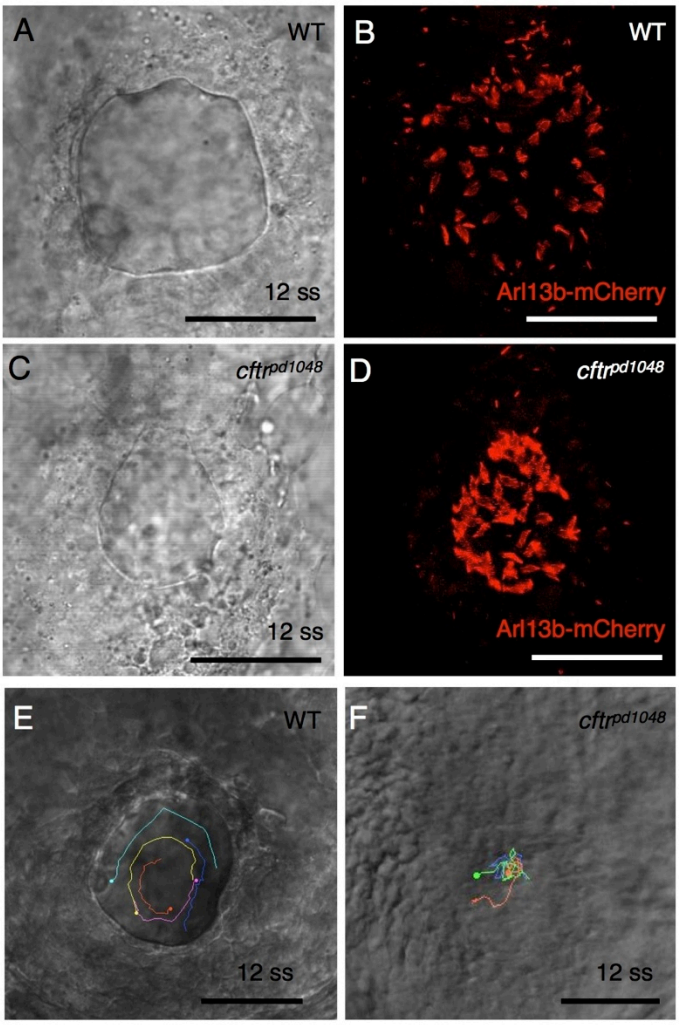

Figure 11: Cilia motility is preserved in *cftr*^{pd1048} mutants.

(A) Brightfield and (B) live confocal imaging of motile cilia marked with Arl13b-mCherry. (C) Brightfield and (D) live confocal image of motile cilia in the hypomorphic *cftr*^{pd1048} KV. (E) Bead tracing in WT and (F) *cftr*^{pd1048} KV. Scale bars: 50 μm.

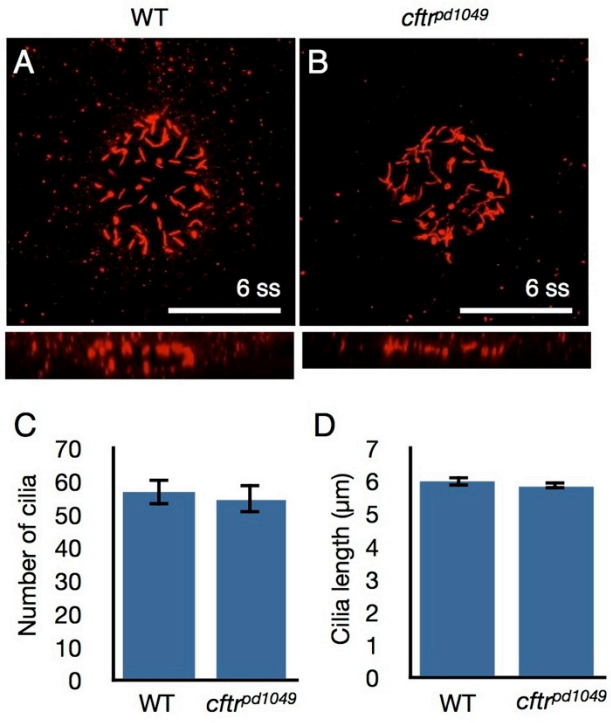

Figure 12: Ciliary development is normal in *cftr*^{pd1049} mutants.

(A,B) Confocal images of WT and mutant KV stained for acetylated tubulin. (C) Quantification of the number of KV cilia. WT KV contained 57.0±4.1 cilia (*n*=5) and mutant KV contained 54.5±4.6 cilia (*n*=8) (*P*=0.69). (D) Quantification of cilia length in WT and mutant KV. WT cilia length was 5.97±0.13 μm (*n*=30) and *cftr*^{pd1049} cilia length was 5.82±0.13 μm (*n*=49) (*p*=0.42). Error bars represent s.e.m. Scale bars: 50 μm.

To examine KV ciliogenesis further in the absence of Cftr function and lumen expansion, we determined the number and average length of cilia in KV. We found no significant difference in either the number or length of cilia between *cftr*^{pd1049} mutants and their WT siblings (Fig. 12A-D), indicating that the volume of the KV lumen does not regulate ciliogenesis.

We next examined the apical-basal polarity of KV in *cftr*^{pd1049} mutants, by investigating the localization of several polarity markers. We characterized membrane polarity by examining the localization of the tight-junction protein ZO-1 and the basolateral marker, Cadherin. In mutant embryos, ZO-1 and Cadherin were properly localized in the absence of lumen expansion (Fig. 13A,B). A higher magnification view of the KV epithelium shows that ZO-1 appears completely apical and Cadherin is absent from the apical membrane in WT and *cftr*^{pd1049} mutant embryos (Fig. 13A'-B'''). We next examined aPKC, a peripheral membrane protein localized to the apical membrane in KV (Amack et al., 2007). In *cftr*^{pd1049} mutants, we observed a plate of aPKC-positive membrane on the center (apical side) of the *sox17:GFP*-positive cluster (Fig. 14A,B). We also generated a transgenic line expressing an integral membrane apical marker, *GFP-podocalyxin* (*GFP-podxl*) (Meder et al., 2005) under the control of a heat shock promoter. We observed that in *cftr*^{pd1049} mutants, at 3 ss, GFP-podxl was also localized in a central plate of apical membrane in KV (Fig. 14C,D). To observe the morphology of the KV lumen in *cftr*^{pd1049} mutants better, we live-imaged the localization of an apical peripheral

membrane protein, RFP-Clic5b, in *Tg(sox17:GFP)*-expressing embryos. Injection of *RFP-clic5b* RNA marked the apical membrane in WT and *cftr*^{pd1049} mutant KV (Fig. 14E,F). Thus, apical-basal polarity in the KV epithelium develops properly in *cftr*^{pd1049} mutants. Altogether, these data indicate that *cftr* is crucial for lumen expansion but not ciliogenesis or apical-basal polarization during KV morphogenesis.

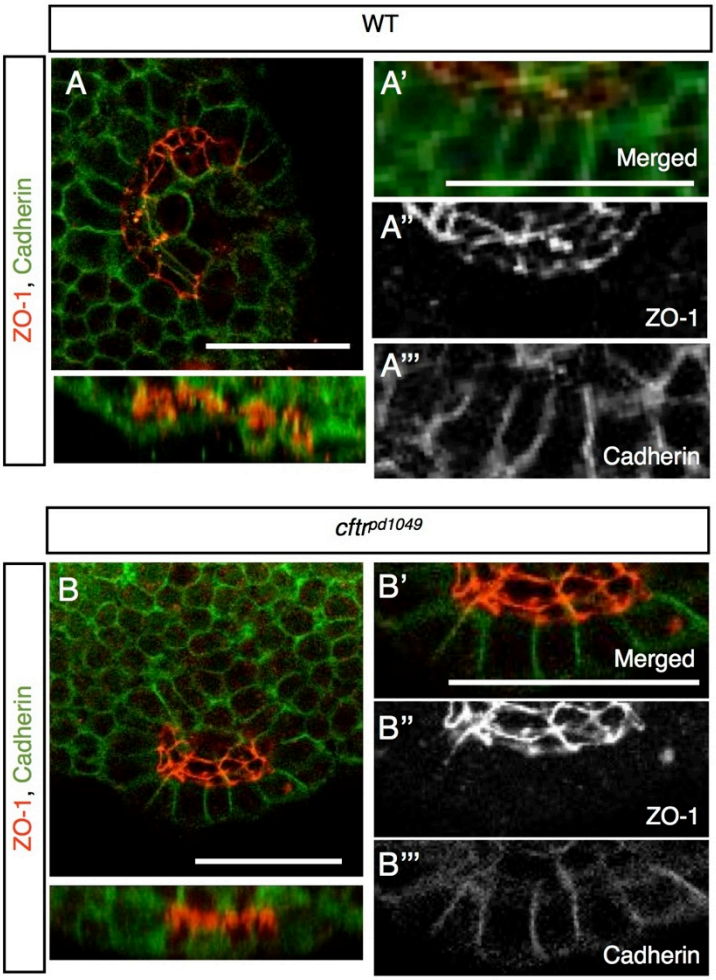

Figure 13: Tight junctions are properly localized in *cftr* mutants.

(A,B) Confocal image and associated orthogonal projections of WT and *cftr*^{pd1049} mutant fish stained for ZO-1 and Cadherin. (A′-A‴,B′-B‴) Magnification of the KV epithelium to show localization of the polarity markers. Scale bars: 50 μm.

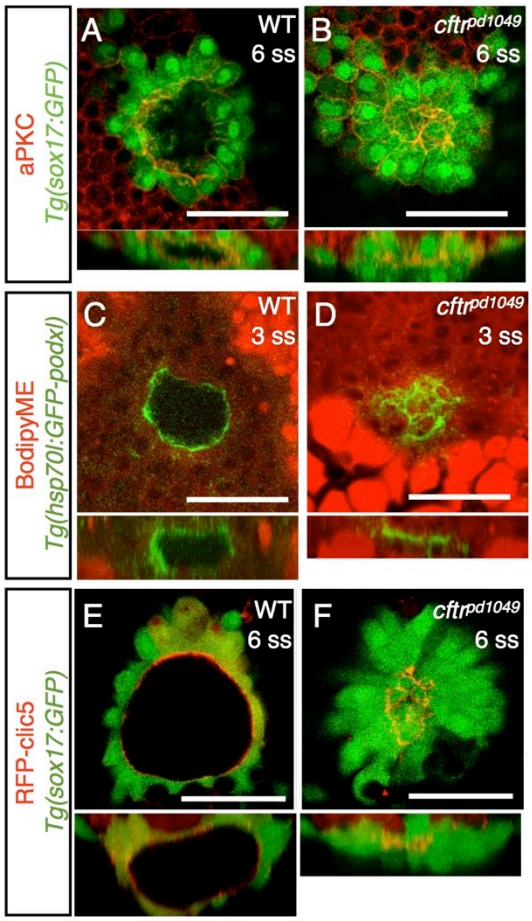

Figure 14: *cftr* mutants retain apical membrane markers.

(A,B) Confocal image and associated orthogonal projections of WT and *cftr*^{pd1049} mutant fish stained for aPKC and expressing *Tg(sox17:GFP)*. (C,D) Confocal image of WT and *cftr*^{pd1049} mutant KV expressing apically localized, GFP-tagged Podocalyxin. (E,F) Live confocal images of WT and *cftr*^{pd1049} mutant fish co-expressing an apical marker, RFP-Clic5b, and *Tg(sox17:GFP)*. Scale bars: 50 μm.

3.5 Expression and localization of cftr in KV

To determine where Cftr functions during KV lumen formation, we examined *cftr* expression using *in situ* hybridization and live imaging. By *in situ* hybridization, *cftr* expression was highly enriched in KV at 3 ss, a stage when the lumen is expanding (Fig. 15A). By 10 ss, the transcript appeared to be downregulated and *cftr* expression was also observed in the chordamesoderm (Fig. 15B).

To better understand the dynamics of Cftr expression and localization in live embryos, we used BAC recombineering to generate a Cftr-GFP fusion protein. Smaller promoter driven constructs often contain insufficient regulatory information to reflect endogenous gene expression. The *cftr* BAC (DKEY-270I2) used contains ~50 kb of genomic DNA upstream and ~100 kb downstream of the coding sequence, and is likely to include critical regulatory information (Fig. 15C). To generate a C-terminal fusion protein, we replaced the stop codon of *cftr* with GFP, separated by a sequence encoding a 20 amino acid spacer to provide some insulation from GFP. C-terminal fusion proteins of human CFTR maintain similar localization and channel activity to untagged CFTR (Benharouga et al., 2003).

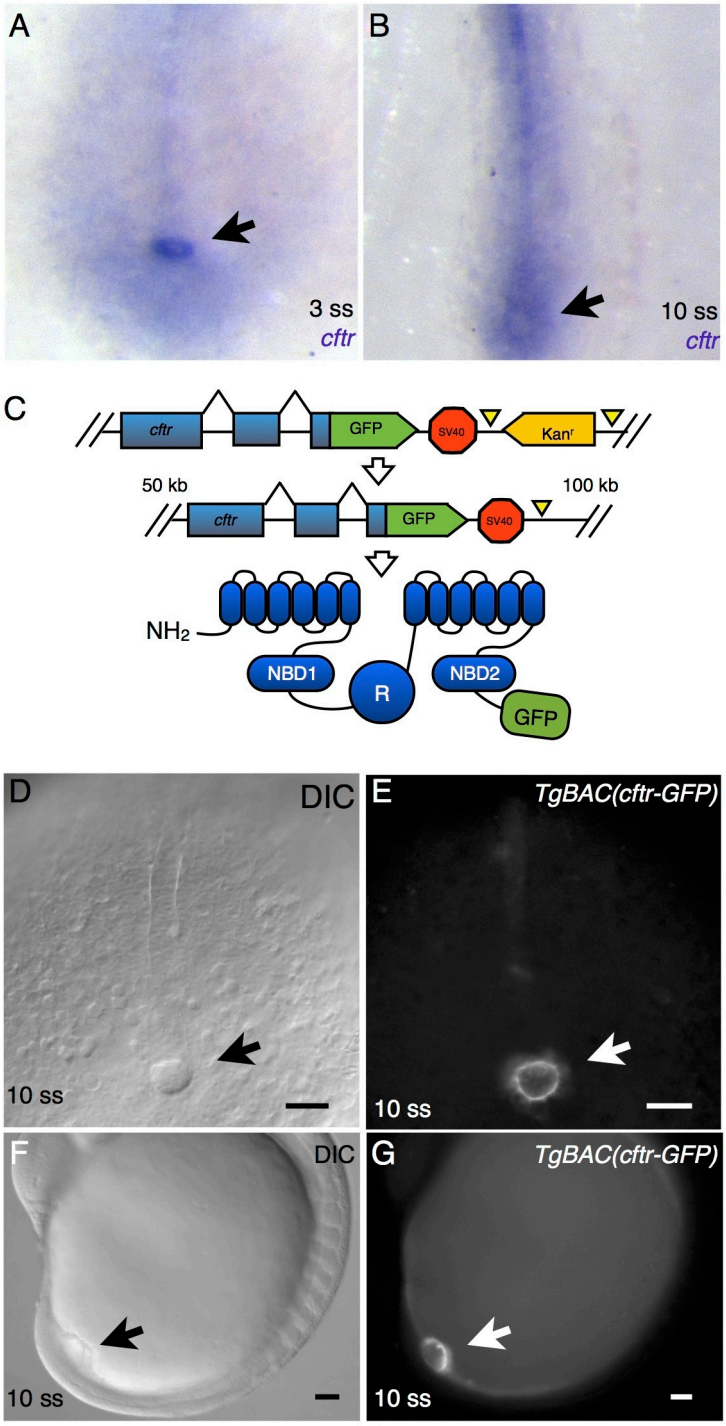

Figure 15: *cftr* is expressed in KV.

Figure 15: *cftr* is expressed in KV. (A) At 3 ss, *in situ* hybridization detects *cftr* expression specifically in KV (arrow). (B) *In situ* hybridization showing *cftr* expression in KV (arrow) and the notochord in 10 ss embryos. (C) Schematic of the BAC recombineering procedure, showing the recombination target and the expected structure of the resulting GFP fusion protein. (D,F) DIC images showing ventral (D) and lateral (F) views of 10 ss embryos expressing *TgBAC(cftr-GFP)*. The arrow marks the characteristic KV structure. (E,G) Whole-mount epifluorescence of the embryos shown in E and G demonstrate specific KV expression of Cftr-GFP (arrows) at 10 ss. Scale bars: 50 μm.

We then repeated the recombineering procedure to generate an RFP fusion and established two transgenic lines, *TgBAC(cftr-GFP)pd1041* and *TgBAC(cftr-RFP)pd1042*, that have identical expression patterns at all stages observed. At 10 ss, by whole-mount epifluorescence, Cftr-GFP was highly restricted to KV (Fig. 15D,F). Next, we performed live, time-lapse imaging of *TgBAC(cftr-RFP)* in conjunction with cytosolic *Tg(sox17:GFP)* and found that Cftr-RFP was localized apically in KV by 1 ss and throughout the initial stages of lumen formation as multiple small lumens coalesced into a single lumen (Fig. 16A,B). By 10 ss, Cftr-RFP remained apically localized as the lumen continued to expand (Fig. 16C,D). At 15 ss, prior to KV disassembly, Cftr-GFP expressed from *TgBAC(cftr-GFP)* remained localized to the apical membrane (Fig. 16E,F). Together, these data indicate that Cftr is expressed and apically localized in KV throughout its morphogenesis.

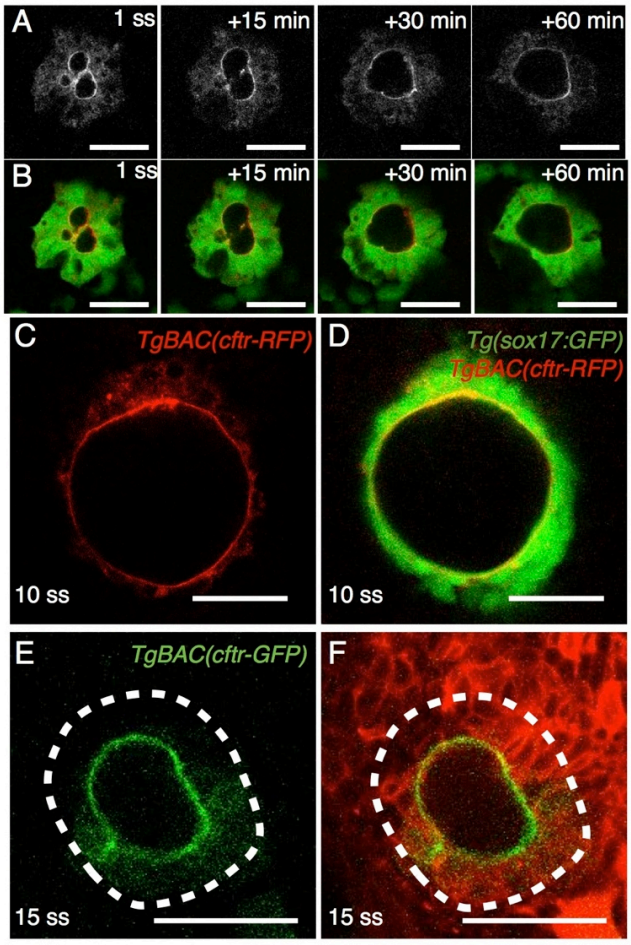

Figure 16: *cftr* is apically localized throughout KV morphogenesis.

(A) Live, time-lapse confocal imaging of Cftr-RFP in *TgBAC(cftr-RFP); Tg(sox17:GFP)* embryos. Cftr-RFP is expressed and apically localized in KV throughout the initial stages of lumen coalescence. (B) Merge of the RFP and GFP channels. (C,D) Live confocal imaging of *TgBAC(cftr-RFP); Tg(sox17:GFP)* embryos at 10 ss shows that Cftr-RFP is localized apically in KV. (D) Merged view of Cftr-RFP and GFP. (E,F) Live confocal imaging of *TgBAC(cftr-GFP)* embryos injected with membrane-RFP RNA shows continued apical localization of Cftr-GFP until 15 ss. The dashed line marks the edge of KV. Scale bars: 50 μm.

3.6 Cftr regulates fluid secretion in KV

Next, we tested whether modulation of Cftr channel activity could regulate the luminal volume of KV. Cftr is strongly activated by phosphorylation of its R-domain by PKA (Berger et al., 1993). To activate Cftr, we treated fish with a cocktail of forskolin and IBMX. These drugs synergistically elevate cAMP levels, rapidly increasing PKA activity, and result in a potent activation of Cftr. PKA activation from 50% epiboly to 12 ss led to a 66% increase in the area of the KV lumen (Fig. 17A-C). We also tested whether the KV lumen could be reduced in size by inhibiting fluid secretion. The ion gradients driving Cftr-dependent fluid secretion are generated by the Na^+/K^+-ATPase. Treatment with low concentrations of ouabain, a potent and specific inhibitor of the Na^+/K^+-ATPase, from 50% epiboly to 10 ss decreased the area of the KV lumen by 33% (Fig. 17D-F). We further investigated the morphology of KV in fish treated with activators or inhibitors of fluid secretion using live confocal imaging and found that, although the lumen size was changed, the structure was otherwise organized properly, including the development of motile cilia (Fig. 17G-I).

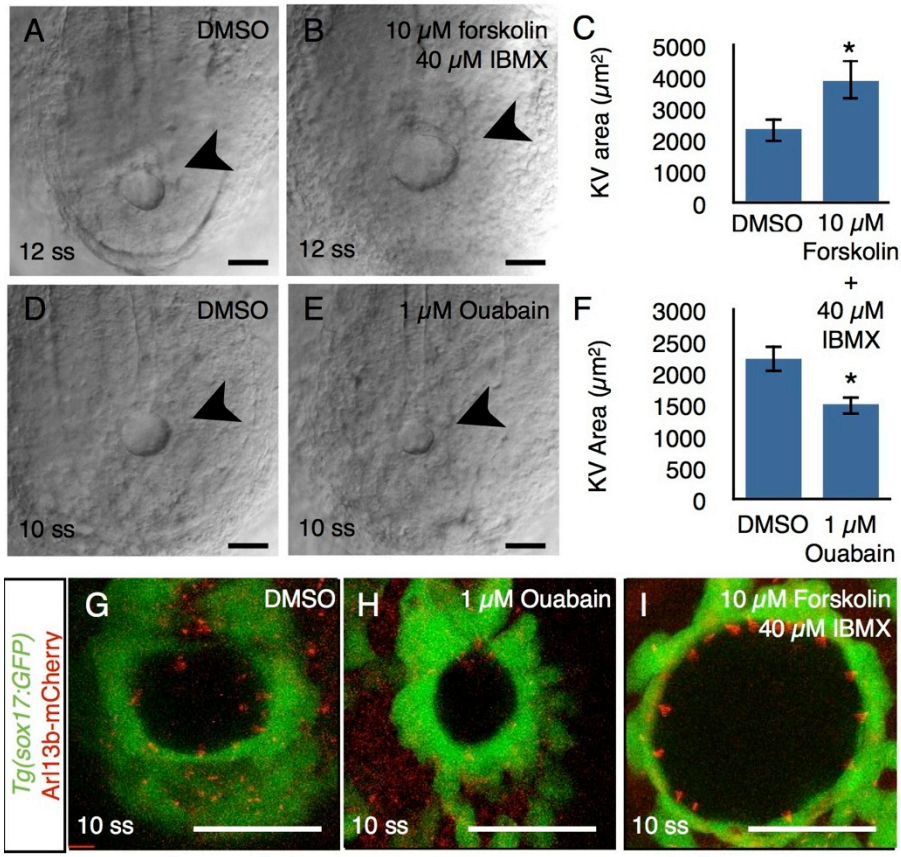

Figure 17: Cftr activity regulates KV lumen size.

(A,B) DIC imaging of KV (arrowheads) in (A) DMSO control and (B) 10 μM forskolin, 40 μM IBMX-treated embryos. (C) The KV area of DMSO and treated fish is quantified. DMSO *n*=15; forskolin + IBMX, *n*=13; **P*<0.01. (D,E) DIC imaging of KV (arrowheads) in (D) DMSO control and (E) 1 μM ouabain-treated embryos at 10 ss. (F) Quantification of KV area in DMSO-and ouabain-treated embryos. DMSO, *n*=10; ouabain, *n*=10; **P*<0.02. (G-I) Live confocal imaging of *Tg(sox17:GFP)*-expressing fish treated with (G) DMSO, (H) ouabain or (I) forskolin and IBMX. Error bars represent s.e.m. Scale bars: 50 μm.

We next tested whether Cftr function is required for fluid secretion in KV by rescuing lumen expansion defects in several ways. We began by injecting WT and *cftr* mutant embryos with RNA encoding a Cftr-GFP fusion. Because we used the KV phenotype to distinguish mutant from WT embryos, we assayed KV rescue by examining the percentage of phenotypically mutant KV in whole clutches. A cross between parents heterozygous for *cftr*^{pd1049} resulted in a failure of KV lumen inflation in 25% of the clutch. Injection of *cftr-GFP* RNA at the one-cell stage reduced the proportion of the clutch that failed to undergo KV lumen expansion to ~10%, indicating that homozygous *cftr*^{pd1049} mutants were partially (~60%) rescued by RNA injection at the one-cell stage (Fig. 18A-D). The failure to completely rescue KV lumen expansion was probably due to mosaicism of the injected RNA (Carmany-Rampey and Moens, 2006). To test whether *cftr* is required in KV, we crossed *cftr*^{pd1049} mutants to the *TgBAC(cftr-GFP)* line, which is almost exclusively expressed in KV during lumen morphogenesis. This transgene was able to completely rescue lumen expansion, whereas non-expressing siblings maintained a 25% failure of KV lumen expansion (n=289) (Fig. 18E). Additionally, all *TgBAC(cftr-GFP)*-expressing fish had normal heart looping, indicating that the transgene was also able to rescue organ laterality. The *TgBAC(cftr-GFP)* rescue indicates that the BAC transgene, which appears to be expressed primarily in KV at this stage, encodes a functional fusion protein capable of rescuing lumen inflation in KV.

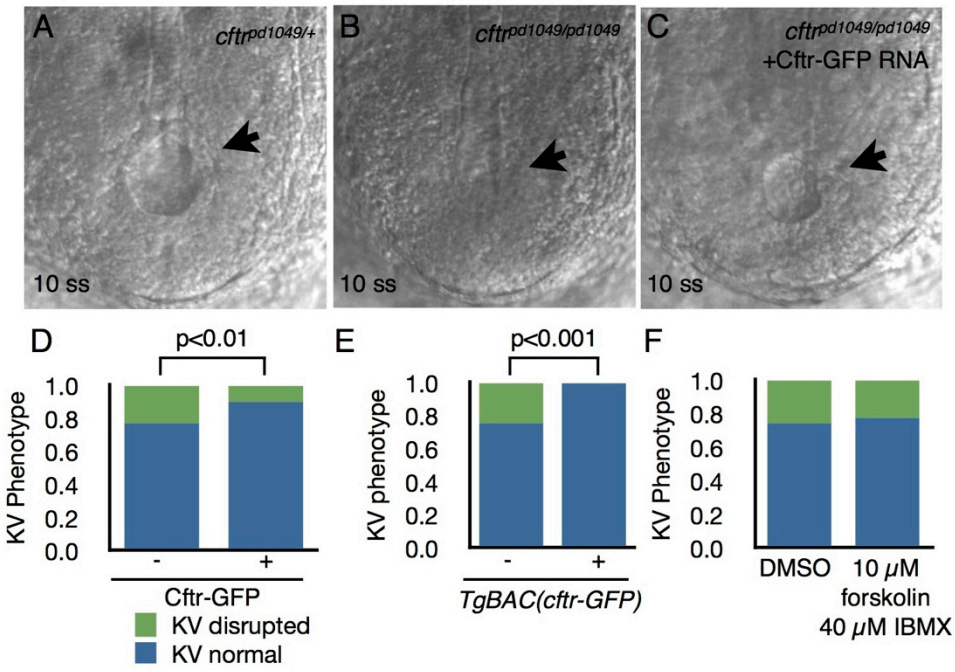

Figure 18: Cftr-GFP expression rescues *cftr* mutant KV lumen expansion.

(A-C) Representative DIC images of KV (arrows) at 10 ss in embryos (A) heterozygous for *cftr*^{pd1049}, (B) homozygous for *cftr*^{pd1049} and (C) in *cftr*^{pd1049} homozygous mutants injected with 150 pg *cftr-GFP* RNA. (D) Quantification of KV phenotype at 10 ss in control and *cftr-GFP*-injected embryos resulting from a cross between *cftr*^{pd1049} heterozygous parents. Control, n=158; Cftr-GFP, n=94; P<0.01. (E) Graph of the KV phenotype at 10 ss in embryos from a *cftr*$^{pd1049/+}$*; TgBAC(cftr-GFP)* × *cftr*$^{pd1049/+}$ cross, compared by whether the embryos were Cftr-GFP positive or negative. Cftr-GFP negative, n=140; Cftr-GFP positive, n=149; P<0.001. (F) Quantification of KV phenotype in embryos treated with DMSO (n=96) or 10 μM forskolin and 40 μM IBMX resulting from a cross between *cftr*^{pd1049} heterozygous parents. n=95; P=0.6374. Scale bars: 50 μm.

We also attempted to phenocopy the *cftr*^{pd1049} KV phenotype by injecting a morpholino against Cftr (Bagnat et al., 2010) into DFCs (Amack and Yost, 2004). We found that DFC-specific injections were unable to prevent KV lumen expansion due to mosaic uptake of the morpholino (Amack and Yost, 2004) (Fig. 19A-F). This is not surprising given that fluid secretion is expected to function non-cell-autonomously.

Next, we determined whether forskolin and IBMX were acting through Cftr in KV by treating WT and *cftr*^{pd1049} mutants with these activators of fluid secretion. Forskolin and IBMX treatment failed to rescue KV lumen expansion in *cftr*^{pd1049} mutants, indicating that cAMP-stimulated fluid secretion acts through Cftr (Fig. 18F). Taken together, these studies demonstrate that in zebrafish, Cftr functions in KV to drive fluid secretion crucial for lumen expansion and morphogenesis of KV and LR patterning of the embryo.

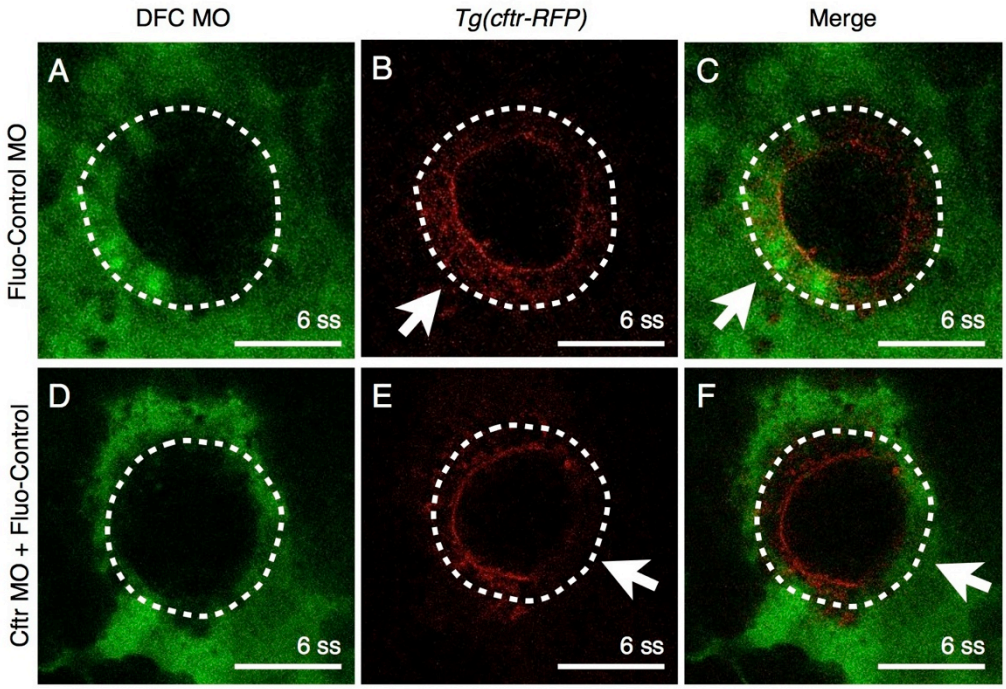

Figure 19: DFC-targeted morpholino injection is mosaically incorporated into KV.

(A) A fluorescently tagged control morpholino incorporated mosaically in the zebrafish KV epithelium after DFC injection. (B) Expression of Cftr-RFP in the KV epithelium. (C) Fluorescent merge. (D) Mosaic incorporation of a fluorescent control morpholino co-injected with a morpholino against Cftr. (E) Cftr-RFP expression is reduced in cells that have incorporated the morpholinos. (F) Fluorescent merge of the fluorescent morpholino and Cftr-RFP channels. Scale bars: 50 μm.

3.7 Discussion

Here, we describe a new role for Cftr in the regulation of fluid secretion necessary for KV morphogenesis and function. Live imaging of KV lumen morphogenesis showed several small lumens that coalesce into a single, central lumen. In the absence of Cftr activity, the KV lumen fails to inflate, indicating that fluid acts as a force driving lumen expansion and might also promote lumen coalescence. The zebrafish gut undergoes a similar process of *de novo* lumen formation, beginning with inflation of multiple small lumens, followed by their coalescence into one (Bagnat et al., 2007) and a similar role in *de novo* lumen formation and expansion has been shown for apical membrane or secreted mucins during tubulogenesis in the vertebrate vasculature (Strilić et al., 2010), the ommatidium (Husain et al., 2006), and hindgut (Syed et al., 2012) in *Drosophila*. The role of luminal content as a driving force during tube formation is most clearly exemplified by the *Drosophila* tracheal system, which becomes filled with a solid chitin matrix, then liquid and finally gas during its development (Tsarouhas et al., 2007). Altogether, these studies signify that the filling of the lumen is crucial for tubulogenesis in metazoans.

Although complete loss of Cftr function abrogated inflation of the KV lumen, it did not affect the specification, migration or the clustering of DFCs. Ciliogenesis has previously been shown to proceed coordinately with KV lumen expansion, raising the possibility of crosstalk between luminal volume and cilia length (Oteíza et al., 2010).

Here, we found that in the absence of fluid secretion into the KV lumen, cilia morphogenesis and motility were unaffected, indicating that fluid secretion and flow are specified largely independently.

Although KV cilia length and number were unchanged in *cftr*^{pd1049} mutants, the absence of a KV lumen resulted in bilateral *spaw* expression. Previous research has demonstrated that bilateral *spaw* expression can be caused by defects in the midline barrier, which functions to prevent the diffusion of Spaw to the right side of the embryo (Long et al., 2003). In *cftr*^{pd1049} mutants, proper midline expression of *ntl* and *lefty1* indicate that midline integrity is not perturbed. Moreover, mutations that affect midline integrity result in heterotaxia, a phenotype rarely observed in *cftr*^{pd1049} mutants. This difference in organ *situs* in *cftr*^{pd1049} mutants can be explained by the fact that a majority of embryos with bilateral *spaw* expression did not show equivalent left and right *spaw*, but rather that expression on one side was more pronounced and extended anteriorly. Previous research in *Xenopus* has demonstrated that in embryos with bilateral *Nodal*, in which one side displays dominant expression, organ position is specified concordantly (Ohi and Wright, 2007). The remaining pool of *cftr*^{pd1049} embryos with equivalent left and right-sided *spaw* expression might have been left-biased in a way *in situ* hybridization was not sensitive enough to detect. Similar patterns of bilateral *spaw* expression have also been observed upon loss of function of the Spaw antagonist Charon (Dand5 – Zebrafish Information Network), which also has no associated midline defect

(Hashimoto et al., 2004). Although we are unable to completely rule out a contribution from the midline, our data strongly suggest that *cftr* is required specifically in KV for proper specification of organ laterality. However, the fact that we observe defects in organ laterality in only ~30% of *cftr*^{pd1049} mutants, instead of a complete randomization of laterality (50% penetrance), suggests that fluid flow in KV is not the only source of asymmetric information in the early zebrafish embryo. Consistent with this interpretation, previous studies in chicken, frog and zebrafish suggested that KV might function to amplify earlier asymmetries, such as differences in H^+/K^+-ATPase activity and thus bias organ laterality in the absence of KV function (Kawakami et al., 2005; Levin et al., 2002).

Although our results demonstrate that Cftr plays an important role in the development of LR asymmetry in the zebrafish, it should be noted that organ laterality defects have not been observed in cystic fibrosis (CF) patients. This is probably due to morphological differences between the teleost KV and the laterality organs in other vertebrates. Whereas KV in zebrafish is an enclosed structure, the node in mammals and the gastrocoel roof plate in *Xenopus* are indentations, where fluid may freely diffuse into the organ (Blum et al., 2007; Shook et al., 2004; Sulik et al., 1994). In fact, passing artificially generated fluid flow over the mouse node is sufficient to reverse organ laterality (Nonaka et al., 2002). It is also unknown whether *cftr* orthologs are expressed in the mouse node or frog gastrocoel roof plate. Further investigation will be required to

determine whether embryonic fluid secretion is specifically required in the laterality organs of other vertebrates or if they utilize fluid secreted from other sources.

In CF patients, reduced fluid secretion leads to mucus buildup in the lungs, liver and pancreas, disrupting their function (Durie and Forstner, 1989; Gaskin et al., 1988; Matsui et al., 1998). The recent development of new animal models of CF will greatly improve understanding of the pathophysiology of CF (Rogers et al., 2008; Sun et al., 2010). Clinical data from patients and new animal models, such as the pig and the ferret, suggest that some defects associated with CF might arise during development (Imrie et al., 1979; Olivier et al., 2012; Sturgess, 1984), a stage that remains difficult to access in these models with limited genetic tools. A developmentally accessible model will provide valuable insights into CFTR regulation and CF pathophysiology in various organs. The development of zebrafish *cftr* mutants provides an *in vivo* model in which to study human CFTR and assay drugs designed to correct the ΔF508-CFTR mutation and other pathologically relevant mutations. Future work may also shed light into the role Cftr plays in the development of the pancreas and other organs.

In summary, this study identifies a new role for Cftr in the regulation of fluid secretion into KV and for the development of LR asymmetry. It also highlights the importance of fluid secretion in lumen expansion during vertebrate morphogenesis. The relative simplicity and experimental accessibility of KV compared with other organs

undergoing *de novo* lumen formation make KV an attractive model for studying fundamental mechanisms of lumen formation in vertebrates.

4. Cftr is required for maintenance of the zebrafish exocrine pancreas

4.1 Introduction

Cystic fibrosis is a hereditary disease caused by defects in the function of a chloride channel, CFTR. CF patients have defects in the function of several organs including the pancreas, lungs, liver, and intestine (Ruzal-Shapiro, 1998). In these organs, lack of fluid secretion leads to mucosal compaction and degradation of organ function. In the pancreas, CFTR function is necessary to hydrate the ductal mucus. Loss of fluid secretion leads to blockage in the pancreatic ducts and is thought to subsequently cause destruction of the exocrine tissue (Wilschanski and Novak, 2013). In the lung, loss of fluid secretion leads to compaction of the airway surface layer, preventing normal ciliary clearance of the airway mucus (Knowles et al., 1997). Defects in lung clearance allows colonization by opportunistic pathogens which drives inflammation and progressive degeneration of lung function (Callaghan and McClean, 2012).

As CF patients age, additional symptoms have become apparent. Over time, many CF patients develop cystic fibrosis related diabetes (CFRD). CFRD patients have fewer β cells and altered responses to changes in blood glucose (Mackie et al., 2003). In the ferret model for CF, changes in the regulation of blood glucose can be observed prior to the exocrine destruction, indicating that the defects in glucose regulation are not a secondary consequence of pancreatic destruction (Olivier et al., 2012). It remains unclear

whether disruption of glucose regulation in CF is due to defects in β cell specification or function.

The defects observed in the infant CF pancreas are reflected in other mammalian models for the disease. In the pig pancreas, severe exocrine destruction is observed at birth (Rogers et al., 2008). In the ferret, exocrine destruction occurs early in neonatal life (Olivier et al., 2012; Sun et al., 2010). Blockage of the pancreatic ducts with dried-out mucus, which restricts transport of digestive enzymes to the intestine, has been proposed to drive the destruction of the exocrine pancreas; however, it remains unclear whether developmental abnormalities underlie CF of the pancreas. The ferret and pig are not developmentally accessible organisms and CFTR mutant mice do not develop severe pancreatic disease observed in other mammals (O'Neal et al., 1993). To determine whether CFTR is required during pancreatic organogenesis, it will be necessary to generate a developmentally accessible model for CF.

Fluid secretion is controlled by osmotic gradients established through coordinated regulation of ion channel activity (Barrett and Keely, 2000). CFTR, a chloride channel, is an integral regulator of vertebrate fluid secretion. Classically, secretion of chloride into the lumen is powered by ATP hydrolysis of the Na^+/K^+-ATPase. In the intestine, the Na^+/K^+-ATPase drives sodium export and potassium import. The external sodium gradient powers import of chloride ions through NKCC1,

which can be apically secreted through CFTR. Increased chloride in the lumen draws sodium to establish an osmotic gradient to draw water into the lumen.

To investigate developmental functions for Cftr-dependent fluid secretion, we examined mutant and transgenic lines at several stages. To identify whether loss of Cftr activity leads to symptoms similar to CF in the zebrafish, we examined the pancreas in adult fish, finding substantial destruction of the exocrine pancreas. We were next interested to determine whether developmental defects underlie the destruction observed in the exocrine pancreas. We found no significant differences between the morphology of the *cftr* mutant ducts or exocrine pancreatic tissue compared to WT siblings in larval zebrafish. We also found that β cells are specified normally and β cell regeneration occurs normally in *cftr* mutant larvae. Our results indicate that the destruction in the exocrine pancreas is likely due to ductal blockage rather than a defect in the early stages of pancreatic morphogenesis.

4.2 cftr is expressed in the adult pancreas

To determine whether *cftr* is similarly required in the zebrafish and mammalian pancreas, we investigated *cftr* expression and function in adult zebrafish. In mammals, CFTR is expressed specifically within the pancreatic ducts, where it regulates fluid secretion necessary for mucosal hydration and delivery of digestive enzymes (Hyde et al., 1997; Marino et al., 1991; Rogers et al., 2008). We sectioned adult pancreata expressing *TgBAC(cftr-GFP)* to observe *cftr* expression and localization. We found that

cftr is expressed in the adult pancreas and co-localized with phalloidin (Fig. 20A-C), a marker of filamentous actin. The expression pattern we observed for Cftr-GFP is very similar to the expression of CFTR in the ducts of the human pancreas and other mammalian models (Hyde et al., 1997; Marino et al., 1991; Rogers et al., 2008). Additionally, filamentous actin is associated with the apical surface of the pancreatic duct epithelium (Fallon et al., 1995; Kesavan et al., 2009). The co-localization observed between Cftr-GFP and phalloidin in the zebrafish pancreas passes between nuclei (Fig. 20A′-C′) indicating that Cftr-GFP likely marks the luminal surface of the pancreatic ducts in the zebrafish.

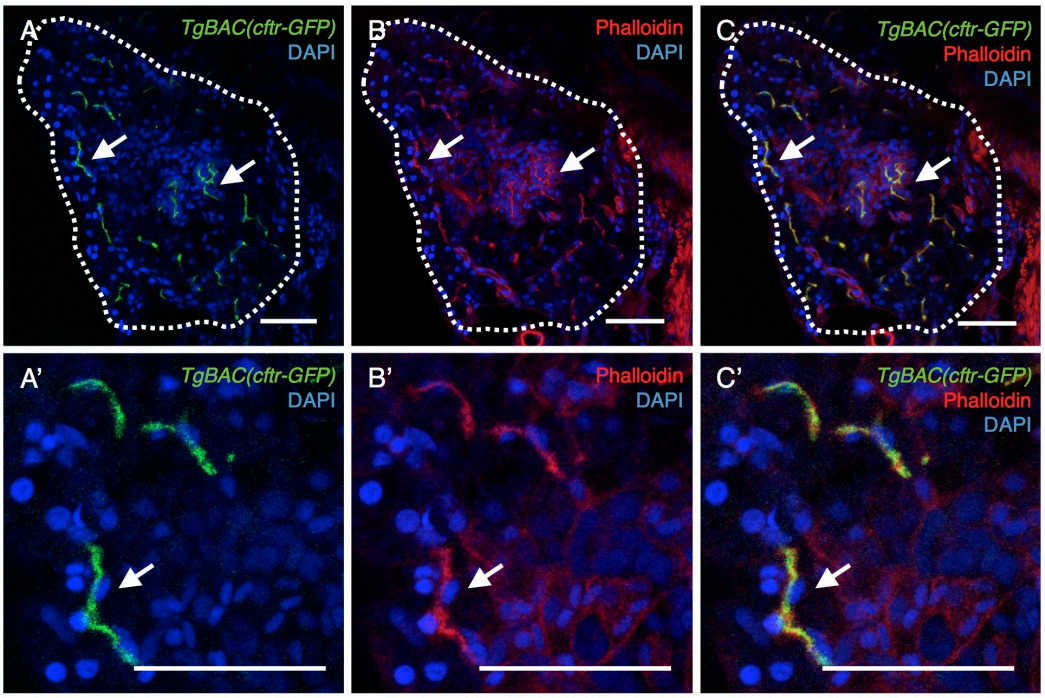

Figure 20: Expression of *cftr* in the adult zebrafish pancreas.

(A) Expression of *TgBAC(cftr-GFP)* in a transverse section of the adult zebrafish pancreas. (B) Phalloidin stains filamentous actin in the adult pancreas. (C) Fluorescent merge of *TgBAC(cftr-GFP)* and phalloidin expression showing co-localization of phalloidin and Cftr-GFP. (A′-C′) Higher magnification view of the above images to highlight the co-localization of Cftr-GFP and phalloidin. Cftr-GFP and phalloidin staining pass between nuclei, suggestive of luminal localization (arrows). Scale bars: 50 μm.

4.3 Maintenance of the adult pancreas requires cftr

To test whether loss of *cftr* function leads to pancreatic phenotypes similar to CF in the zebrafish, we examined the morphology of adult *cftr*^{pd1049} mutants. We first examined adult *Tg(ela:GFP, lfabp:dsRed)*; *Tg(ins:dsRed)* (2CLIP) expressing fish, a transgenic line which marks the exocrine pancreas in green, the liver in red, and the β cells in the pancreatic islets in red. In 3 month old WT zebrafish, the pancreas, marked by GFP expression, extends along the length of the liver and looped intestine (Fig. 21A,A'). Conversely, in age-matched *cftr*^{pd1049} mutant siblings, GFP expression was largely absent, detectable only in small patches where the exocrine pancreas would be expected, suggesting that the pancreas in *cftr*^{pd1049} mutant adults loses substantial exocrine tissue (Fig. 21B,B'). The visceral organs collected from *cftr* mutants are noticeably smaller due to growth restriction, likely due in part to loss of exocrine pancreatic function.

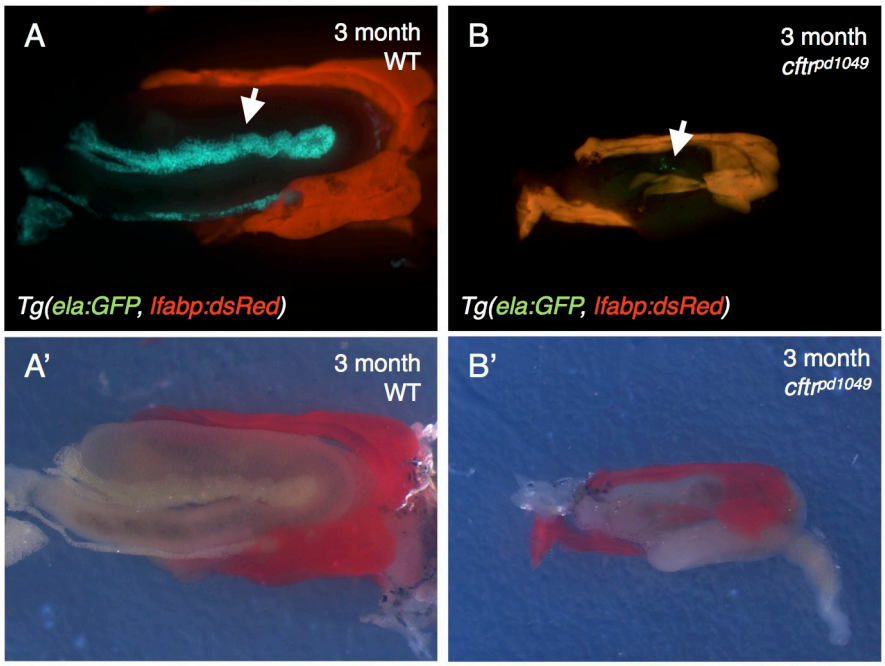

Figure 21: Exocrine pancreatic morphology in adult *cftr* mutants.

(A,B) Epifluorescent images of adult whole-mount internal organs from (A) WT and (B) *cftr*^{pd1049} zebrafish pancreas expressing *ela:GFP*. Arrows indicate *ela:GFP* expression in the exocrine pancreas. (A',B') Brightfield image of the same (A') WT and (B') *cftr*^{pd1049} mutant samples.

Pancreatic destruction is common among CF patients and frequently leads to PI and defects in growth rate (Imrie et al., 1979; Sproul and Huang, 1964; Sturgess, 1984). Prior to oral enzyme treatments, loss of pancreatic function was a primary cause of mortality in CF patients (Ruzal-Shapiro, 1998). To investigate the morphology of the *cftr*^{pd1049} mutant pancreas in greater detail, we sectioned 2CLIP; *cftr*^{pd1049} mutant pancreata in 3 month old adult zebrafish. In WT zebrafish at this age, *ela:GFP* is broadly expressed throughout the pancreas, where it marks exocrine tissue and is excluded from the endocrine and ductal tissue (Fig. 22A). Embedded within the exocrine tissue are pancreatic islets expressing *ins:dsRed* (Fig. 22A). In contrast to the broad GFP expression in WT pancreata, *cftr*^{pd1049} mutant pancreata contain sporadic *ela:GFP* expression surrounding a core of actin rich unlabeled tissue (Fig. 22B). The islets appear intact and largely spared from the morphological changes that have occurred in the exocrine tissue. The *cftr*^{pd1049} mutant zebrafish pancreas has substantially less tissue expressing an exocrine marker. Additionally, the phalloidin staining in unmarked tissue suggests the exocrine tissue may be replaced by fibrotic tissue, indicating that the *cftr* mutant zebrafish may undergo destruction of exocrine pancreatic tissue, consistent with CF in humans and other mammalian models (Imrie et al., 1979; Rogers et al., 2008; Sturgess, 1984; Sun et al., 2010).

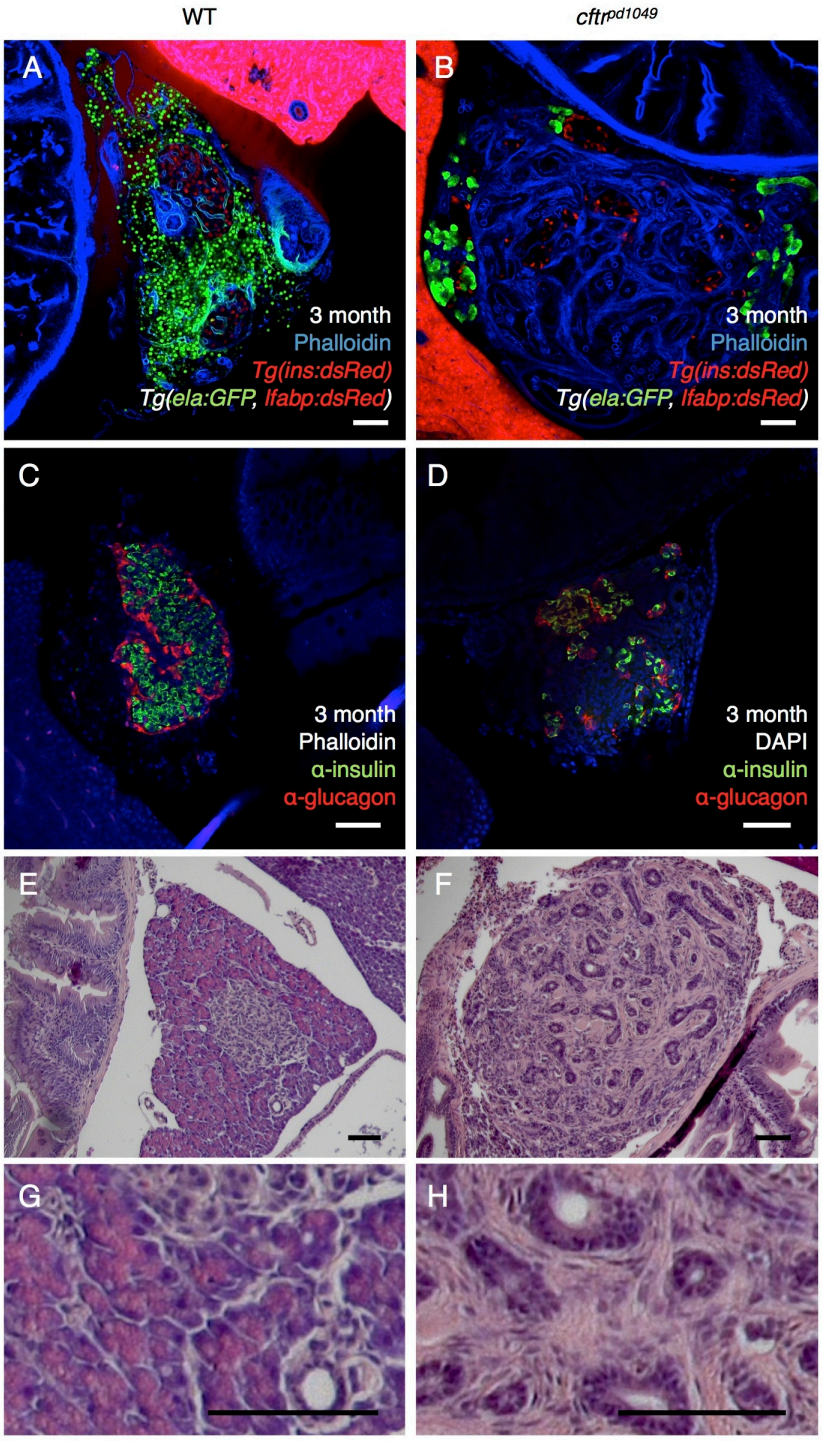

Figure 22: Adult *cftr* mutants lose exocrine pancreatic tissue.

Figure 22: Adult *cftr* mutants lose exocrine pancreatic tissue. (A,B) *Tg(ela:GFP, lfabp:dsRed)* expresses in the exocrine tissue of (A) WT and (B) *cftr*^{pd1049} mutant adult pancreas sections at 3 months old. (C,D) Sections of 3 month old WT and *cftr*^{pd1049} pancreata stained for insulin (green) and glucagon (red). (E,F) Hematoxylin and eosin (H&E) stained sections of WT and *cftr*^{pd1049} adult pancreata. (G,H) Higher magnification view of WT and *cftr*^{pd1049} H&E stained pancreata. Scale bars: 50 μm.

To determine the morphology and composition of the adult pancreatic islets, we examined expression of key markers of endocrine tissue, insulin and glucagon. In WT zebrafish at 3 months old, islets are interspersed throughout the pancreas and contain a core of insulin-producing β cells surrounded by glucagon-producing α cells (Fig. 22C). In *cftr*^{pd1049} mutant siblings, the endocrine cells are organized into a larger number of smaller islets although the organization of these islets is similar to the larger WT islets (Fig. 22D). An important consideration is that the age-matched *cftr*^{pd1049} mutants are typically smaller than their WT siblings, so while differences in islet size are likely to be observed, the increased number of islets in *cftr*^{pd1049} mutants is unexpected from differences in size alone. Importantly, this morphology is similar to observations in the pig and ferret models of cystic fibrosis (Olivier et al., 2012; Rogers et al., 2008; Sun et al., 2010). The mechanisms that restrict preferential destruction of the exocrine pancreas while sparing other cell-types within the pancreas remain unclear, although it is typical of CF in the pancreas of humans and mammalian CF models.

To further examine the morphology of the *cftr*^{pd1049} mutant pancreas, we performed basic histology on adult zebrafish pancreatic sections. In contrast to the exocrine and endocrine tissue observed in WT adult pancreata (Fig. 22E,G), we observed that the exocrine tissue in the mutant pancreas was predominantly replaced by a core of fibrotic tissue (Fig. 22F,H). Importantly, the ducts of the *cftr*^{pd1049} mutant pancreata are expanded in comparison to their WT siblings, suggestive of mucosal blockage (Fig.

22G,H). Lacking *cftr* function, the adult zebrafish pancreas undergoes substantial destruction similar to the phenotypes observed in CF. Together, these results suggest that the adult *cftr*^{pd1049} mutant zebrafish models pancreatic disease observed in CF.

We next investigated whether differences in pancreatic composition are observed in earlier stages in *cftr*^{pd1049} mutant zebrafish. By 3 wpf, the *cftr*^{pd1049} mutant zebrafish are significantly smaller than their WT siblings (Fig. 23A). To determine whether there is less exocrine pancreatic tissue in *cftr* mutants at this stage, we examined pancreata from 3 wpf *cftr*^{pd1049} mutants. By this stage, we observe loss of the exocrine marker carboxypeptidase in the center of the pancreas (Fig. 23B,C). A small number of carboxypeptidase expressing cells surround a core of unmarked tissue in the *cftr*^{pd1049} mutant pancreas at 3 wpf. As observed in later stages, the islets at 3 wpf appear to be spared from the surrounding exocrine destruction.

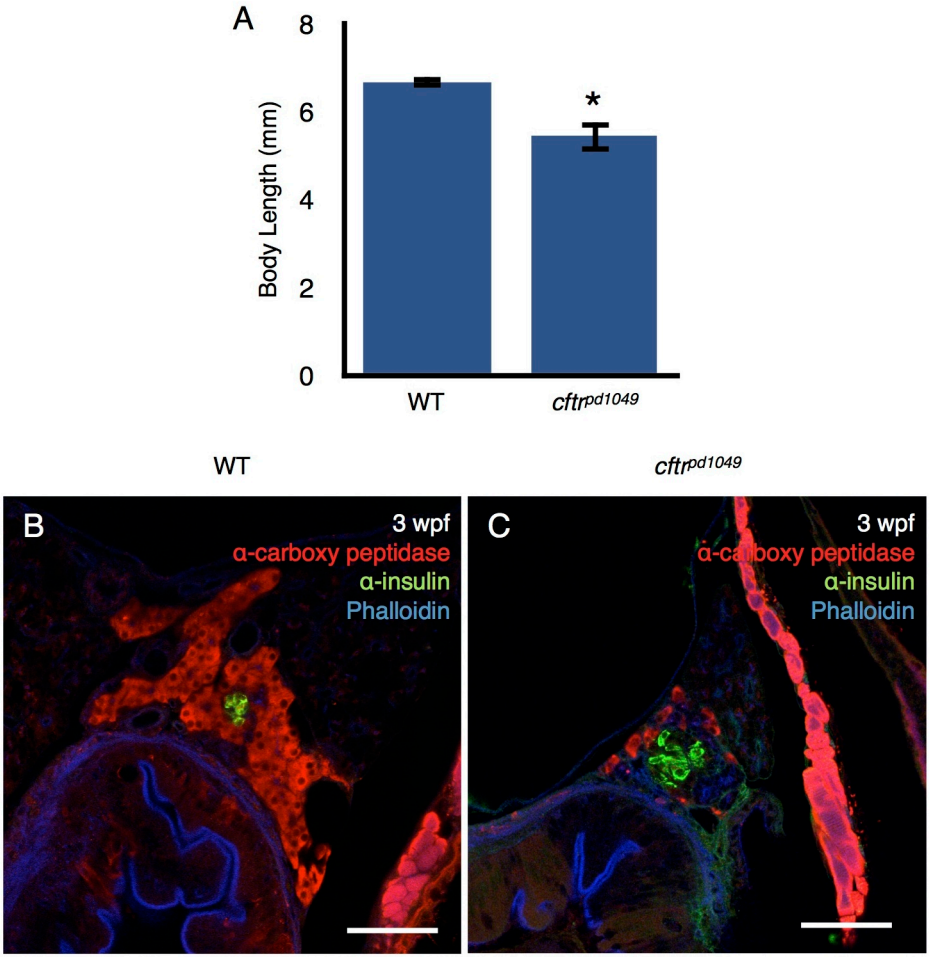

Figure 23: Exocrine pancreatic tissue is reduced in 3 wpf *cftr* mutant zebrafish.

(A) Quantification of body length of 3 wpf zebrafish. *P<0.002 (B,C) 3 wpf transverse section of WT and *cftr*^{pd1049} mutant pancreas stained with anti-carboxypeptidase (red) to mark exocrine cells and anti-insulin (green) to mark β cells of the islet. Error bars represent s.e.m. Scale bars: 50 μm.

Over time, many CF patients develop CFRD due to loss and dysfunction of β cells. CFRD is characterized by increased fasting blood glucose and abnormal responses to glucose tolerance tests. We were interested to determine whether the adult zebrafish develop CFRD-like symptoms. We tested fasting blood glucose in *cftr*^{pd1049} mutant adults, finding no significant difference between fasting glucose levels in *cftr*^{pd1049} mutants or their WT siblings (Fig. 24). This result suggests that blood glucose is properly maintained in the *cftr*^{pd1049} mutants. Alternatively, we may not observe defects in glucose regulation because fish that develop defects in endocrine pancreatic function may be preferentially lost as the fish age. An important indicator of CFRD in humans is the glucose tolerance test. We were unable to test glucose tolerance in the zebrafish due to the small volume of adult zebrafish blood, which precludes collection of multiple blood samples from a single fish.

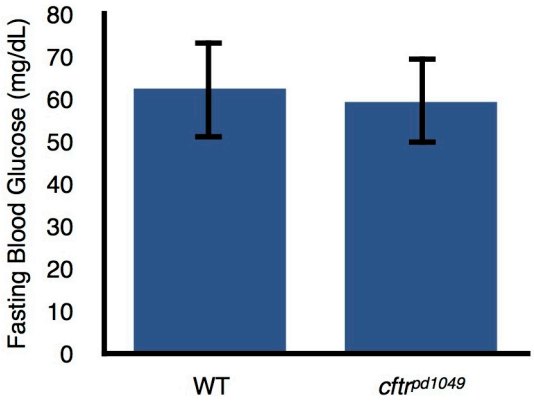

Figure 24: Blood glucose levels in *cftr* mutant zebrafish.

Quantification of fasting blood glucose levels in adult WT and *cftr*^{pd1049} zebrafish. Error bars represent s.e.m.

We were also interested in whether *cftr*^{pd1049} mutant zebrafish have other symptoms characteristic of CF. Male CF patients are frequently infertile due to blockage and degeneration of the vas deferens. In several large zebrafish clutches produced by natural mating of homozygous *cftr*^{pd1049} males, we never observed fertilization of any oocytes indicating that the *cftr*^{pd1049} mutant male zebrafish have fertility defects. Future work will be important to determine whether the fish develops absence of the vas deferens similar to human CF patients. The *cftr*^{pd1049} mutant zebrafish develops several phenotypes characteristic of CF and establishes the zebrafish as a model of pancreatic disease in CF.

4.3 cftr is expressed in the larval pancreatic duct

Pancreatic degeneration in the adult pancreas has been well documented and extensively studied in CF patients and mammalian models. Analysis of the newborn CF ferret suggests that inflammation and degeneration of the exocrine pancreas occurs rapidly after birth (Olivier et al., 2012). In newborn CF pigs, the pancreas is severely degenerated at birth (Rogers et al., 2008). It remains unclear whether developmental defects lead to the pathophysiology characteristic of the CF pancreas or whether progressive rounds of inflammation due to ductal blockage destroy the exocrine pancreas. We sought to address whether defects arise early in pancreatic development.

We examined developmental expression of *cftr* using whole-mount *in situ* hybridization and live imaging of *cftr* reporters. By *in situ* hybridization, we detected *cftr*

expression at 3 dpf in a thin stripe along the right side of the larvae, consistent with pancreatic localization (Fig. 25A,C). By 5 dpf, *in situ* hybridization detects *cftr* expression in a branched network along the right side of the larvae, likely marking the fine details of the pancreatic duct at this stage (Fig. 25B,D). These expression patterns are consistent with ductal localization, but lack the resolution to make a definitive conclusion.

To examine *cftr* expression in greater detail, we imaged expression and localization using BAC transgenic lines expressing fluorescently tagged Cftr. To confirm that the *cftr* transgenes are expressed within the pancreas at this stage, we imaged sections of zebrafish expressing fluorescently labeled Cftr in conjunction with well-characterized transgenic or immunofluorescent markers of the pancreas. We first examined 3 dpf *TgBAC(cftr-GFP)*; *TgBAC(ptf1a:Gal4)*; *Tg(UAS:mCherry)* expressing larvae. The *ptf1a:Gal4* expression is localized to the exocrine pancreas and excludes the pancreatic duct. At this stage, Cftr-GFP expression is observed in the pancreatic duct, distinct from the surrounding exocrine *ptf1a* expression. The separation between Cftr-GFP and *ptf1a* expression suggests that Cftr-GFP may be apically localized in the ductal epithelium (Fig. 25E). At 5 dpf, we analyzed *TgBAC(cftr-GFP)* expression in sections stained with ZN-5, a marker that labels the total pancreas. Again, we observe Cftr-GFP expressed in the pancreatic duct and excluded from other cells within the pancreas (Fig. 25F). Cftr is expressed within the pancreatic ducts throughout their morphogenesis.

To observe expression of *cftr* throughout the pancreatic ducts, we performed live imaging of 5 dpf zebrafish expressing transgenic markers of the pancreas. We examined 5 dpf larvae expressing *TgBAC(cftr-GFP)* and *Tg(ins:dsRed)* which marks the pancreatic duct as it branches around the principal islet and extends toward the tail of the pancreas (Fig. 25G). We next observed the pancreatic ductal network in live fish expressing *TgBAC(cftr-RFP)*; *Tg(ela:GFP, lfabp:dsRed)*. In these larvae, Cftr-RFP can clearly be seen labeling the pancreatic duct embedded within the exocrine pancreas, labeled by *ela:GFP* expression (Fig. 25H). Cftr is expressed within the pancreatic ducts throughout their morphogenesis, indicating that *cftr* may play a key role in the development of the pancreatic ducts.

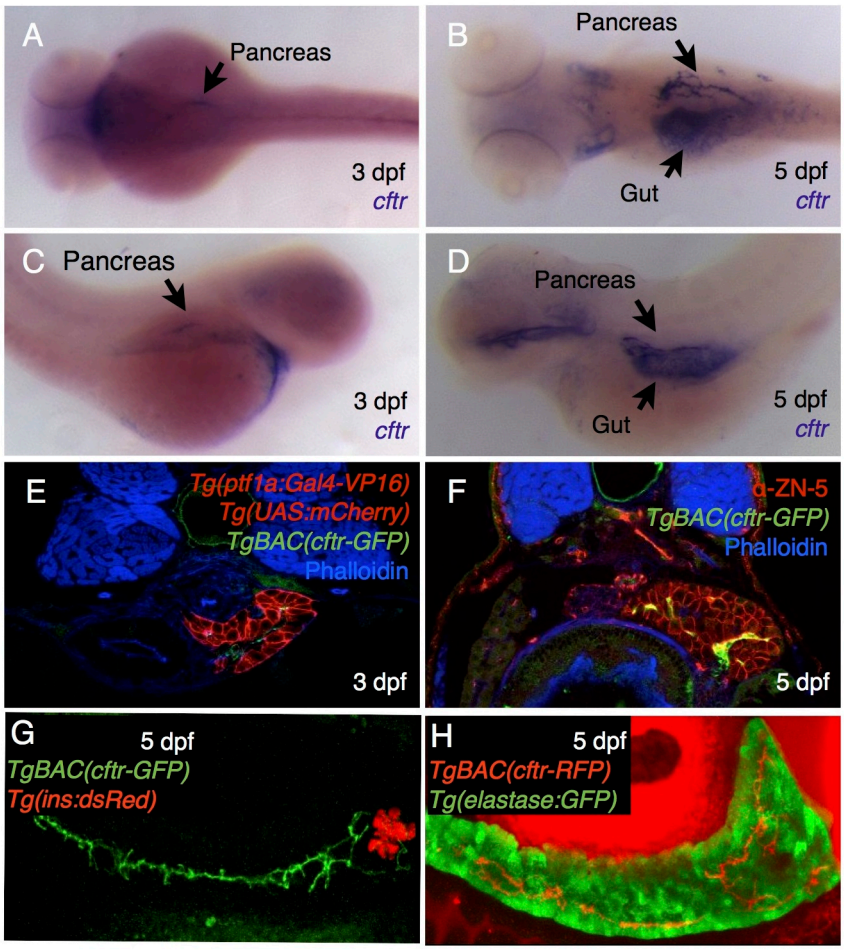

Figure 25: *cftr* is expressed in the larval pancreatic duct.

(A,B) Dorsal view of *in situ* hybridization for *cftr* at (A) 3 dpf and (B) 5 dpf. (C,D) Lateral view of *cftr* expression detected by *in situ* hybridization at (C) 3 dpf and (D) 5 dpf. (E) Transverse section of a 3 dpf zebrafish expressing Cftr-GFP in the pancreatic duct. (F) Transverse section of a 5 dpf zebrafish expressing Cftr-GFP in the pancreatic duct. (G,H) Live confocal images of (G) *TgBAC(cftr-GFP)* and (H) *TgBAC(cftr-RFP)* expression in 5 dpf pancreatic ducts.

To examine *cftr* function during ductal morphogenesis, we required a clear marker of the duct. The zebrafish lacks a high quality, specific marker of the pancreatic duct epithelium. The expression of *cftr* makes it an ideal marker of the pancreatic duct; however, the BAC transgenic lines generated express functional copies of Cftr, which rescue *cftr* mutant zebrafish (Fig. 18E). To examine ductal morphogenesis, we developed a *cftr* BAC transgenic expressing Gal4 at the start codon to block transcription of the native *cftr* transcript and prevent rescue of the mutant allele. Importantly, the binary design of the Gal4/UAS expression system (Fig. 26A) can amplify low levels of expression, increasing fluorescence compared with direct *cftr* BAC transgenic lines. Gal4 drivers can also be paired with alternative UAS-driven genes, allowing a single Gal4 line to express a wide variety of transgenic reagents.

We examined expression of *TgBAC(cftr:Gal4)*; *Tg(UAS:GFP)* at 5 dpf to confirm *cftr:Gal4* was expressed in a similar pattern to the other *cftr* BAC transgenic lines. At 5 dpf, *cftr:Gal4* drives *UAS:GFP* expression in the notochord, pancreatic duct, and intestine, characteristic of other *cftr* lines in the zebrafish (Fig. 26B). This line also allowed us to more precisely examine the localization of Cftr within the pancreatic epithelium to determine whether Cftr localizes to the luminal membrane of the pancreatic duct. In 5 dpf zebrafish expressing *TgBAC(cftr-RFP)*; *TgBAC(cftr:Gal4)*; *Tg(UAS:GFP)*, the Cftr-RFP fusion protein localization is associated with filamentous actin, known to be localized apically within the pancreatic duct (Fig. 26C-C′′) (Fallon et

al., 1995; Kesavan et al., 2009). The *TgBAC(cftr:Gal4)* driver provides a robust, versatile marker of the pancreatic duct throughout pancreatic morphogenesis.

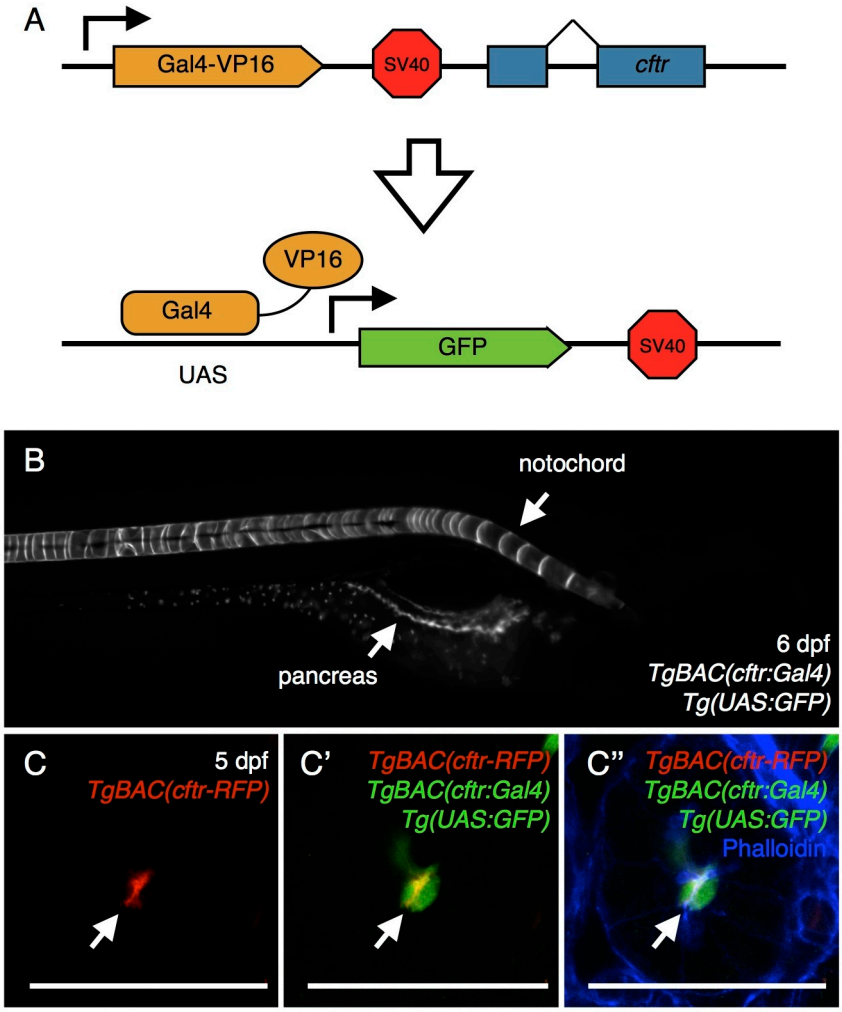

Figure 26: *cftr:Gal4* drives expression in *cftr* expressing cells.

(A) Schematic representation of a Gal4/UAS expression system. (B) Live epifluorescent image of a zebrafish expressing *cftr:Gal4* and *UAS:GFP* in the notochord, pancreatic duct, and individual cells along the intestinal epithelium. (C-C'') Cftr-RFP is localized apically within the pancreatic duct at 5 dpf. Arrow indicates the pancreatic duct. (C') Fluorescent merge of Cftr-RFP localization in conjunction with *cftr:Gal4* driving cytosolic *UAS:GFP* in the pancreatic duct. (C'') Fluorescent merge with phalloidin to mark filamentous actin at the apical membrane of the duct. Scale bars: 50 μm.

4.4 Pancreatic development in cftr mutants

Given the reduction of exocrine pancreatic tissue evident in *cftr* mutant adult zebrafish, we were interested to determine whether *cftr* mutants have defects in pancreatic morphogenesis. We first examined development of the exocrine pancreas marked by *ela:GFP* expression. At 5 dpf, the mutant pancreas is morphologically similar to WT siblings and expresses exocrine markers throughout the pancreas (Fig. 27A,B). To determine whether the pancreas undergoes defects in exocrine development as the pancreas grows, we examined 10 dpf zebrafish expressing *ela:GFP*. These fish express *ela:GFP* throughout the exocrine tissue, suggesting exocrine specification is normal throughout larval development (Fig. 27C,D).

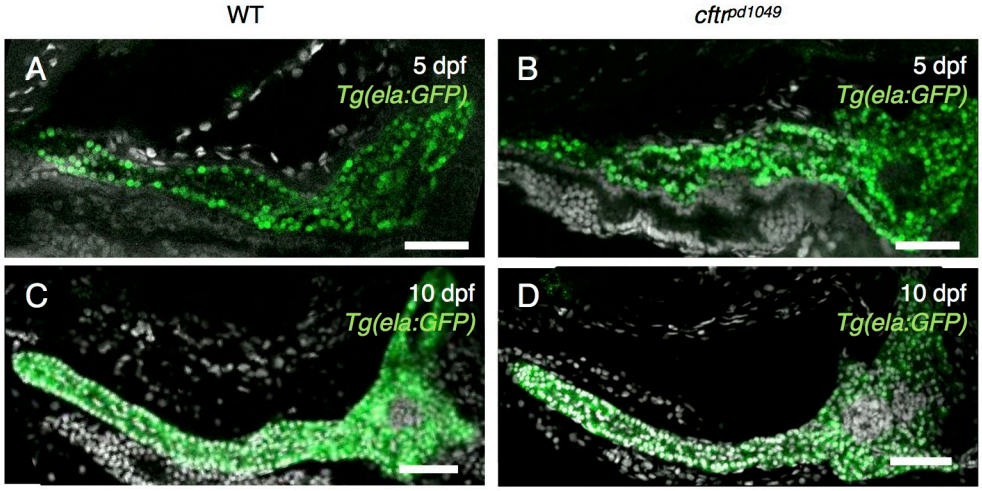

Figure 27: Development of the exocrine pancreas in *cftr* mutants.

(A,B) Confocal images of morphologically similar WT and *cftr*^{pd1049} pancreata expressing similar amounts of *ela:GFP* at 5 dpf. (C,D) Confocal images of WT and *cftr*^{pd1049} pancreata with similar morphology and expressing similar *ela:GFP* levels at 10 dpf. Scale bars: 50 μm.

In the pancreas, *cftr* is highly expressed in the ductal epithelium. To determine whether the loss of *cftr* function leads to defects in the specification of ductal epithelial cells, we examined development of the pancreatic ducts using a combination of transgenic, antibody, and lipid markers. We stained *cftr* mutant zebrafish with an antibody against carboxypeptidase to mark the exocrine tissue and phalloidin to mark filamentous actin to examine the morphology of the pancreatic duct. In WT zebrafish, actin at the luminal surface of the ductal epithelium clearly extends down the length of the pancreatic tail (Fig. 28A,A'). Similarly, the *cftr*^{pd1049} mutant pancreas broadly expresses the exocrine marker, carboxypeptidase (Fig. 28B). The mutant duct also appears contiguous down the length of the pancreatic tail (Fig. 28B') indicating that specification of the ductal epithelium is successful in *cftr*^{pd1049} mutant zebrafish. This result is likely similar to our observation of KV morphogenesis early in development. In the *cftr* mutant KV, the apical membrane is properly specified, but *cftr* function is necessary for fluid secretion and expansion of the lumen. In contrast to the KV lumen, the lumen of the pancreatic duct does not undergo obvious expansion during larval stages in WT fish.

To further test whether *cftr*^{pd1049} mutant zebrafish have defects in formation of the lumen of the pancreatic duct, we examined the localization of a BODIPY-C_5 fatty acid, which localizes to the duct upon feeding (Carten et al., 2011). In WT zebrafish, the fatty acid is localized to the duct at low levels in comparison to fluorescence observed in the

gut (Fig. 28C). It is unclear why the lipid is discontinuous in the WT pancreas, but localization in the tail of the pancreas suggests that the lipid can diffuse through the duct (Fig. 28C, arrow). In *cftr*^{pd1049} mutants, the lipid can similarly be observed at the posterior tail of the pancreas (Fig. 28D, arrow). Alternatively, the dye may enter the pancreatic duct through transcytosis of the dye through the exocrine pancreatic cells rather than diffusion from the intestine. In either case, a ductal lumen appears in *cftr*^{pd1049} mutants, but if the dye enters the duct by diffusion, the observation of the dye in the tail of the pancreas suggests that the pancreatic duct is contiguous in *cftr*^{pd1049} mutant zebrafish at 6 dpf.

In contrast to the large inflation observed in the KV lumen, pancreatic ducts have very small lumens. Due to the small luminal volume, is unclear whether the *cftr*^{pd1049} mutant pancreas has defects in lumen expansion at this stage. Finally, we examined specification of the pancreatic ductal cells using the *TgBAC(cftr:Gal4)* driver. At 5 dpf, the pancreatic ducts appear to develop similarly in WT and *cftr*^{pd1049} mutant larvae (Fig. 28E,F), indicating that the ductal epithelial cells are specified properly in *cftr*^{pd1049} mutants. These results suggest that pancreatic development and specification occur normally in *cftr*^{pd1049} mutant zebrafish.

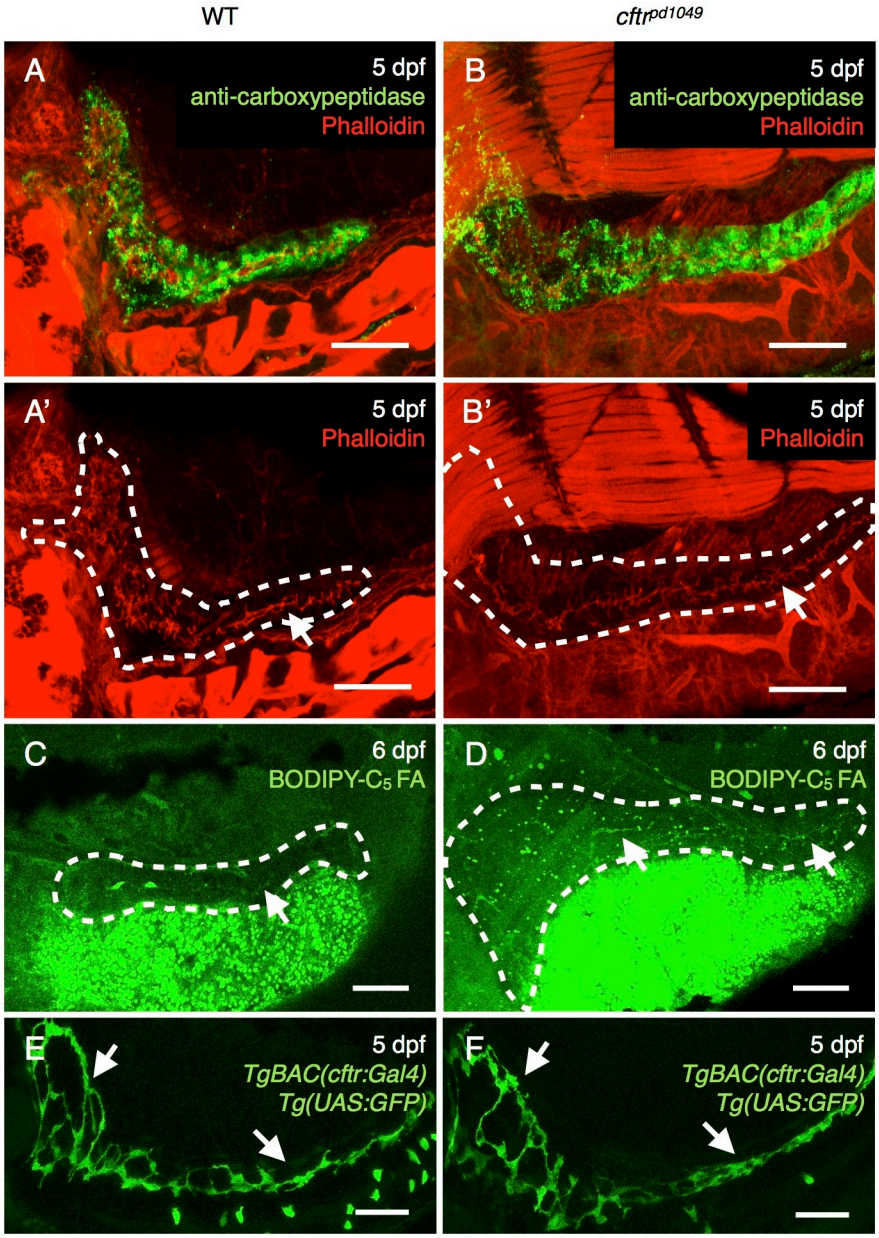

Figure 28: Development of the pancreatic duct in *cftr* mutants.

Figure 28: Development of the pancreatic duct in *cftr* mutants. (A) Whole-mount z-projection of WT and (B) *cftr*^{pd1049} mutant pancreata stained with anti-carboxypeptidase to mark the exocrine tissue and phalloidin to mark filamentous actin. (A′,B′) Z-projection of phalloidin channel only. (C) Z-projection of WT and (D) mutant pancreata fed BODIPY-C_5-FA to mark the pancreatic duct. The pancreas is outlined with a dashed line and the duct is indicated with a white arrow. (E) Z-projection of live *TgBAC(cftr:Gal4)*; *Tg(UAS:GFP)* expression in WT and (F) *cftr*^{pd1049} mutant pancreata. Scale bars: 50 μm.

Over time, many CF patients develop CFRD, caused by loss and dysfunction of insulin producing β cells in the pancreatic islets (Mackie et al., 2003). We were interested to determine whether *cftr* is required for pancreatic islet development in general or for the specification of β cells. Although *cftr* is not known to be expressed in the islet, expression in the ducts may play a direct role in the specification of new β cells. Lineage tracing experiments have determined that mammalian islets and zebrafish secondary islets arise from ductal progenitors (Parsons et al., 2009; Solar et al., 2009), where *cftr* function may be required for β cell differentiation. Additionally, cAMP signaling in the pancreatic ducts has been implicated in β cell regeneration (Andersson et al., 2012). Increased cAMP signaling has been shown to increase the rate of β cell regeneration in the pancreatic islets (Andersson et al., 2012). These studies suggest a mechanism whereby *cftr*, a cAMP dependent chloride channel, can function during the specification of new β cells from ductal progenitors.

To determine whether *cftr* is important for β cell specification, we first examined the development of the principal islet. The development of β cells was observed using the *Tg(ins:dsRed)* line or an insulin antibody. We stained whole-mount 3 dpf larvae with an antibody against insulin to quantify the number of β cells in the principal islet (Fig. 29A,B). We found no significant difference between the number of β cells between WT and *cftr*^{pd1049} mutants (Fig. 29C). Similar numbers of β cells is not surprising since the

principal islet β cells are specified independently of the ductal progenitors that give rise to secondary islets.

Secondary islets in the zebrafish develop through a mechanism similar to the development of mammalian islets, which arise from ductal progenitors (Parsons et al., 2009). To determine whether *cftr* is necessary for the specification of secondary islets, we began by examining the number and size of the secondary islets in *cftr*^{pd1049} mutants. Secondary islets form late in the development of the zebrafish pancreas (Parsons et al., 2009). The first secondary islet β cells can be observed at 6 dpf, with more β cells added slowly as development continues. We examined the number of endogenous β cells at 14 dpf, finding no significant difference in secondary islets or total number of β cells in *cftr*^{pd1049} mutants (Fig. 29D,E).

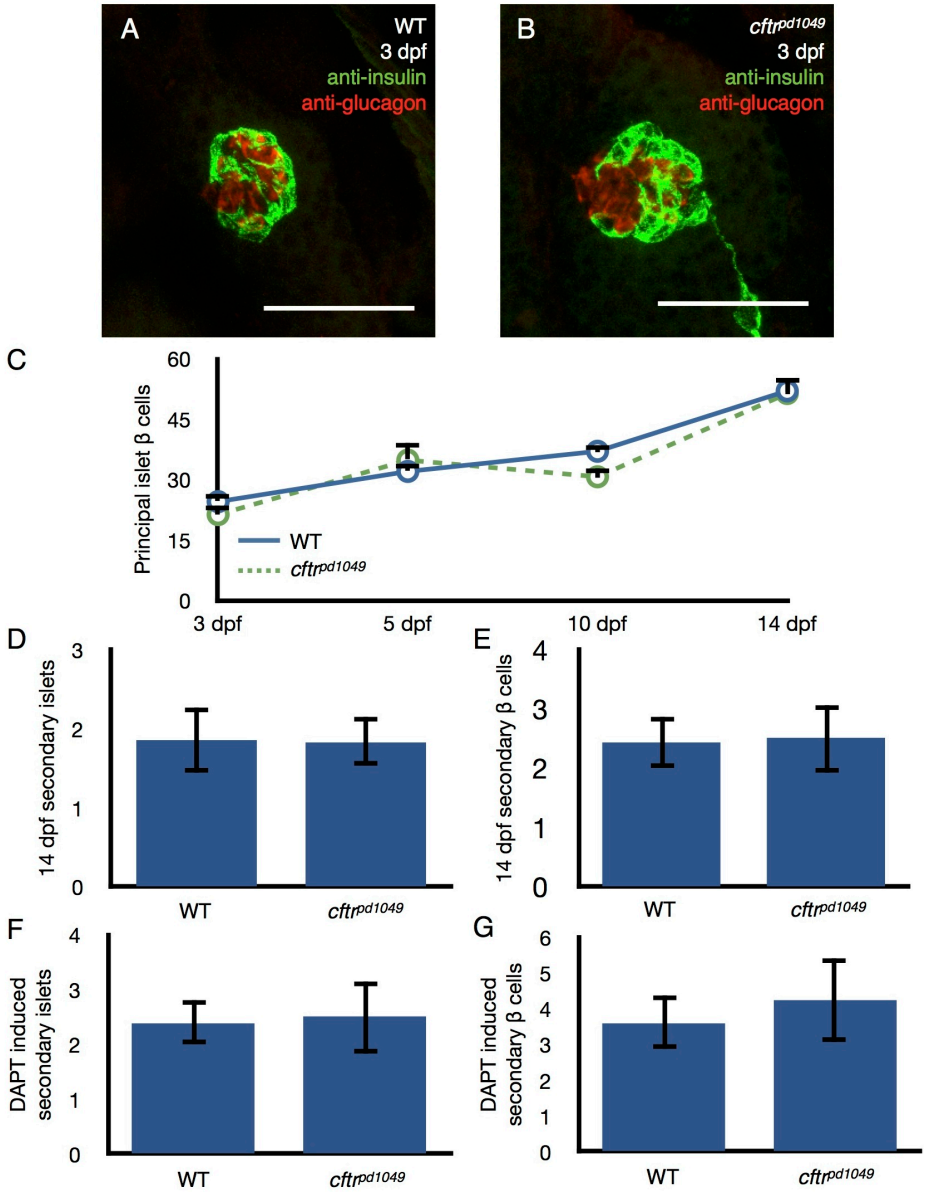

Figure 29: Pancreatic islet development in *cftr* mutants.

(A-B) Representative Z-projection of islets stained with anti-insulin for quantifying the number of β cells and counter-stained with anti-glucagon. (C) Quantification of total number of β cells in a confocal stack of the principal islet through 14 dpf. (D) Quantification of secondary islets observed at 14 dpf and (E) total β cells observed at 14 dpf. (F) Quantification of the number of DAPT induced secondary islets and (G) total number of β cells at 6 dpf. Scale bars: 50 μm. Error bars represent s.e.m.

The sporadic development of secondary islets complicated analysis at early time points, so we induced precocious secondary islet formation by pharmacologically inhibiting Notch signaling using DAPT, a gamma secretase inhibitor. This pharmacological agent stimulates increased differentiation of new β cells from the pancreatic duct (Parsons et al., 2009). After treatment with DAPT, we found no significant difference between the number of precocious secondary islets or β cells marked by *Tg(ins:dsRed)* in *cftr*^{pd1049} mutants and their siblings (Fig. 29F,G). Altogether, these results suggest that *cftr* is not required for the specification of primary or secondary islets during the early stages of zebrafish development.

Since defects in islet composition become more evident with age, we next tested whether *cftr* was required for β cell regeneration. To test the recovery of β cells, we used nitroreductase (NTR), an enzyme that can catalyze the formation of a toxic compound from metronidazole (MTZ). We expressed NTR under the control of the insulin promoter, *Tg(ins:NTR-mCherry)*. This line, treated with MTZ, has been previously characterized to ablate developing β cells, allowing for analysis of β cell regeneration (Pisharath et al., 2007). MTZ alone is toxic to zebrafish at high levels, so treatments were restricted to 10 mM. In accordance with previous studies (Pisharath et al., 2007), we treated 56 hpf *cftr* mutants expressing *Tg(ins:NTR-mCherry)* for 48 hours with MTZ and examined regeneration of the principal islet after allowing the fish to recover for another 48 hours (Fig. 30A). We found that *cftr*^{pd1049} mutants again recovered a similar number of

β cells as their WT controls indicating that β cell regeneration is not dependent on Cftr activity (Fig. 30C).

Given the differences between the development of principal and secondary islets in the zebrafish, we also investigated β cell recovery in the secondary islets. Since islet development occurs late and sporadically under normal conditions, we induced development of precocious secondary islets by treating 72 hpf larvae with DAPT and beginning MTZ ablation at 5 dpf (Fig. 30B). We again found that the recovery of secondary islets was not significantly different between WT and *cftr*^{pd1049} mutants (Fig. 30D). Altogether, these results suggest that *cftr* is not required for β cell development in the larval pancreas.

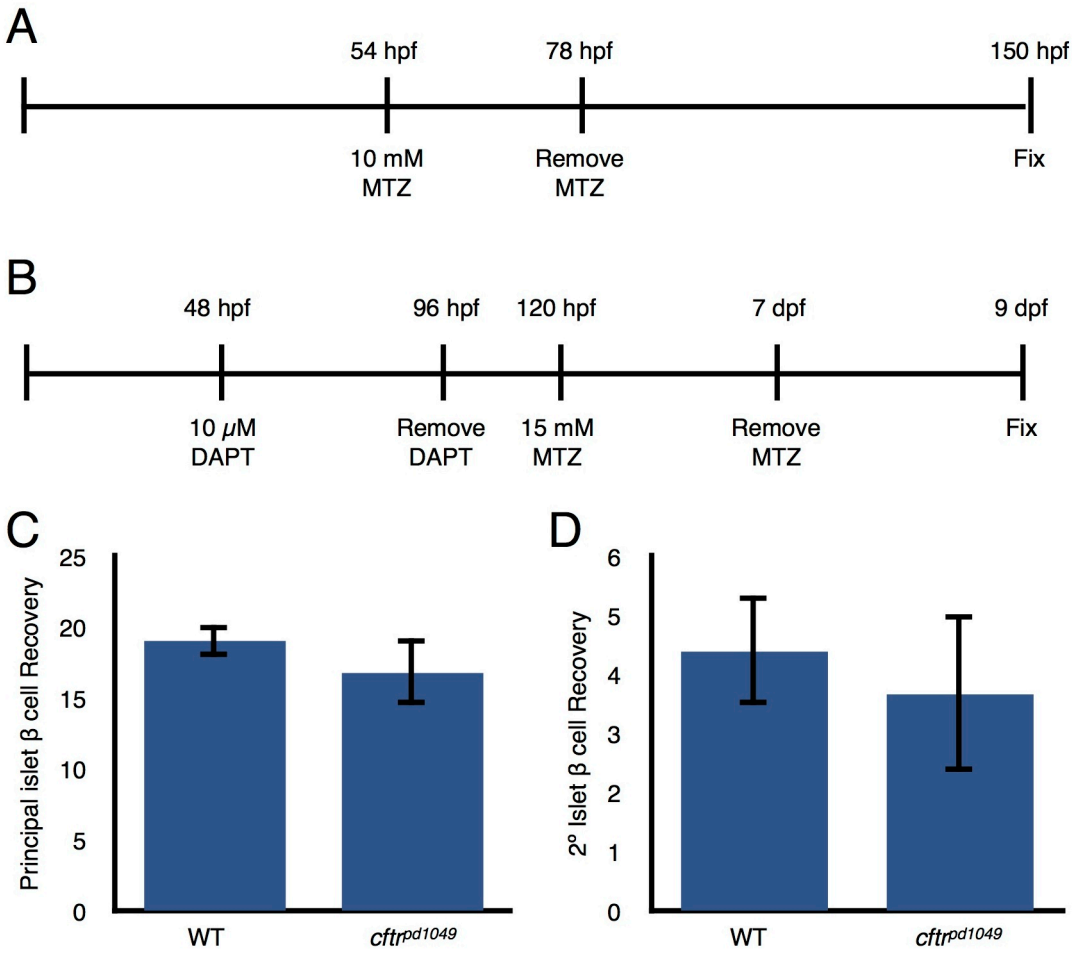

Figure 30: β cell regeneration in *cftr* mutants.

(A) Treatment schedule for principal islet β cell ablation by metronidazole in *Tg(ins:NTR-mCherry)* expressing fish. (B) Treatment schedule for ablating preciously induced β cells in *Tg(ins:NTR-mCherry)* expressing fish. (C) Quantification of β cell recovery in the principal islet. (D) Quantification of β cell recovery in the induced secondary islets. Error bars represent s.e.m.

4.5 Discussion

Here we describe a new model system for the study of CF. The adult *cftr* mutant zebrafish shares many characteristics with human CF. We found severe destruction of the zebrafish exocrine pancreas consistent with CF (Imrie et al., 1979; Ruzal-Shapiro, 1998; Sturgess, 1984). The zebrafish also displays many other defects characteristic of CF including blockages in the pancreatic ducts, reduced growth rate, and male infertility. These results suggest that Cftr function is similar in humans and zebrafish and highlight conserved roles for fluid secretion in vertebrates.

Although defects in ductal function have been proposed to drive destruction of the surrounding exocrine pancreas, the precise sequence of developmental events leading to pancreatic disease in CF has remained elusive. Here we report the generation of a developmentally accessible model for understanding CF. We found that during larval development, the exocrine pancreas and pancreatic ducts are specified normally. Importantly, we also observed that the pancreatic duct appears to form a single contiguous lumen. Actin staining and incorporation of a fatty acid to the tail of the pancreatic duct further suggests that the duct is contiguous in *cftr*^{pd1049} mutants. This result is consistent with our observations of lumen formation in KV and the roles of fluid secretion in other systems. In the zebrafish neural tube, loss of fluid secretion prevents opening of the brain ventricles, but specification of the enclosing epithelium is otherwise normal (Lowery and Sive, 2005). In the zebrafish gut, it was recently

demonstrated that lumen coalescence and fluid secretion are independent, co-incident events (Alvers et al., 2014). Due to the small size of the lumen of the pancreatic duct, we were unable to identify defects in lumen inflation as we observed in the *cftr* mutant KV. In each of these systems, organ function depends on fluid secretion, which is not evident until later stages in the pancreas. A more detailed analysis of the early stages of pancreatic destruction will be important to determine the precise sequence of events that underlie pancreatic disease in CF.

The mechanisms driving the specific destruction of the exocrine pancreas in CF are poorly understood. It will first be important to investigate the function of the exocrine pancreas over time. Pancreatic function can be assayed using quenched reporters of enzymes produced by the pancreas, EnzChek and PED6, which fluoresce after cleavage by digestive enzymes (Hama et al., 2009). Understanding the progression of pancreatic function over time will be important to understand the mechanisms underlying pancreatic disease in *cftr* mutant zebrafish. The prevailing hypothesis suggests that blockage of the pancreatic duct by dried-out mucus causes digestive enzymes to accumulate within the pancreas. Once these enzymes become activated, they likely digest the cells that produced them and the exocrine pancreas is replaced by fibrotic tissue. Recently, an alternative hypothesis has been proposed that instead suggests pancreatitis may be driven by inflammation stimulated by the innate immune system in a chemically induced mouse model of pancreatitis (Sendler et al., 2013). In this

model, neutrophils migrate to the exocrine pancreas triggering the activation of digestive enzymes, which cause the exocrine pancreatic cells to digest themselves. Intriguingly, the immune system is known to be hyper-activated in CF patients, consistent with an early role for the immune system in pancreatitis (Bruscia et al., 2011).

To better understand the changes occurring in the CF pancreas, it will be important to observe the precise events preceding pancreatic destruction using transgenic markers of the exocrine pancreas. The contribution of the immune system to pancreatic disease can also be observed by imaging transgenic markers of inflammation and immune cells. Additionally, the role of the innate immune system during the progression of pancreatic disease may be tested using the tools to ablate or block the migration of neutrophils in *cftr* mutants (Davison et al., 2007; Elks et al., 2011; Wang et al., 2014). Understanding the progression of pancreatic disease in *cftr* mutant zebrafish may provide new insights into pancreatic disease in CF patients.

There are some differences between CF in humans and the *cftr* mutant zebrafish. In human patients, loss of the exocrine pancreas leads to defects in digestion requiring supplementation with digestive enzymes (Wilschanski and Novak, 2013). The *cftr* mutant zebrafish are not provided external digestive enzymes, suggesting that the exocrine pancreas retains some function, although the growth rate for mutant fish is dramatically slower than WT siblings. Cftr function within the pancreatic duct may be examined by driving Cftr with a duct-specific promoter. Although the fish lacks highly

specific markers of the pancreatic duct, *sox9b* has been characterized as a marker of the pancreatic duct and other tissues (Manfroid et al., 2012). Analysis of Cftr function specifically within the duct will provide key insights into the progression of the disease and may help dissect the precise tissue-specific requirements for Cftr.

In adult *cftr* mutants, function of the endocrine pancreas appears intact. There are several possibilities underlying the preservation of endocrine function in adult *cftr* mutants. Severely affected fish may die before they can be analyzed. More detailed analysis of β cell function in the fish is complicated by their small size, which limits sampling. The volume of blood necessary for a standard glucose test is a large percentage of a zebrafish's total blood volume. The most frequent protocols for extracting blood are only able to test fish once per day (Zang et al., 2013) while glucose tolerance tests require several collections in the span of a few hours. Alternatively, endocrine function could be preserved because the pancreatic islets may be less affected by the destruction of the surrounding exocrine tissue than mammalian models. The mammalian pancreatic islets are largely spared, but are typically compressed by encroaching fibrotic tissue. In the fish, the *cftr*^{pd1049} mutant islets appear smaller and more numerous than in WT siblings. Addition of new β cells to zebrafish secondary islets is not well understood and these results may indicate that newly formed β cells are unable to properly incorporate into existing islets due to the fibrotic tissue throughout the adult pancreas.

A common symptom of CF is male infertility due to congenital bilateral absence of the vas deferens (Kaplan et al., 1968). We have observed that *cftr* mutant male zebrafish have defects in fertility, suggesting that they may develop a similar disease. In humans, accumulation of mucus within the lumen is thought to cause blockage and degeneration of the vas deferens (Oppenheimer and Esterly, 1969). Analysis of vas deferens development in the *cftr* mutant zebrafish may provide further insight into fundamental roles for fluid secretion during lumen formation and maintenance.

The phenotypes we observe in the zebrafish $cftr^{pd1049}$ mutants indicate that the zebrafish can be a complementary model for studying the pathophysiology of CF. Although zebrafish are more distantly related to humans than the mammalian pig and ferret models, the zebrafish has several unparalleled strengths including developmental accessibility, large clutch sizes, and amenability to genetic screening. Recently, substantial effort has focused on identifying modifiers of CF to identify target genes which may point to new treatments for CF (Drumm et al., 2005). In the zebrafish, modifiers of CF may be alternatively identified through forward genetics (Patton and Zon, 2001). A suppressor screen may uncover novel genes that rescue loss of *cftr* function in the zebrafish. The zebrafish is also amenable to pharmacological screens (Zon and Peterson, 2005). Although several correctors of CFTR-ΔF508 have been developed, few are functional *in vivo*, due to differences between the screening methodology and native CFTR function (Lukacs and Verkman, 2012). A screen for

CFTR-ΔF508 correctors in the zebrafish may identify new compounds that more effectively function *in vivo*. The development of a more accessible *in vivo* model for CF is likely to catalyze a deeper understanding of the progression of CF and provide insights into new therapeutic strategies.

The transgenic lines described here provide new reagents for marking the pancreatic duct. The Cftr-GFP and Cftr-RFP lines mark the apical membrane of the duct and are observed throughout pancreatic morphogenesis. Additionally, the *TgBAC(cftr:Gal4)* driver in conjunction with UAS-driven reagents is likely to be a useful reagent for analyzing tissue-specific gene function within the duct. These lines can be observed marking the pancreatic duct as early as 3 dpf and throughout adulthood. These reagents will be valuable tools for analysis of the pancreatic duct in other contexts.

Contrary to a role for *cftr* during the specification of the developing pancreas, we instead observe that pancreatic destruction is likely due to defects in the function of the pancreatic ducts. Mucosal blockage has been proposed to drive pancreatic degeneration, but developmental evidence for this hypothesis has previously been lacking. Importantly, we describe a new zebrafish model for investigating CF of the pancreas. We also characterize important new markers of the developing pancreatic duct, which has lacked specific markers in the zebrafish. Altogether, the results described here demonstrate that *cftr* in the pancreatic ducts is necessary for pancreatic function and homeostasis.

5. Conclusions and future directions

The work described here identifies key roles for Cftr during the regulation of fluid secretion necessary for organ morphogenesis and function. These results present several exciting new research directions including basic investigations into the process of lumen formation to specific studies of the progression of CF. The proposed studies leverage the strengths of the zebrafish and the reagents generated during the above work, including live imaging of morphogenetic processes and the accessibility of the zebrafish model. Understanding other functions for Cftr in the zebrafish will likely provide key insights into many other symptoms of CF.

5.1 cftr function the notochord

Cftr is highly expressed in the zebrafish notochord throughout development. The notochord performs several roles in the zebrafish embryo including several signaling and mechanical functions. Initially the structure serves as an early hydrostatic skeleton, helping to elongate the embryo (Adams et al., 1990). The notochord also participates in vertebral development by serving as a substrate around which the vertebrae develop (Ellis et al., 2013). Structurally, the zebrafish notochord is composed of a rod of cells that contain large fluid-filled vacuoles (Adams et al., 1990; Waddington and Perry, 1962). Identifying the function of *cftr* in the notochord may provide insights into the regulation of hydration and mechanical properties of the large vacuolated cells of the notochord.

Cftr expression can be detected by *in situ* hybridization in the notochord as early as 2 ss (Fig. 15A,B). The *cftr* transcript continues to be detected throughout larval development. Using the *TgBAC(cftr-GFP)* line, we observe that Cftr is present on the plasma membrane of the vacuolated cells rather than the internal vacuole membrane, as evidenced by Cftr-GFP localization passing the exterior of nuclei (Fig. 31A). By 20 ss, Cftr-GFP appears to be localized intracellularly, which shifts to the plasma membrane as the vacuoles expand. By 4 dpf, high levels of expression are observed in the notochord and expression continues through 21 dpf (Fig. 31B,C). It is tempting to hypothesize several possible functions for Cftr-regulated fluid secretion in the large vacuolated cells of the notochord, but we have been unable to identify a defect in the development of the notochord. Mutant embryos have normal vacuole development and normal extension of the body (Fig. 9G-J). To rule out the possibility that a maternal contribution of *cftr* masks the zygotic *cftr* mutant, we generated maternal-zygotic *cftr*^{pd1049} mutants and found that they also demonstrate normal notochord development.

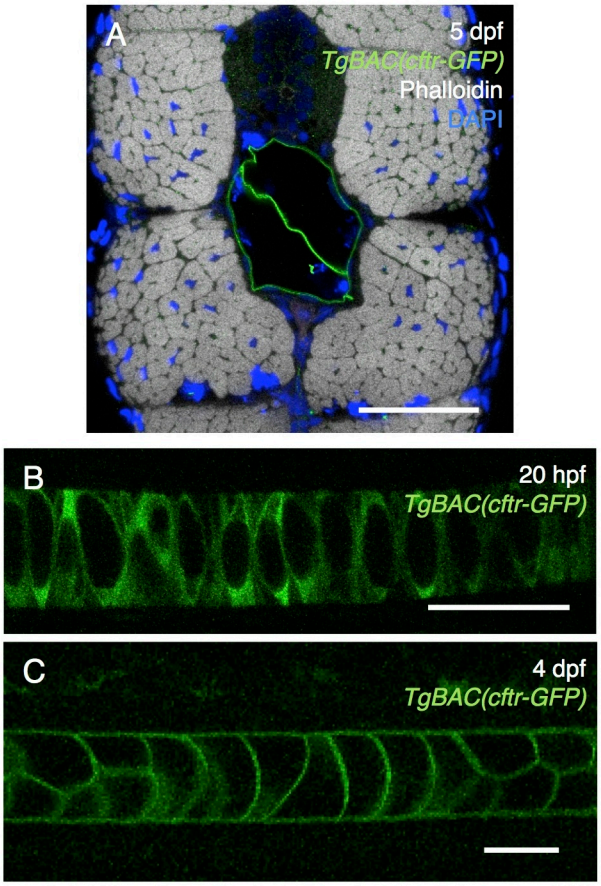

Figure 31: Cftr is expressed in the notochord.

(A) Transverse section of a zebrafish expressing *TgBAC(cftr-GFP)* in the notochord at 5 dpf. (B) Live confocal image of Cftr-GFP expression at 20 hpf demonstrating Cftr-GFP localization primarily in the cytoplasm of the vacuolated cells of the notochord. (C) Live confocal image of Cftr-GFP expression at 4 dpf. Scale bars: 50 μm.

There are several possibilities for the lack of notochord defects observed in *cftr*^{pd1049} mutants. Most simply, there may be alternative channels that compensate for the lack of Cftr activity. This is somewhat unlikely since there are comparatively few anion channels encoded in the vertebrate genome. Tissue-specific transcriptional profiling will be important to identify whether there are alternative anion channels expressed in the vacuolated cells of the notochord. Alternatively, the notochord vacuoles have been traditionally thought to be filled with glycoproteins or glycosaminoglycans which attract water to form a shock absorbent material (Waddington and Perry, 1962). Loss of *cftr* may impede normal delivery of water to negatively charged molecules in the notochord vacuoles, altering their mechanical properties.

Intriguingly, structural abnormalities have been observed in the spines of CF patients leading to slight spinal curvature and pain in a large number of CF patients (Elkin et al., 2001; Ross et al., 1987). By 15 years old, more than 75% of female CF patients have been observed to develop spinal curvature due to changes in vertebral morphology, which become more wedge-shaped (Henderson and Specter, 1994). The late onset of spinal curvature suggests that the disease develops over time. The cause has been proposed to be due to defects in mineral absorption and osteopenia in CF patients (Elkin et al., 2001; Henderson and Specter, 1994). Alternatively, CFTR may be important for the mechanical properties of the nucleus pulposus, the adult remnant of the notochord, which buffers compressive forces in the vertebrae (Hunter et al., 2004;

McCann et al., 2012). Changes in the resistance of the nucleus pulposus may result in increased stresses in the vertebrae leading to changes in their shape.

It would be interesting to determine whether *cftr* mutant zebrafish develop spinal curvature consistent with CF. To determine whether *cftr* mutant zebrafish develop spinal curvature, it will be necessary to first examine adult zebrafish vertebrae for the wedge shape characteristic of the CF vertebrae. To test whether Cftr function is required specifically within the notochord, tissue specific knockdown would be particularly informative. Genetically encoded shRNAs may be sufficient to disrupt *cftr* expression (Dong et al., 2009b) and isolate *cftr* function in the notochord, independent of the loss of digestive function.

One of the primary functions of the notochord is to axially direct mechanical forces. In response to contraction of skeletal muscle, notochord vacuoles can be observed undergoing substantial deformation. Mechanical analysis of notochord vacuoles in *cftr* mutants may indicate whether Cftr is required for vacuole function. Qualitative analysis of the degree of deformation in the notochord vacuoles in *cftr* mutants may reveal functional abnormalities in the notochord that may underlie defects in vertebral maintenance.

The notochord membrane experiences dramatic stresses throughout development. During the initial stages of vacuole inflation the membrane is rapidly expanded and during swimming, the notochord membrane is stressed as the somitic

muscles contract. One mechanism cells use to buffer membrane stress is to stud the membrane with caveolae. In response to increased membrane tension, the caveolae can be rapidly disassembled, providing additional surface area to the plasma membrane (Kozera et al., 2009). The principal component of caveolae are caveolins (Hansen and Nichols, 2010). Interestingly, *caveolin-1* (*cav1*) is highly expressed in the notochord of a wide variety of vertebrate systems suggesting it performs an integral role during notochord development (Nixon et al., 2007). To examine *cav1* localization, we developed a zebrafish BAC transgenic encoding a C-terminal Cav1-GFP fusion, *TgBAC(cav1-GFP)*. This transgene expresses *cav1* in the notochord in addition to a wide variety of other tissues known to express *cav1* (Fig. 32A,B). In addition to buffering mechanical stress, caveolae are also thought to participate in intercellular signaling and facilitate a subset of intracellular trafficking (Kawamura et al., 2003; Sedding et al., 2005; Yazbi et al., 2008).

To determine whether caveolae are necessary for the formation and function of the zebrafish notochord, we developed zebrafish *cav1* mutants using TALENs. *Caveolin 1* has two isoforms, an α and β transcript defined by different transcription start sites (Fig. 32C). We generated two mutant alleles, the first to target the α transcript and the second disrupting the α and β transcripts (Fig. 32D). Morpholinos against the *cav1α* isoform have been previously reported to disrupt formation of the zebrafish notochord (Fang et al., 2006; Nixon et al., 2007). Curiously, in our preliminary analysis of the these mutants, neither homozygous *cav1α* or *cav1αβ* mutants develop similar defects in the formation of

notochord vacuoles in contrast to previous reports of *cav1* knockdown. To determine whether *cav1* functions to buffer membrane stress it will be important to determine whether *cav1* is maternally loaded by analyzing the development of maternal-zygotic mutants for both isoforms. Additionally it will be important to determine whether the notochord in *cav1* mutants responds differently to acute membrane stress than their WT siblings. Further, it will be important to determine whether the *cav1* mutants also develop defects in vertebral morphogenesis or maintenance, which may be indicative of mechanical abnormalities in the nucleus pulposus. These studies will reveal whether mechanical forces induced by fluid pressure are important drivers of vertebral morphogenesis and maintenance.

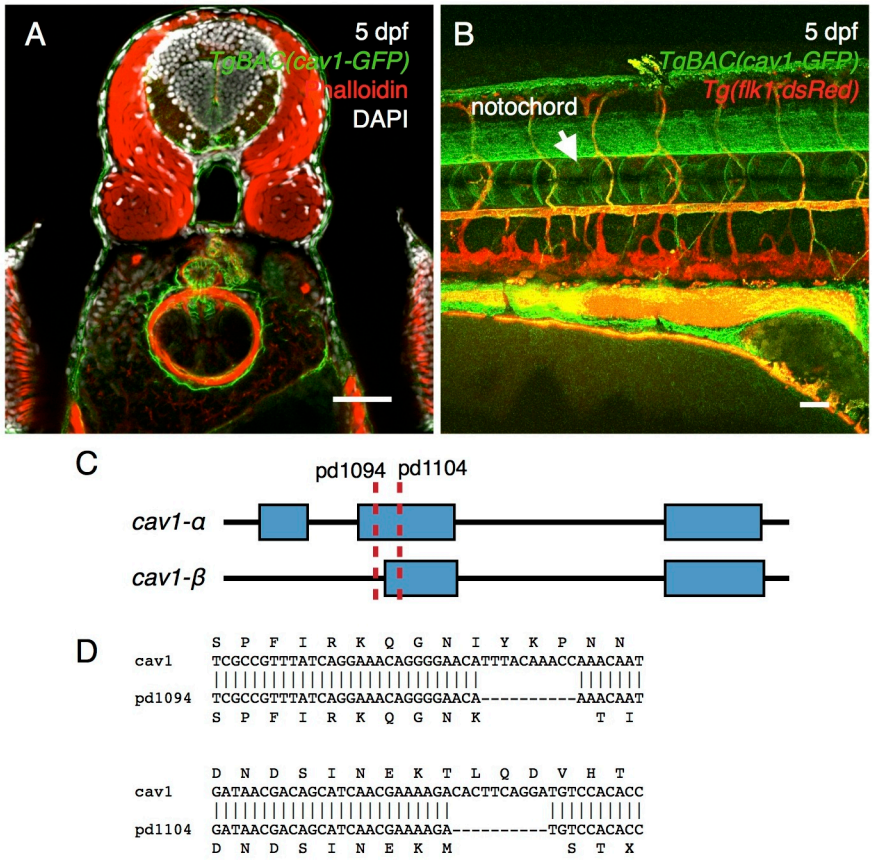

Figure 32: *cav1* expression and mutagenesis.

(A) Transverse section of a 5 dpf zebrafish expressing *TgBAC(cav1-GFP)*. (B) Sagittal, live confocal image of a fish expressing *TgBAC(cav1-GFP)* and *Tg(flk1:dsRed)*. (C) Schematic of *cav1α* and *cav1β* transcripts. (D) Alignment of WT *cav1* to the *cav1*^{pd1094} and *cav1*^{pd1104} mutant alleles. Scale bars: 50 μm.

5.2 Lumen formation in KV

Our analysis of *cftr* function highlights the strengths of KV as a model for studying lumen formation. KV forms from a cluster of unpolarized cells which generate several small lumens that coalesce into a single lumen (Fig. 16A,B) (Amack et al., 2007). The structure has several strengths unparalleled in other systems. Importantly, KV is an *in vivo* model for cord hollowing and it develops rapidly; the early stages of lumen formation normally occur between 13 and 15 hpf. The lumen develops very close to the surface of the embryo, allowing lumen formation to be easily observed from the initial stages of its formation to its disassembly around 22 hpf. Finally, defects in LR asymmetric gene expression can be used as a functional readout of luminal defects.

An important strength for investigating KV development is the power of zebrafish genetics. To drive gene expression in a modular fashion within KV, we utilized the Gal4/UAS system. The *TgBAC(cftr:Gal4)* driver strongly expresses GFP in the KV epithelium by 2 ss (Fig. 33A,B). In this way, otherwise toxic genes can be expressed in the developing KV. Importantly, *cftr* is much more specific for KV than other well characterized transgenes, including the widely used *Tg(sox17:GFP)* line.

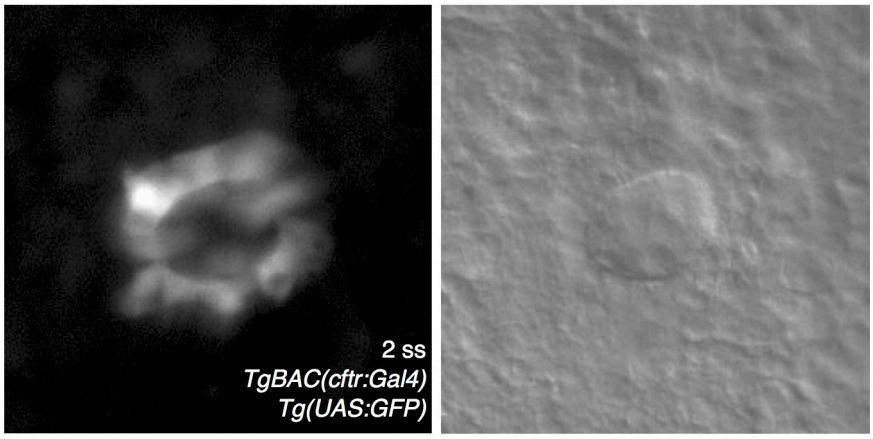

Figure 33: *cftr:Gal4* drives expression in KV.

(A) Whole-mount epifluorescent image of *UAS:GFP* expression in KV driven by *cftr:Gal4*. (B) Associated DIC image of 2 ss KV lumen.

The importance of achieving expression specifically within KV and throughout the KV epithelium is highlighted by our attempts to test *cftr* function in KV using traditional DFC-specific injection techniques. Tissue specificity in KV has previously been achieved by injecting morpholinos and mRNAs into the yolk at the 512-1024 cell stage, when only a small proportion of cells in the embryo retain a syncytium with the yolk (Amack and Yost, 2004). Among these cells are the dorsal forerunner cells, a population that in part gives rise to KV. Although this system has been instrumental in examining function of several genes in KV by preventing incorporation into the notochord, these genes are likely to have cell autonomous effects on KV morphogenesis. To test *cftr* function specifically in KV, we attempted DFC-specific injections of a morpholino against *cftr*, but were unable to prevent lumen inflation. It has been suggested that relatively low levels of *cftr* activity are sufficient to drive normal fluid secretion, so we sought to determine whether the DFC-specific injections incorporate into the entire KV epithelium or a subset, data we could not find previously reported. We injected a green fluorescently labeled control morpholino in conjunction with our morpholino against *cftr* using DFC-specific injections into *TgBAC(cftr-RFP)* transgenics. In all instances, we observed mosaic incorporation of the fluorescently labeled morpholino into KV. To demonstrate the efficacy of the *cftr* morpholino, we observed that the morpholino blocked expression of Cftr-RFP in cells that had incorporated the fluorescent morpholino. This may also explain the reduced penetrance of morpholino

phenotypes when analyzed by DFC-specific injection (Vandenberg and Levin, 2013). To reliably examine gene function specifically within KV, it will be necessary to drive expression throughout the KV epithelium.

One application for the *TgBAC(cftr:Gal4)* transgenic is testing the function of various components of the intracellular trafficking pathways regulated by Rab GTPases during cord hollowing. Previous studies of cord hollowing in the zebrafish gut have demonstrated that Rab11a is crucial for endosomal recycling that mediates lumen coalescence (Alvers et al., 2014). In addition to testing whether endosomal recycling is important in different types of organs, several types of dominant-negative Rab GTPases driven by UAS elements have been generated, which function in various intracellular trafficking pathways (Clark et al., 2011). Crossing these lines to *cftr:Gal4* will reveal the relationship between intracellular trafficking and lumen formation during cord hollowing in live animals. As an *in vivo* model of cord hollowing accessible to live imaging, KV may represent an important complementary model system for examining lumen morphogenesis.

5.3 Mechanisms regulating LR asymmetry in cftr mutants

The defects in LR asymmetry observed in *cftr* mutants may help inform a deeper understanding of early events in the establishment of organ laterality. Instead of a complete randomization of LR asymmetry in *cftr* mutants, we instead observe only about 30% reversal of organ laterality, indicating that there may be additional signals

that bias normal organ positioning. In contrast, defects in the function of the mouse node lead to complete randomization of organ asymmetry.

One possible explanation for incomplete randomization of organ laterality in *cftr* mutants is that KV may retain some signaling function. We tested whether calcium signaling is impaired in KV that lack fluid secretion by examining the expression of *charon*, a gene responsive to KV calcium signaling. *Charon* is typically expressed asymmetrically, with lower levels of expression on the left side of the animal. In KV with overactive calcium signaling, *charon* expression is dramatically reduced (Superina et al., 2014). In *cftr*^{pd1049} mutants, which lack an inflated lumen, *charon* expression is increased and symmetric (Fig. 34A,B). This result indicates that calcium signaling within KV is lost and is unlikely to be responsible for the incomplete penetrance of organ reversal. To test whether fluid secretion acts directly through calcium signaling in KV, it will be necessary to specifically drive asymmetric calcium signaling. Using optogenetics, we can activate a light-activated calcium channel on specific sides of the zebrafish KV (Zhang et al., 2006). Expressed in mutants, this will definitively demonstrate the relationship between calcium signaling and *charon* expression and determine whether fluid flow is necessary for calcium signaling in the KV epithelium.

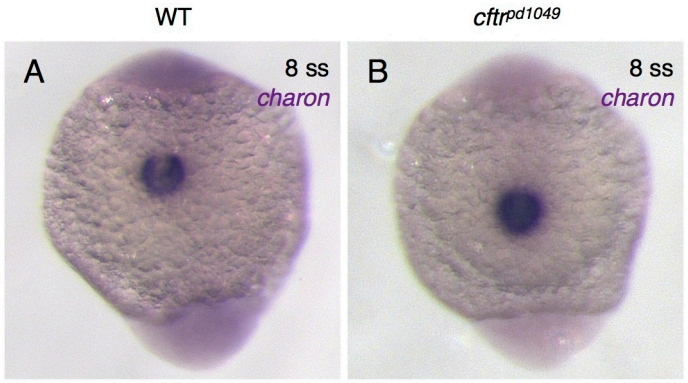

Figure 34: *charon* is symmetrically overexpressed in *cftr* mutants

(A,B) *In situ* hybridization for *charon* in (A) WT and (B) *cftr*^{pd1049} mutant zebrafish.

Prior to formation of KV and homologous structures in other vertebrates, H^+/K^+-ATPase function has been shown to drive early LR signaling. In the frog, chick, and zebrafish, defects in the activity of H^+/K^+-ATPase perturb the development of LR asymmetry (Kawakami et al., 2005; Levin et al., 2002). The H^+/K^+-ATPase functions early in development, before the onset of zygotic gene transcription. In the frog and fish, asymmetric signaling is driven by changes in channel activity rather than protein expression. It remains unclear why many vertebrates retain two types of asymmetric signaling. Several hypotheses have been proposed, including that each embryo may stochastically use one type or another to specify organ laterality, or that KV acts to amplify biases established by earlier mechanisms (Vandenberg and Levin, 2013). The *cftr* mutant may offer a way to test the relationship between early and later LR signaling events. It would first be interesting to determine whether blocking H^+/K^+-ATPase activity in *cftr* mutants completely randomizes organ laterality. This would indicate that these are the sole two processes that specify organ laterality in the zebrafish embryo.

5.4 Innate immune function in CF

In addition to buildup of mucus in several organs, CF patients also have abnormal responses to pathogens by the innate immune system (Bruscia et al., 2011). Opportunistic bacteria frequently colonize the lungs of CF patients. Many CF patients develop *Pseudomonas aueruginosa* infections, which lead to increased lung inflammation. More seriously, infection by *Burkholderia cepacia* typically leads to dramatic declines in

lung function in CF patients (Callaghan and McClean, 2012). Dysfunction in the innate immune system is thought to be caused by several defects. The CF immune system often responds to challenges with excessive inflammation (Bruscia et al., 2011). Additionally, previous studies have shown that neutrophils lacking *cftr* function have impaired migration. A study using morpholino knockdown of *cftr* in zebrafish identified that neutrophil migration specifically toward *Pseudomonas* infection was compromised (Phennicie et al., 2010). Once the CF macrophages identify and engulf bacterial pathogens, they are less efficient at bacterial killing (Di et al., 2006). Bacterial killing is mediated by delivering high concentrations of chloride to the phagocytic compartment. CFTR is thought to be essential for delivering the chloride ions necessary for bacterial killing. Understanding the changes in the CF immune system will be vital to managing infectious diseases that have become characteristic of CF.

The underlying defects in the CF immune system are poorly understood *in vivo*. The zebrafish may represent an ideal system to examine the innate immune system in CF. In fish, the adaptive immune system does not develop until adulthood, so the larvae allows isolated analysis of innate immune function (Trede et al., 2004). Additionally, the transparency of the zebrafish embryo allows the immune system to be monitored *in vivo*. Several existing transgenic lines that specifically mark neutrophils and macrophages have been developed and are known to respond to immune challenges (Gray et al., 2011; Hall et al., 2007). Examination of innate immune system function *in vivo* is likely to

provide key insights into the changes present in the CF immune system. To investigate the kinetics of bacterial killing in the immune system, *cftr* mutants expressing *Tg(lysC:dsRed)* (Hall et al., 2007) to mark neutrophils or *TgBAC(fms:Gal4)* (Gray et al., 2011) to mark macrophages can be imaged after infection with fluorescently labeled pathogens. Zebrafish can be monitored for extended periods of time to determine the precise kinetics of bacterial killing *in vivo*, which will reveal whether there are defects in innate immune function in the *cftr* mutant zebrafish. Additionally, the zebrafish may provide key insights into the role of inflammation during tissue destruction.

In the CF pancreas, once the ducts are blocked, the exocrine tissue becomes inflamed and is later replaced by fibrosis. We also observed similar destruction in the zebrafish adult *cftr* mutant pancreas. It will be important to understand the mechanisms that drive tissue destruction to better understand the progression of CF. To determine when the pancreatic duct becomes blocked, we will express a secreted protein in the exocrine tissue of the *cftr* mutant pancreas. During normal function, the protein is expected to localize in the duct as it is transported to the intestine, but as the duct becomes plugged with mucus, the secreted protein should accumulate within the pancreas. Expression in exocrine tissue can be driven by the *TgBAC(ptf1a:Gal4)* (Parsons et al., 2009) driver crossed to a transgenic zebrafish encoding a fluorescently-tagged secreted protein driven by a UAS element.

An important early signal for inflammation is tumor necrosis factor α (TNFa) (Locksley et al., 2001). A transgenic marker for TNFa expression would allow for precise timing of the initial inflammatory responses in live fish. Identification of the onset of inflammation will focus further investigations on a specific time-point to identify the cellular changes that precede tissue destruction. Molecular markers of inflammation, neutrophils, macrophages, and ductal function will be important to understand the progression of pancreatic disease in CF patients. Altogether, these studies will provide key insights into the role of the innate immune system during the progression of pancreatic disease in CF.

5.5 Trafficking and cell-specific function of Cftr during intestinal fluid secretion

During normal intestinal function, the epithelium secretes large volumes of fluid into the lumen. Fluid secretion in the mammalian intestine occurs in the crypts and flows outward into the lumen (Barrett and Keely, 2000; Frizzell and Hanrahan, 2012). Although the physiology of fluid secretion has been well studied in the intestine, the specific cell-types driving fluid secretion remain unclear. Recently, a population of cells was described in the mammalian intestine that express high levels of CFTR and other ion transporters (Fan et al., 2012; Jakab et al., 2013). These cells, termed *cftr* high expressers (CHE), are scattered throughout the intestine with an enterocyte-like morphology. In these cells, CFTR is typically found in subapical vesicles. Upon stimulation of pharmacological agonists of fluid secretion, CFTR is delivered to the

apical membrane, consistent with a role in the regulation of fluid secretion in these cells (Jakab et al., 2013). The high levels of ion channel expression suggest that these cells may be the principal regulators of fluid secretion in the intestine. The zebrafish models we have developed may be instrumental for defining the precise function for CHE cells in the intestine.

We have observed that *cftr* is highly expressed in a small population of cells along the length of the gut in the *TgBAC(cftr-GFP)* line, similar to observations of the mammalian intestine (Fig. 35A,C). The CHE cells are distinct from enterocytes, marked by *Tg(ifabp:dsRed)* (Kanther et al., 2011) expression (Fig. 35B). This expression pattern is consistent in two of our other *cftr* BAC lines, *TgBAC(cftr-RFP)* and *TgBAC(cftr:Gal4)*, suggesting that it is specific to the *cftr* locus rather than a position specific effect of insertion. Imaging the Cftr-GFP fusion protein in these cells reveals a similar subapical distribution of Cftr-GFP (Fig. 35D). Furthermore, treatment of these cells with IBMX and Cftr activator causes the localization of Cftr-GFP to shift to the apical membrane (Fig. 35E). Together these results indicate that the cells we observe in the zebrafish gut are similar to the CHE cells characterized in the mammalian intestine.

Using the tools available in the zebrafish system, we may be able to directly address whether these cells are the primary drivers of fluid secretion in the intestine. To test whether the CHE cells are the primary regulators of intestinal fluid secretion, the *TgBAC(cftr:Gal4)* can be used to drive *Tg(UAS:NTR-mCherry)* in the CHE cells.

Treatment with MTZ will ablate the CHE cells. Cftr is also expressed in the pancreatic ducts and notochord, which may complicate analysis of intestinal fluid flow. To achieve some specificity, it will be important to deliver the MTZ to the intestinal lumen by gavage. Once the cells are ablated, fluid secretion can be stimulated with IBMX and Cftr activator to determine whether the fish lacking CHE cells fail to accumulate fluid within the intestinal lumen. It is important to note that we do not see the *cftr:Gal4* construct driving expression in the neighboring enterocytes, likely because the Gal4 is not expressed at a high enough level to activate the UAS promoter, indicating that metronidazole ablation of CHE cells would spare the enterocytes. These studies would demonstrate a clear requirement for CHE cells during fluid secretion in the intestine.

The powerful imaging techniques available to the zebrafish will allow a deeper characterization of the mechanisms that regulate CFTR trafficking in CHE and other epithelial cells. The *TgBAC(cftr-GFP)* line reflects Cftr localization within resting and activated CHE cells. Co-expression of *TgBAC(cftr-GFP)* and *TgBAC(cftr:Gal4)* with various dominant negative Rab GTPases expressed under the control of a UAS promoter will allow for fine dissection of the molecular regulators of Cftr trafficking. In cells expressing Cftr-GFP, and dominant negative Rab GTPases, localization of Cftr-GFP in response to activators of fluid secretion can be quickly analyzed. One likely candidate to disrupt Cftr localization is Rab11a, which is associated with recycling endosomes. Fish expressing Cftr-GFP and associated Rab GTPases can be simply imaged using live

confocal microscopy to determine whether Cftr-GFP is delivered to the apical membrane. Understanding the mechanisms regulating Cftr delivery to the apical surface has important implications for treating CF, since CFTR-ΔF508 is not properly maintained on the apical surface. Additionally, lessons about the regulation of CFTR localization inform basic mechanisms underlying intracellular trafficking.

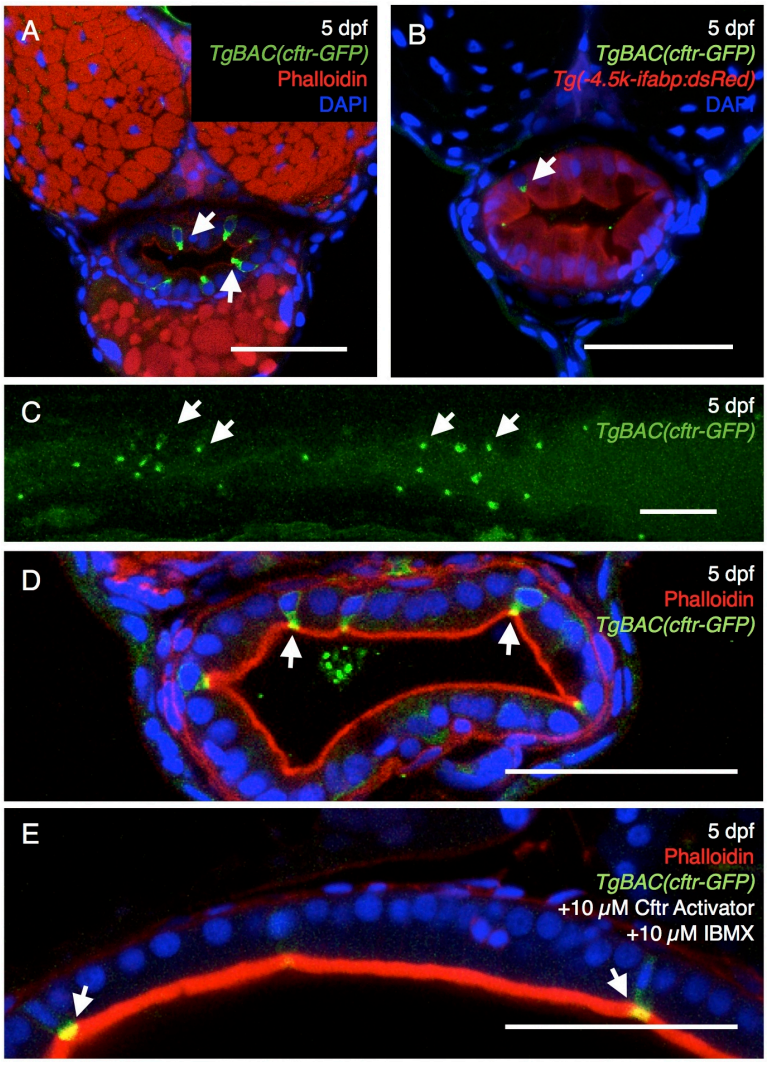

Figure 35: Cftr expression and localization in CHE cells.

(A) Transverse section of 5 dpf larvae expressing Cftr-GFP within a sub-population of intestinal epithelial cells. (B) Transverse section 5 dpf larvae demonstrating Cftr-GFP expression excluded from enterocyte-specific *ifabp:dsRed* expression. (C) Live sagittal confocal z-projection showing the pattern of Cftr-GFP expression in the larval intestine. (D) Cftr-GFP is primarily localized subcellularly. (E) Treatment with IBMX and Cftr activator translocates Cftr-GFP to the apical, brush border membrane. Arrows indicate CHE cells. Scale bars: 50 μm.

5.6 Summary

Here I have established that Cftr-dependent fluid secretion is an essential component of organ morphogenesis and function. In KV, Cftr activity within the epithelium drives lumen expansion where fluid secretion is necessary for KV function during the specification of LR asymmetry. Importantly, live imaging of transgenic lines I generated during the course of this work revealed that *cftr* is expressed throughout KV morphogenesis. In the pancreas, I demonstrated that the *cftr* mutant zebrafish develops pancreatic disease reminiscent of CF, including substantial destruction of the exocrine pancreas. Within the zebrafish pancreas, I observed *cftr* expression specifically in the pancreatic ducts throughout morphogenesis. Cftr function in the pancreas is not evident in the early stages of pancreatic specification, but is essential for later ductal function and pancreatic maintenance. Altogether, the work described here demonstrates that *cftr* is necessary for fluid secretion, organ morphogenesis, and function in the zebrafish.

This work lays a foundation for diverse studies that may result from the generation of a new model for investigating *cftr*-dependent fluid secretion. Although the pathophysiology of CF has been well characterized, a highly accessible experimental system for dissecting the precise mechanisms at work in the disease has been lacking. The zebrafish may provide an ideal system to gain a deeper understanding of CF by providing insight into the function of the processes regulating intracellular trafficking of CFTR, function of the innate immune system, and in vertebral maintenance. Similarly,

cftr mutant zebrafish will allow investigations into more basic questions including the processes that drive lumen formation and how the cells in the notochord mediate mechanical forces throughout the body. Examining the function of *cftr* in the zebrafish models established here will continue to provide insights into fundamental developmental processes and illuminate the pathophysiology of cystic fibrosis, which will contribute to a more complete understanding of the disease.

References

Abu-El-Haija, M., Ramachandran, S., Meyerholz, D. K., Abu-El-Haija, M., Griffin, M., Giriyappa, R. L., Stoltz, D. A., Welsh, M. J., McCray, P. B. and Uc, A. (2012). Pancreatic damage in fetal and newborn cystic fibrosis pigs involves the activation of inflammatory and remodeling pathways. *Am. J. Pathol.* **181**, 499–507.

Adams, D. S., Keller, R. and Koehl, M. A. (1990). The mechanics of notochord elongation, straightening and stiffening in the embryo of Xenopus laevis. *Development (Cambridge, England)* **110**, 115–130.

Alvers, A. L., Ryan, S., Scherz, P. J., Huisken, J. and Bagnat, M. (2014). Single continuous lumen formation in the zebrafish gut is mediated by smoothened-dependent tissue remodeling. *Development (Cambridge, England)* **141**, 1110–1119.

Amack, J. D. and Yost, H. J. (2004). The T box transcription factor no tail in ciliated cells controls zebrafish left-right asymmetry. *Curr Biol* **14**, 685–690.

Amack, J. D., Wang, X. and Yost, H. J. (2007). Two T-box genes play independent and cooperative roles to regulate morphogenesis of ciliated Kupffer's vesicle in zebrafish. *Developmental Biology* **310**, 196–210.

Andersen, D. H. (1938). Cystic fibrosis of the pancreas and its relation to celiac disease: a clinical and pathological study. *Am J Dis Child* **56**, 344–399.

Anderson, M. P., Gregory, R. J., Thompson, S., Souza, D. W., Paul, S., Mulligan, R. C., Smith, A. E. and Welsh, M. J. (1991). Demonstration that CFTR is a chloride channel by alteration of its anion selectivity. *Science (New York, NY)* **253**, 202–205.

Andersson, O., Adams, B. A., Yoo, D., Ellis, G. C., Gut, P., Anderson, R. M., German, M. S. and Stainier, D. Y. R. (2012). Adenosine signaling promotes regeneration of pancreatic β cells in vivo. *Cell Metab* **15**, 885–894.

Aw, S., Adams, D. S., Qiu, D. and Levin, M. (2008). H,K-ATPase protein localization and Kir4.1 function reveal concordance of three axes during early determination of left-right asymmetry. *Mechanisms of Development* **125**, 353–372.

Baetens, D., Malaisse-Lagae, F., Perrelet, A. and Orci, L. (1979). Endocrine pancreas: three-dimensional reconstruction shows two types of islets of langerhans. *Science (New York, NY)* **206**, 1323–1325.

Bagnat, M., Cheung, I. D., Mostov, K. E. and Stainier, D. Y. R. (2007). Genetic control of

single lumen formation in the zebrafish gut. *Nat Cell Biol* **9**, 954–960.

Bagnat, M., Navis, A., Herbstreith, S., Brand-Arzamendi, K., Curado, S., Gabriel, S., Mostov, K. E., Huisken, J. and Stainier, D. Y. R. (2010). Cse1l is a negative regulator of CFTR-dependent fluid secretion. *Curr Biol* **20**, 1840–1845.

Barrett, K. E. and Keely, S. J. (2000). Chloride secretion by the intestinal epithelium: molecular basis and regulatory aspects. *Annu Rev Physiol* **62**, 535–572.

Benharouga, M., Sharma, M., So, J., Haardt, M., Drzymala, L., Popov, M., Schwapach, B., Grinstein, S., Du, K. and Lukacs, G. L. (2003). The role of the C terminus and Na+/H+ exchanger regulatory factor in the functional expression of cystic fibrosis transmembrane conductance regulator in nonpolarized cells and epithelia. *J Biol Chem* **278**, 22079–22089.

Berger, H. A., Travis, S. M. and Welsh, M. J. (1993). Regulation of the cystic fibrosis transmembrane conductance regulator Cl- channel by specific protein kinases and protein phosphatases. *J Biol Chem* **268**, 2037–2047.

Bisgrove, B. W., Essner, J. J. and Yost, H. J. (1999). Regulation of midline development by antagonism of lefty and nodal signaling. *Development (Cambridge, England)* **126**, 3253–3262.

Bisgrove, B. W., Snarr, B. S., Emrazian, A. and Yost, H. J. (2005). Polaris and Polycystin-2 in dorsal forerunner cells and Kupffer's vesicle are required for specification of the zebrafish left-right axis. *Developmental Biology* **287**, 274–288.

Blum, M., Andre, P., Muders, K., Schweickert, A., Fischer, A., Bitzer, E., Bogusch, S., Beyer, T., van Straaten, H. W. M. and Viebahn, C. (2007). Ciliation and gene expression distinguish between node and posterior notochord in the mammalian embryo. *Differentiation* **75**, 133–146.

Borovina, A., Superina, S., Voskas, D. and Ciruna, B. (2010). Vangl2 directs the posterior tilting and asymmetric localization of motile primary cilia. *Nat Cell Biol* **12**, 407–412.

Brennan, J., Norris, D. P. and Robertson, E. J. (2002). Nodal activity in the node governs left-right asymmetry. *Genes Dev* **16**, 2339–2344.

Bruscia, E. M., Zhang, P.-X., Satoh, A., Caputo, C., Medzhitov, R., Shenoy, A., Egan, M. E. and Krause, D. S. (2011). Abnormal trafficking and degradation of TLR4 underlie the elevated inflammatory response in cystic fibrosis. *J. Immunol.* **186**, 6990–6998.

Buechner, M. (2002). Tubes and the single C. elegans excretory cell. *Trends Cell Biol* **12**, 479–484.

Callaghan, M. and McClean, S. (2012). Bacterial host interactions in cystic fibrosis. *Curr Opin Microbiol* **15**, 71–77.

Carmany-Rampey, A. and Moens, C. B. (2006). Modern mosaic analysis in the zebrafish. *Methods* **39**, 228–238.

Carson, M. R., Travis, S. M. and Welsh, M. J. (1995). The two nucleotide-binding domains of cystic fibrosis transmembrane conductance regulator (CFTR) have distinct functions in controlling channel activity. *J Biol Chem* **270**, 1711–1717.

Carten, J. D., Bradford, M. K. and Farber, S. A. (2011). Visualizing digestive organ morphology and function using differential fatty acid metabolism in live zebrafish. *Developmental Biology* **360**, 276–285.

Cartwright, J. H. E., Piro, O. and Tuval, I. (2009). Fluid dynamics in developmental biology: moving fluids that shape ontogeny. *Hfsp J* **3**, 77–93.

Cermak, T., Doyle, E. L., Christian, M., Wang, L., Zhang, Y., Schmidt, C., Baller, J. A., Somia, N. V., Bogdanove, A. J. and Voytas, D. F. (2011). Efficient design and assembly of custom TALEN and other TAL effector-based constructs for DNA targeting. *Nucleic Acids Res* **39**, e82.

Chen, S., Li, C., Yuan, G. and Xie, F. (2007). Anatomical and histological observation on the pancreas in adult zebrafish. *Pancreas* **34**, 120–125.

Cheng, S. H., Rich, D. P., Marshall, J., Gregory, R. J., Welsh, M. J. and Smith, A. E. (1991). Phosphorylation of the R domain by cAMP-dependent protein kinase regulates the CFTR chloride channel. *Cell* **66**, 1027–1036.

Clark, B. S., Winter, M., Cohen, A. R. and Link, B. A. (2011). Generation of Rab-based transgenic lines for in vivo studies of endosome biology in zebrafish. *Dev Dyn* **240**, 2452–2465.

Colledge, W., Abella, B., Southern, K., Ratcliff, R., Jiang, C., Cheng, S., MacVinish, L., Anderson, J., Cuthbert, A. and Evans, M. (1995). Generation and characterization of a DF508 cystic fibrosis mouse model. *Nat Genet* **10**, 445–452.

Consortium, T. C. F. G.-P. (1993). Correlation between genotype and phenotype in patients with cystic fibrosis. The Cystic Fibrosis Genotype-Phenotype Consortium.

New England Journal of Medicine **329**, 1308–1313.

Dahlem, T. J., Hoshijima, K., Jurynec, M. J., Gunther, D., Starker, C. G., Locke, A. S., Weis, A. M., Voytas, D. F. and Grunwald, D. J. (2012). Simple Methods for Generating and Detecting Locus-Specific Mutations Induced with TALENs in the Zebrafish Genome. *PLoS Genet* **8**, e1002861.

Davison, J. M., Akitake, C. M., Goll, M. G., Rhee, J. M., Gosse, N., Baier, H., Halpern, M. E., Leach, S. D. and Parsons, M. J. (2007). Transactivation from Gal4-VP16 transgenic insertions for tissue-specific cell labeling and ablation in zebrafish. *Developmental Biology* **304**, 811–824.

Dean, M. and Annilo, T. (2005). Evolution of the ATP-binding cassette (ABC) transporter superfamily in vertebrates. *Annual review of genomics and human genetics* **6**, 123–142.

Deng, W., Nies, F., Feuer, A., Bocina, I., Oliver, D. and Jiang, D. (2013). Anion translocation through an Slc26 transporter mediates lumen expansion during tubulogenesis. *Proc Natl Acad Sci USA* **110**, 14972–14977.

Di Sant'Agnese, P. A., Darling, R. C., Perera, G. A. and Shea, E. (1953). Abnormal electrolyte composition of sweat in cystic fibrosis of the pancreas; clinical significance and relationship to the disease. *Pediatrics* **12**, 549–563.

Di, A., Brown, M. E., Deriy, L. V., Li, C., Szeto, F. L., Chen, Y., Huang, P., Tong, J., Naren, A. P., Bindokas, V., et al. (2006). CFTR regulates phagosome acidification in macrophages and alters bactericidal activity. *Nat Cell Biol* **8**, 933–944.

DiMagno, E. P., Go, V. L. and Summerskill, W. H. (1973). Relations between pancreatic enzyme ouputs and malabsorption in severe pancreatic insufficiency. *New England Journal of Medicine* **288**, 813–815.

Dong, B., Horie, T., Denker, E., Kusakabe, T., Tsuda, M., Smith, W. C. and Jiang, D. (2009a). Tube formation by complex cellular processes in Ciona intestinalis notochord. *Developmental Biology* **330**, 237–249.

Dong, M., Fu, Y.-F., Du, T.-T., Jing, C.-B., Fu, C.-T., Chen, Y., Jin, Y., Deng, M. and Liu, T. X. (2009b). Heritable and Lineage-Specific Gene Knockdown in Zebrafish Embryo. *PLoS ONE* **4**, e6125.

Dong, P. D. S., Munson, C. A., Norton, W., Crosnier, C., Pan, X., Gong, Z., Neumann, C. J. and Stainier, D. Y. R. (2007). Fgf10 regulates hepatopancreatic ductal system

patterning and differentiation. *Nat Genet* **39**, 397–402.

Doyle, E. L., Booher, N. J., Standage, D. S., Voytas, D. F., Brendel, V. P., VanDyk, J. K. and Bogdanove, A. J. (2012). TAL Effector-Nucleotide Targeter (TALE-NT) 2.0: tools for TAL effector design and target prediction. *Nucleic Acids Res* **40**, W117–22.

Drumm, M. L., Konstan, M. W., Schluchter, M. D., Handler, A., Pace, R., Zou, F., Zariwala, M., Fargo, D., Xu, A., Dunn, J. M., et al. (2005). Genetic Modifiers of Lung Disease in Cystic Fibrosis. *N Engl J Med* **353**, 1443–1453.

Durie, P. R. and Forstner, G. G. (1989). Pathophysiology of the exocrine pancreas in cystic fibrosis. *J R Soc Med* **82 Suppl 16**, 2–10.

Elkin, S. L., Fairney, A., Burnett, S., Kemp, M., Kyd, P., Burgess, J., Compston, J. E. and Hodson, M. E. (2001). Vertebral deformities and low bone mineral density in adults with cystic fibrosis: a cross-sectional study. *Osteoporos Int* **12**, 366–372.

Elks, P. M., van Eeden, F. J., Dixon, G., Wang, X., Reyes-Aldasoro, C. C., Ingham, P. W., Whyte, M. K. B., Walmsley, S. R. and Renshaw, S. A. (2011). Activation of hypoxia-inducible factor-1α (Hif-1α) delays inflammation resolution by reducing neutrophil apoptosis and reverse migration in a zebrafish inflammation model. *Blood* **118**, 712–722.

Ellis, K., Bagwell, J. and Bagnat, M. (2013). Notochord vacuoles are lysosome-related organelles that function in axis and spine morphogenesis. *J Cell Biol* **200**, 667–679.

Essner, J. J., Amack, J. D., Nyholm, M. K., Harris, E. B. and Yost, H. J. (2005). Kupffer's vesicle is a ciliated organ of asymmetry in the zebrafish embryo that initiates left-right development of the brain, heart and gut. *Development (Cambridge, England)* **132**, 1247–1260.

Essner, J. J., Vogan, K. J., Wagner, M. K., Tabin, C. J., Yost, H. J. and Brueckner, M. (2002). Conserved function for embryonic nodal cilia. *Nature* **418**, 37–38.

Fallon, M. B., Gorelick, F. S., Anderson, J. M., Mennone, A., Saluja, A. and Steer, M. L. (1995). Effect of cerulein hyperstimulation on the paracellular barrier of rat exocrine pancreas. *Gastroenterology* **108**, 1863–1872.

Fan, S., Harfoot, N., Bartolo, R. C. and Butt, A. G. (2012). CFTR is restricted to a small population of high expresser cells that provide a forskolin-sensitive transepithelial Cl- conductance in the proximal colon of the possum, Trichosurus vulpecula. *J Exp Biol* **215**, 1218–1230.

Fang, P.-K., Solomon, K. R., Zhuang, L., Qi, M., McKee, M., Freeman, M. R. and Yelick, P. C. (2006). Caveolin-1alpha and -1beta perform nonredundant roles in early vertebrate development. *Am. J. Pathol.* **169**, 2209–2222.

Farooq, M., Sulochana, K. N., Pan, X., To, J., Sheng, D., Gong, Z. and Ge, R. (2008). Histone deacetylase 3 (hdac3) is specifically required for liver development in zebrafish. *Developmental Biology* **317**, 336–353.

Field, H. A., Dong, P. D. S., Beis, D. and Stainier, D. Y. R. (2003). Formation of the digestive system in zebrafish. II. Pancreas morphogenesis. *Developmental Biology* **261**, 197–208.

Field, M., Fromm, D., Al-Awqati, Q. and Grennough, W. B., III (1972). Effect of Cholera Enterotoxin on Ion Transport across Isolated Ileal Mucosa. *Journal of Clinical Investigation* **51**, 796–804.

Field, S., Riley, K.-L., Grimes, D. T., Hilton, H., Simon, M., Powles-Glover, N., Siggers, P., Bogani, D., Greenfield, A. and Norris, D. P. (2011). Pkd1l1 establishes left-right asymmetry and physically interacts with Pkd2. *Development (Cambridge, England)* **138**, 1131–1142.

Frizzell, R. A. and Hanrahan, J. W. (2012). Physiology of epithelial chloride and fluid secretion. *Cold Spring Harb Perspect Med* **2**, a009563.

Fujita, H., Hamazaki, Y., Noda, Y., Oshima, M. and Minato, N. (2012). Claudin-4 Deficiency Results in Urothelial Hyperplasia and Lethal Hydronephrosis. *PLoS ONE* **7**, e52272.

Furuse, M., Hata, M., Furuse, K., Yoshida, Y., Haratake, A., Sugitani, Y., Noda, T., Kubo, A. and Tsukita, S. (2002). Claudin-based tight junctions are crucial for the mammalian epidermal barrier: a lesson from claudin-1-deficient mice. *J Cell Biol* **156**, 1099–1111.

Gaskin, K. J., Waters, D. L., Howman-Giles, R., de Silva, M., Earl, J. W., Martin, H. C., Kan, A. E., Brown, J. M. and Dorney, S. F. (1988). Liver disease and common-bile-duct stenosis in cystic fibrosis. *New England Journal of Medicine* **318**, 340–346.

Gittes, G. K. (2009). Developmental biology of the pancreas: a comprehensive review. *Developmental Biology* **326**, 4–35.

Gray, C., Loynes, C. A., Whyte, M. K. B., Crossman, D. C., Renshaw, S. A. and Chico, T. J. A. (2011). Simultaneous intravital imaging of macrophage and neutrophil

behaviour during inflammation using a novel transgenic zebrafish. *Thromb. Haemost.* **105**, 811–819.

Gros, J., Feistel, K., Viebahn, C., Blum, M. and Tabin, C. J. (2009). Cell movements at Hensen's node establish left/right asymmetric gene expression in the chick. *Science (New York, NY)* **324**, 941–944.

Hall, C., Flores, M. V., Storm, T., Crosier, K. and Crosier, P. (2007). The zebrafish lysozyme C promoter drives myeloid-specific expression in transgenic fish. *BMC Developmental Biology 2005 5:2* **7**, 42.

Hama, K., Provost, E., Baranowski, T. C., Rubinstein, A. L., Anderson, J. L., Leach, S. D. and Farber, S. A. (2009). In vivo imaging of zebrafish digestive organ function using multiple quenched fluorescent reporters. *Am. J. Physiol. Gastrointest. Liver Physiol.* **296**, G445–53.

Hanaoka, K., Devuyst, O., Schwiebert, E. M., Wilson, P. D. and Guggino, W. B. (1996). A role for CFTR in human autosomal dominant polycystic kidney disease. *Am J Physiol* **270**, C389–99.

Hansen, C. G. and Nichols, B. J. (2010). Exploring the caves: cavins, caveolins and caveolae. *Trends Cell Biol* **20**, 177–186.

Hashimoto, H., Rebagliati, M., Ahmad, N., Muraoka, O., Kurokawa, T., Hibi, M. and Suzuki, T. (2004). The Cerberus/Dan-family protein Charon is a negative regulator of Nodal signaling during left-right patterning in zebrafish. *Development (Cambridge, England)* **131**, 1741–1753.

Henderson, R. C. and Specter, B. B. (1994). Kyphosis and fractures in children and young adults with cystic fibrosis. *J. Pediatr.* **125**, 208–212.

Hirokawa, N., Tanaka, Y., Okada, Y. and Takeda, S. (2006). Nodal flow and the generation of left-right asymmetry. *Cell* **125**, 33–45.

Hogan, B. L. M. and Kolodziej, P. A. (2002). Organogenesis: molecular mechanisms of tubulogenesis. *Nat Rev Genet* **3**, 513–523.

Horne-Badovinac, S., Rebagliati, M. and Stainier, D. Y. R. (2003). A cellular framework for gut-looping morphogenesis in zebrafish. *Science (New York, NY)* **302**, 662–665.

Hou, J., Renigunta, A., Yang, J. and Waldegger, S. (2010). Claudin-4 forms paracellular chloride channel in the kidney and requires claudin-8 for tight junction localization.

Proc Natl Acad Sci USA **107**, 18010–18015.

Huang, P., Xiao, A., Zhou, M., Zhu, Z., Lin, S. and Zhang, B. (2011). Heritable gene targeting in zebrafish using customized TALENs. *Nat Biotechnol* **29**, 699–700.

Hunter, C. J., Matyas, J. R. and Duncan, N. A. (2004). Cytomorphology of notochordal and chondrocytic cells from the nucleus pulposus: a species comparison. *J Anat* **205**, 357–362.

Husain, N., Pellikka, M., Hong, H., Klimentova, T., Choe, K.-M., Clandinin, T. R. and Tepass, U. (2006). The agrin/perlecan-related protein eyes shut is essential for epithelial lumen formation in the Drosophila retina. *Dev Cell* **11**, 483–493.

Hyde, K., Reid, C. J., Tebbutt, S. J., Weide, L., Hollingsworth, M. A. and Harris, A. (1997). The cystic fibrosis transmembrane conductance regulator as a marker of human pancreatic duct development. *Gastroenterology* **113**, 914–919.

Imrie, J. R., Fagan, D. G. and Sturgess, J. M. (1979). Quantitative evaluation of the development of the exocrine pancreas in cystic fibrosis and control infants. *Am. J. Pathol.* **95**, 697–708.

Jakab, R. L., Collaco, A. M. and Ameen, N. A. (2013). Characterization of CFTR High Expresser cells in the intestine. *AJP: Gastrointestinal and Liver Physiology* **305**, G453–65.

Kamei, M., Saunders, W. B., Bayless, K. J., Dye, L., Davis, G. E. and Weinstein, B. M. (2006). Endothelial tubes assemble from intracellular vacuoles in vivo. *Nature* **442**, 453–456.

Kanther, M., Sun, X., Mühlbauer, M., Mackey, L. C., Flynn, E. J., Bagnat, M., Jobin, C. and Rawls, J. F. (2011). Microbial colonization induces dynamic temporal and spatial patterns of NF-κB activation in the zebrafish digestive tract. *Gastroenterology* **141**, 197–207.

Kaplan, E., Shwachman, H., Perlmutter, A. D., Rule, A., Khaw, K. T. and Holsclaw, D. S. (1968). Reproductive failure in males with cystic fibrosis. *New England Journal of Medicine* **279**, 65–69.

Kawakami, Y., Raya, A., Raya, R. M., Rodríguez-Esteban, C. and Izpisúa Belmonte, J.-C. (2005). Retinoic acid signalling links left-right asymmetric patterning and bilaterally symmetric somitogenesis in the zebrafish embryo. *Nature* **435**, 165–171.

Kawamura, S., Miyamoto, S. and Brown, J. H. (2003). Initiation and transduction of stretch-induced RhoA and Rac1 activation through caveolae: cytoskeletal regulation of ERK translocation. *J Biol Chem* **278**, 31111–31117.

Kesavan, G., Sand, F. W., Greiner, T. U., Johansson, J. K., Kobberup, S., Wu, X., Brakebusch, C. and Semb, H. (2009). Cdc42-mediated tubulogenesis controls cell specification. *Cell* **139**, 791–801.

Khan, L. A., Zhang, H., Abraham, N., Sun, L., Fleming, J. T., Buechner, M., Hall, D. H. and Göbel, V. (2013). Intracellular lumen extension requires ERM-1-dependent apical membrane expansion and AQP-8-mediated flux. *Nat Cell Biol* **15**, 143–156.

Kim, H. Y., Varner, V. D. and Nelson, C. M. (2013). Apical constriction initiates new bud formation during monopodial branching of the embryonic chicken lung. *Development (Cambridge, England)* **140**, 3146–3155.

Knowles, M. R., Robinson, J. M., Wood, R. E., Pue, C. A., Mentz, W. M., Wager, G. C., Gatzy, J. T. and Boucher, R. C. (1997). Ion composition of airway surface liquid of patients with cystic fibrosis as compared with normal and disease-control subjects. *J Clin Invest* **100**, 2588–2595.

Kolotuev, I., Hyenne, V., Schwab, Y., Rodriguez, D. and Labouesse, M. (2013). A pathway for unicellular tube extension depending on the lymphatic vessel determinant Prox1 and on osmoregulation. *Nat Cell Biol* **15**, 157–168.

Kozera, L., White, E. and Calaghan, S. (2009). Caveolae act as membrane reserves which limit mechanosensitive I(Cl,swell) channel activation during swelling in the rat ventricular myocyte. *PLoS ONE* **4**, e8312.

Kramer-Zucker, A. G., Olale, F., Haycraft, C. J., Yoder, B. K., Schier, A. F. and Drummond, I. A. (2005). Cilia-driven fluid flow in the zebrafish pronephros, brain and Kupffer's vesicle is required for normal organogenesis. *Development (Cambridge, England)* **132**, 1907–1921.

Kwan, K. M., Fujimoto, E., Grabher, C., Mangum, B. D., Hardy, M. E., Campbell, D. S., Parant, J. M., Yost, H. J., Kanki, J. P. and Chien, C.-B. (2007). The Tol2kit: a multisite gateway-based construction kit for Tol2 transposon transgenesis constructs. *Dev Dyn* **236**, 3088–3099.

Lee, E. C., Yu, D., Martinez de Velasco, J., Tessarollo, L., Swing, D. A., Court, D. L., Jenkins, N. A. and Copeland, N. G. (2001). A highly efficient Escherichia coli-based chromosome engineering system adapted for recombinogenic targeting and

subcloning of BAC DNA. *Genomics* **73**, 56–65.

Lenhart, K. F., Lin, S.-Y., Titus, T. A., Postlethwait, J. H. and Burdine, R. D. (2011). Two additional midline barriers function with midline lefty1 expression to maintain asymmetric Nodal signaling during left-right axis specification in zebrafish. *Development (Cambridge, England)* **138**, 4405–4410.

Levi, B. P., Ghabrial, A. S. and Krasnow, M. A. (2006). Drosophila talin and integrin genes are required for maintenance of tracheal terminal branches and luminal organization. *Development (Cambridge, England)* **133**, 2383–2393.

Levin, M. (2005). Left-right asymmetry in embryonic development: a comprehensive review. *Mechanisms of Development* **122**, 3–25.

Levin, M., Thorlin, T., Robinson, K. R., Nogi, T. and Mercola, M. (2002). Asymmetries in H+/K+-ATPase and cell membrane potentials comprise a very early step in left-right patterning. *Cell* **111**, 77–89.

Li, N., Wei, C., Olena, A. F. and Patton, J. G. (2011). Regulation of endoderm formation and left-right asymmetry by miR-92 during early zebrafish development. *Development (Cambridge, England)* **138**, 1817–1826.

Locksley, R. M., Killeen, N. and Lenardo, M. J. (2001). The TNF and TNF receptor superfamilies: integrating mammalian biology. *Cell* **104**, 487–501.

Long, S., Ahmad, N. and Rebagliati, M. (2003). The zebrafish nodal-related gene southpaw is required for visceral and diencephalic left-right asymmetry. *Development (Cambridge, England)* **130**, 2303–2316.

Lowery, L. A. and Sive, H. (2005). Initial formation of zebrafish brain ventricles occurs independently of circulation and requires the nagie oko and snakehead/atp1a1a.1 gene products. *Development (Cambridge, England)* **132**, 2057–2067.

Löhr, M., Goertchen, P., Nizze, H., Gould, N. S., Gould, V. E., Oberholzer, M., Heitz, P. U. and Klöppel, G. (1989). Cystic fibrosis associated islet changes may provide a basis for diabetes. An immunocytochemical and morphometrical study. *Virchows Arch A Pathol Anat Histopathol* **414**, 179–185.

Lubarsky, B. and Krasnow, M. A. (2003). Tube morphogenesis: making and shaping biological tubes. *Cell* **112**, 19–28.

Lukacs, G. L. and Verkman, A. S. (2012). CFTR: folding, misfolding and correcting the

ΔF508 conformational defect. *Trends Mol Med* **18**, 81–91.

Lyczak, J. B., Cannon, C. L. and Pier, G. B. (2002). Lung infections associated with cystic fibrosis. *Clin. Microbiol. Rev.* **15**, 194–222.

Mackie, A. D. R., Thornton, S. J. and Edenborough, F. P. (2003). Cystic fibrosis-related diabetes. *Diabet. Med.* **20**, 425–436.

Mailleux, A. A., Overholtzer, M., Schmelzle, T., Bouillet, P., Strasser, A. and Brugge, J. S. (2007). BIM regulates apoptosis during mammary ductal morphogenesis, and its absence reveals alternative cell death mechanisms. *Dev Cell* **12**, 221–234.

Manfroid, I., Ghaye, A., Naye, F., Detry, N., Palm, S., Pan, L., Ma, T. P., Huang, W., Rovira, M., Martial, J. A., et al. (2012). Zebrafish sox9b is crucial for hepatopancreatic duct development and pancreatic endocrine cell regeneration. *Developmental Biology* **366**, 268–278.

Marino, C. R., Matovcik, L. M., Gorelick, F. S. and Cohn, J. A. (1991). Localization of the cystic fibrosis transmembrane conductance regulator in pancreas. *J Clin Invest* **88**, 712–716.

Marjoram, L. and Wright, C. (2011). Rapid differential transport of Nodal and Lefty on sulfated proteoglycan-rich extracellular matrix regulates left-right asymmetry in Xenopus. *Development (Cambridge, England)* **138**, 475–485.

Marques, S., Borges, A. C., Silva, A. C., Freitas, S., Cordenonsi, M. and Belo, J. A. (2004). The activity of the Nodal antagonist Cerl-2 in the mouse node is required for correct L/R body axis. *Genes Dev* **18**, 2342–2347.

Matsui, H., Grubb, B. R., Tarran, R., Randell, S. H., Gatzy, J. T., Davis, C. W. and Boucher, R. C. (1998). Evidence for periciliary liquid layer depletion, not abnormal ion composition, in the pathogenesis of cystic fibrosis airways disease. *Cell* **95**, 1005–1015.

McCann, M. R., Tamplin, O. J., Rossant, J. and Séguin, C. A. (2012). Tracing notochord-derived cells using a Noto-cre mouse: implications for intervertebral disc development. *Dis Model Mech* **5**, 73–82.

McGrath, J., Somlo, S., Makova, S., Tian, X. and Brueckner, M. (2003). Two populations of node monocilia initiate left-right asymmetry in the mouse. *Cell* **114**, 61–73.

Meder, D., Shevchenko, A., Simons, K. and Füllekrug, J. (2005). Gp135/podocalyxin and NHERF-2 participate in the formation of a preapical domain during polarization of MDCK cells. *J Cell Biol* **168**, 303–313.

Melnick, M. and Jaskoll, T. (2000). Mouse submandibular gland morphogenesis: a paradigm for embryonic signal processing. *Crit Rev Oral Biol Med* **11**, 199–215.

Miller, J. C., Tan, S., Qiao, G., Barlow, K. A., Wang, J., Xia, D. F., Meng, X., Paschon, D. E., Leung, E., Hinkley, S. J., et al. (2011). A TALE nuclease architecture for efficient genome editing. *Nat Biotechnol* **29**, 143–148.

Moss, J. B., Koustubhan, P., Greenman, M., Layer, R., Walter, I. and Moss, L. G. (2009). Regeneration of the Pancreas in Adult Zebrafish. *Diabetes* **58**, 1844–1851.

Moyer, J. H., Lee-Tischler, M. J., Kwon, H. Y., Schrick, J. J., Avner, E. D., Sweeney, W. E., Godfrey, V. L., Cacheiro, N. L., Wilkinson, J. E. and Woychik, R. P. (1994). Candidate gene associated with a mutation causing recessive polycystic kidney disease in mice. *Science (New York, NY)* **264**, 1329–1333.

Muto, S., Hata, M., Taniguchi, J., Tsuruoka, S., Moriwaki, K., Saitou, M., Furuse, K., Sasaki, H., Fujimura, A., Imai, M., et al. (2010). Claudin-2-deficient mice are defective in the leaky and cation-selective paracellular permeability properties of renal proximal tubules. *Proc Natl Acad Sci USA* **107**, 8011–8016.

Nakamura, T., Mine, N., Nakaguchi, E., Mochizuki, A., Yamamoto, M., Yashiro, K., Meno, C. and Hamada, H. (2006). Generation of robust left-right asymmetry in the mouse embryo requires a self-enhancement and lateral-inhibition system. *Dev Cell* **11**, 495–504.

Nauli, S. M., Alenghat, F. J., Luo, Y., Williams, E., Vassilev, P., Li, X., Elia, A. E. H., Lu, W., Brown, E. M., Quinn, S. J., et al. (2003). Polycystins 1 and 2 mediate mechanosensation in the primary cilium of kidney cells. *Nat Genet* **33**, 129–137.

Nixon, S. J., Carter, A., Wegner, J., Ferguson, C., Floetenmeyer, M., Riches, J., Key, B., Westerfield, M. and Parton, R. G. (2007). Caveolin-1 is required for lateral line neuromast and notochord development. *J Cell Sci* **120**, 2151–2161.

Nonaka, S., Shiratori, H., Saijoh, Y. and Hamada, H. (2002). Determination of left-right patterning of the mouse embryo by artificial nodal flow. *Nature* **418**, 96–99.

O'Neal, W., Hasty, P., McCray, P., Casey, B., RiveraPerez, J., Welsh, M., Beaudet, A. and Bradley, A. (1993). A severe phenotype in mice with a duplication of exon 3 in

the cystic fibrosis locus. *Human Molecular Genetics* **2**, 1561–1569.

Ohi, Y. and Wright, C. V. E. (2007). Anteriorward shifting of asymmetric Xnr1 expression and contralateral communication in left-right specification in Xenopus. *Developmental Biology* **301**, 447–463.

Olivier, A. K., Yi, Y., Sun, X., Sui, H., Liang, B., Hu, S., Xie, W., Fisher, J. T., Keiser, N. W., Lei, D., et al. (2012). Abnormal endocrine pancreas function at birth in cystic fibrosis ferrets. *J Clin Invest* **122**, 3755–3768.

Oppenheimer, E. H. and Esterly, J. R. (1969). Observations on cystic fibrosis of the pancreas. V. Developmental changes in the male genital system. *J. Pediatr.* **75**, 806–811.

Oteíza, P., Köppen, M., Concha, M. L. and Heisenberg, C.-P. (2008). Origin and shaping of the laterality organ in zebrafish. *Development (Cambridge, England)* **135**, 2807–2813.

Oteíza, P., Köppen, M., Krieg, M., Pulgar, E., Farias, C., Melo, C., Preibisch, S., Müller, D., Tada, M., Hartel, S., et al. (2010). Planar cell polarity signalling regulates cell adhesion properties in progenitors of the zebrafish laterality organ. *Development (Cambridge, England)* **137**, 3459–3468.

Parsons, M. J., Pisharath, H., Yusuff, S., Moore, J. C., Siekmann, A. F., Lawson, N. D. and Leach, S. D. (2009). Notch-responsive cells initiate the secondary transition in larval zebrafish pancreas. *Mechanisms of Development* **126**, 898–912.

Patton, E. E. and Zon, L. I. (2001). The art and design of genetic screens: zebrafish. *Nat Rev Genet* **2**, 956–966.

Pennekamp, P., Karcher, C., Fischer, A., Schweickert, A., Skryabin, B., Horst, J., Blum, M. and Dworniczak, B. (2002). The ion channel polycystin-2 is required for left-right axis determination in mice. *Curr Biol* **12**, 938–943.

Phennicie, R. T., Sullivan, M. J., Singer, J. T., Yoder, J. A. and Kim, C. H. (2010). Specific resistance to Pseudomonas aeruginosa infection in zebrafish is mediated by the cystic fibrosis transmembrane conductance regulator. *Infection and immunity* **78**, 4542–4550.

Pisharath, H., Rhee, J. M., Swanson, M. A., Leach, S. D. and Parsons, M. J. (2007). Targeted ablation of beta cells in the embryonic zebrafish pancreas using E. coli nitroreductase. *Mechanisms of Development* **124**, 218–229.

Quinton, P. M. (1990). Cystic fibrosis: a disease in electrolyte transport. *The FASEB Journal* **4**, 2709.

Riordan, J. R. (2008). CFTR function and prospects for therapy. *Annu Rev Biochem* **77**, 701–726.

Riordan, J. R., Rommens, J. M., Kerem, B., Alon, N., Rozmahel, R., Grzelczak, Z., Zielenski, J., Lok, S., Plavsic, N. and Chou, J. L. (1989). Identification of the cystic fibrosis gene: cloning and characterization of complementary DNA. *Science (New York, NY)* **245**, 1066–1073.

Rogers, C. S., Stoltz, D. A., Meyerholz, D. K., Ostedgaard, L. S., Rokhlina, T., Taft, P. J., Rogan, M. P., Pezzulo, A. A., Karp, P. H., Itani, O. A., et al. (2008). Disruption of the CFTR Gene Produces a Model of Cystic Fibrosis in Newborn Pigs. *Science (New York, NY)* **321**, 1837–1841.

Rosenstein, B. J. and Cutting, G. R. (1998). The diagnosis of cystic fibrosis: a consensus statement. Cystic Fibrosis Foundation Consensus Panel.pp. 589–595.

Ross, J., Gamble, J., Schultz, A. and Lewiston, N. (1987). Back pain and spinal deformity in cystic fibrosis. *Am J Dis Child* **141**, 1313–1316.

Ruzal-Shapiro, C. (1998). Cystic fibrosis. An overview. *Radiol Clin North Am* **36**, 143–161.

Saijoh, Y., Oki, S., Ohishi, S. and Hamada, H. (2003). Left-right patterning of the mouse lateral plate requires nodal produced in the node. *Developmental Biology* **256**, 160–172.

Sakaguchi, T., Kikuchi, Y., Kuroiwa, A., Takeda, H. and Stainier, D. Y. R. (2006). The yolk syncytial layer regulates myocardial migration by influencing extracellular matrix assembly in zebrafish. *Development (Cambridge, England)* **133**, 4063–4072.

Sarmah, B., Latimer, A. J., Appel, B. and Wente, S. R. (2005). Inositol polyphosphates regulate zebrafish left-right asymmetry. *Dev Cell* **9**, 133–145.

Sawyer, J. M., Harrell, J. R., Shemer, G., Sullivan-Brown, J., Roh-Johnson, M. and Goldstein, B. (2010). Apical constriction: a cell shape change that can drive morphogenesis. *Developmental Biology* **341**, 5–19.

Schottenfeld, J., Sullivan-Brown, J. and Burdine, R. D. (2007). Zebrafish curly up encodes a Pkd2 ortholog that restricts left-side-specific expression of southpaw. *Development (Cambridge, England)* **134**, 1605–1615.

Schweickert, A., Weber, T., Beyer, T., Vick, P., Bogusch, S., Feistel, K. and Blum, M. (2007). Cilia-driven leftward flow determines laterality in Xenopus. *Curr Biol* **17**, 60–66.

Sedding, D. G., Hermsen, J., Seay, U., Eickelberg, O., Kummer, W., Schwencke, C., Strasser, R. H., Tillmanns, H. and Braun-Dullaeus, R. C. (2005). Caveolin-1 facilitates mechanosensitive protein kinase B (Akt) signaling in vitro and in vivo. *Circ Res* **96**, 635–642.

Semova, I., Carten, J. D., Stombaugh, J., Mackey, L. C., Knight, R., Farber, S. A. and Rawls, J. F. (2012). Microbiota regulate intestinal absorption and metabolism of fatty acids in the zebrafish. *Cell Host Microbe* **12**, 277–288.

Sendler, M., Dummer, A., Weiss, F. U., Krüger, B., Wartmann, T., Scharffetter-Kochanek, K., van Rooijen, N., Malla, S. R., Aghdassi, A., Halangk, W., et al. (2013). Tumour necrosis factor α secretion induces protease activation and acinar cell necrosis in acute experimental pancreatitis in mice. *Gut* **62**, 430–439.

Shih, H. P., Wang, A. and Sander, M. (2013). Pancreas Organogenesis: From Lineage Determination to Morphogenesis. *Annu Rev Cell Dev Biol* **29**, 81–105.

Shook, D. R., Majer, C. and Keller, R. (2004). Pattern and morphogenesis of presumptive superficial mesoderm in two closely related species, Xenopus laevis and Xenopus tropicalis. *Developmental Biology* **270**, 163–185.

Snelson, C. D., Santhakumar, K., Halpern, M. E. and Gamse, J. T. (2008). Tbx2b is required for the development of the parapineal organ. *Development (Cambridge, England)* **135**, 1693–1702.

Solar, M., Cardalda, C., Houbracken, I., Martín, M., Maestro, M. A., De Medts, N., Xu, X., Grau, V., Heimberg, H., Bouwens, L., et al. (2009). Pancreatic exocrine duct cells give rise to insulin-producing beta cells during embryogenesis but not after birth. *Dev Cell* **17**, 849–860.

Sproul, A. and Huang, N. (1964). Growth patterns in children with cystic fibrosis. *J. Pediatr.* **65**, 664–676.

Strilić, B., Eglinger, J., Krieg, M., Zeeb, M., Axnick, J., Babál, P., Muller, D. J. and Lammert, E. (2010). Electrostatic cell-surface repulsion initiates lumen formation in developing blood vessels. *Curr Biol* **20**, 2003–2009.

Sturgess, J. M. (1984). Structural and developmental abnormalities of the exocrine

pancreas in cystic fibrosis. *J. Pediatr. Gastroenterol. Nutr.* **3 Suppl 1**, S55–66.

Sulik, K., Dehart, D. B., Iangaki, T., Carson, J. L., Vrablic, T., Gesteland, K. and Schoenwolf, G. C. (1994). Morphogenesis of the murine node and notochordal plate. *Dev Dyn* **201**, 260–278.

Sun, X., Sui, H., Fisher, J. T., Yan, Z., Liu, X., Cho, H.-J., Joo, N. S., Zhang, Y., Zhou, W., Yi, Y., et al. (2010). Disease phenotype of a ferret CFTR-knockout model of cystic fibrosis. *J Clin Invest* **120**, 3149–3160.

Sun, Z., Amsterdam, A., Pazour, G. J., Cole, D. G., Miller, M. S. and Hopkins, N. (2004). A genetic screen in zebrafish identifies cilia genes as a principal cause of cystic kidney. *Development (Cambridge, England)* **131**, 4085–4093.

Superina, S., Borovina, A. and Ciruna, B. (2014). Analysis of maternal-zygotic ugdh mutants reveals divergent roles for HSPGs in vertebrate embryogenesis and provides new insight into the initiation of left-right asymmetry. *Developmental Biology* **387**, 154–166.

Suster, M. L., Sumiyama, K. and Kawakami, K. (2009). Transposon-mediated BAC transgenesis in zebrafish and mice. *BMC Genomics* **10**, 477.

Syed, Z. A., Bougé, A.-L., Byri, S., Chavoshi, T. M., Tång, E., Bouhin, H., van Dijk-Härd, I. F. and Uv, A. (2012). A luminal glycoprotein drives dose-dependent diameter expansion of the Drosophila melanogaster hindgut tube. *PLoS Genet* **8**, e1002850.

Tanner, M. S. and Taylor, C. J. (1995). Liver disease in cystic fibrosis. *Arch. Dis. Child.* **72**, 281–284.

Thibodeau, P. H., Brautigam, C. A., Machius, M. and Thomas, P. J. (2005). Side chain and backbone contributions of Phe508 to CFTR folding. *Nature Structural & Molecular Biology* **12**, 10–16.

Tiso, N., Moro, E. and Argenton, F. (2009). Zebrafish pancreas development. *Mol. Cell. Endocrinol.* **312**, 24–30.

Trede, N. S., Langenau, D. M., Traver, D., Look, A. T. and Zon, L. I. (2004). The use of zebrafish to understand immunity. *Immunity* **20**, 367–379.

Tsarouhas, V., Senti, K.-A., Jayaram, S. A., Tiklová, K., Hemphälä, J., Adler, J. and Samakovlis, C. (2007). Sequential pulses of apical epithelial secretion and

endocytosis drive airway maturation in Drosophila. *Dev Cell* **13**, 214–225.

Tucker, A. S. (2007). Salivary gland development. *Semin Cell Dev Biol* **18**, 237–244.

Unger, R. H. (1985). Glucagon physiology and pathophysiology in the light of new advances. *Diabetologia* **28**, 574–578.

Uv, A., Cantera, R. and Samakovlis, C. (2003). Drosophila tracheal morphogenesis: intricate cellular solutions to basic plumbing problems. *Trends Cell Biol* **13**, 301–309.

van Doorninck, J. H., French, P. J., Verbeek, E., Peters, R. H., Morreau, H., Bijman, J. and Scholte, B. J. (1995). A mouse model for the cystic fibrosis delta F508 mutation. *EMBO J* **14**, 4403–4411.

Vandenberg, L. N. and Levin, M. (2013). A unified model for left-right asymmetry? Comparison and synthesis of molecular models of embryonic laterality. *Developmental Biology* **379**, 1–15.

Veerkamp, J., Rudolph, F., Cseresnyes, Z., Priller, F., Otten, C., Renz, M., Schaefer, L. and Abdelilah-Seyfried, S. (2013). Unilateral dampening of Bmp activity by nodal generates cardiac left-right asymmetry. *Dev Cell* **24**, 660–667.

Waddington, C. H. and Perry, M. M. (1962). Ultrastructure of the developing urodele notochord. *P Roy Soc Lond B Bio* **156**, 459–482.

Wang, G., Cadwallader, A. B., Jang, D. S., Tsang, M., Yost, H. J. and Amack, J. D. (2011a). The Rho kinase Rock2b establishes anteroposterior asymmetry of the ciliated Kupffer's vesicle in zebrafish. *Development (Cambridge, England)* **138**, 45–54.

Wang, X., Robertson, A. L., Li, J., Chai, R. J., Haishan, W., Sadiku, P., Ogryzko, N. V., Everett, M., Yoganathan, K., Luo, H. R., et al. (2014). Inhibitors of neutrophil recruitment identified using transgenic zebrafish to screen a natural product library. *Dis Model Mech* **7**, 163–169.

Wang, Y., Rovira, M., Yusuff, S. and Parsons, M. J. (2011b). Genetic inducible fate mapping in larval zebrafish reveals origins of adult insulin-producing β-cells. *Development (Cambridge, England)* **138**, 609–617.

Warming, S., Costantino, N., Court, D. L., Jenkins, N. A. and Copeland, N. G. (2005). Simple and highly efficient BAC recombineering using galK selection. *Nucleic Acids Res* **33**, e36.

Waters, D. L., Dorney, S. F., Gaskin, K. J., Gruca, M. A., O'Halloran, M. and Wilcken, B. (1990). Pancreatic function in infants identified as having cystic fibrosis in a neonatal screening program. *New England Journal of Medicine* **322**, 303–308.

Wilschanski, M. and Novak, I. (2013). The cystic fibrosis of exocrine pancreas. *Cold Spring Harb Perspect Med* **3**, a009746–a009746.

Wilson, P. D. (2004). Polycystic kidney disease. *N Engl J Med* **350**, 151–164.

Wilson, S. M., Olver, R. E. and Walters, D. V. (2007). Developmental regulation of lumenal lung fluid and electrolyte transport. *Respir Physiol Neurobiol* **159**, 247–255.

Wright, E. M. and Loo, D. D. (2000). Coupling between Na+, sugar, and water transport across the intestine. *Ann. N. Y. Acad. Sci.* **915**, 54–66.

Yang, B., Sonawane, N. D., Zhao, D., Somlo, S. and Verkman, A. S. (2008). Small-molecule CFTR inhibitors slow cyst growth in polycystic kidney disease. *Journal of the American Society of Nephrology* **19**, 1300–1310.

Yang, Z., Zimmerman, S., Brakeman, P. R., Beaudoin, G. M., Reichardt, L. F. and Marciano, D. K. (2013). De novo lumen formation and elongation in the developing nephron: a central role for afadin in apical polarity. *Development (Cambridge, England)* **140**, 1774–1784.

Yazbi, El, A. F., Cho, W. J., Cena, J., Schulz, R. and Daniel, E. E. (2008). Smooth muscle NOS, colocalized with caveolin-1, modulates contraction in mouse small intestine. *J. Cell. Mol. Med.* **12**, 1404–1415.

Yelon, D., Horne, S. A. and Stainier, D. Y. R. (1999). Restricted expression of cardiac myosin genes reveals regulated aspects of heart tube assembly in zebrafish. *Developmental Biology* **214**, 23–37.

Zaghloul, N. A. and Katsanis, N. (2011). Zebrafish assays of ciliopathies. *Methods Cell Biol* **105**, 257–272.

Zang, L., Shimada, Y., Nishimura, Y., Tanaka, T. and Nishimura, N. (2013). A Novel, Reliable Method for Repeated Blood Collection from Aquarium Fish. *Zebrafish* 130513085856008.

Zeiher, B., Eichwald, E., Zabner, J., Smith, J., Puga, A., McCray, P., Jr, Capecchi, M., Welsh, M. and Thomas, K. (1995). A mouse model for the delta F508 allele of cystic fibrosis. *Journal of Clinical Investigation* **96**, 2051.

Zhang, F., Wang, L.-P., Boyden, E. S. and Deisseroth, K. (2006). Channelrhodopsin-2 and optical control of excitable cells. *Nat Meth* **3**, 785–792.

Zhang, J., Piontek, J., Wolburg, H., Piehl, C., Liss, M., Otten, C., Christ, A., Willnow, T. E., Blasig, I. E. and Abdelilah-Seyfried, S. (2010). Establishment of a neuroepithelial barrier by Claudin5a is essential for zebrafish brain ventricular lumen expansion. *Proc Natl Acad Sci USA* **107**, 1425–1430.

Zon, L. I. and Peterson, R. T. (2005). In vivo drug discovery in the zebrafish. *Nat Rev Drug Discov* **4**, 35–44.

Biography

Adam Navis was born August 12, 1983 in La Crosse, Wisconsin to Randy and Laura Navis. He received a Bachelor of Science in Molecular Biosciences and Biotechnology from Arizona State University in 2008, performing undergraduate research in Alan Rawls' lab. Adam joined the Development and Stem Cell Biology Training Program at Duke University in 2008 and joined Michel Bagnat's lab in the Department of Cell Biology in 2009.

Publications

Navis, A., Marjoram, L., and Bagnat, M. (2013). Cftr controls lumen expansion and function of Kupffer's vesicle in zebrafish. *Development* 140, 1703–1712.

Navis, A., Bagnat, M. Chapter 4: Apico-basal polarity and lumen formation during development. *Cell Polarity*. Springer-Verlag, Submitted

Bagnat, M., Navis, A., Herbstreith, S., Brand-Arzamendi, K., Curado, S., Gabriel, S., Mostov, K.E., Huisken, J., and Stainier, D.Y.R. (2010). Cse1l is a negative regulator of CFTR-dependent fluid secretion. *Curr Biol* 20, 1840–1845.